Spring 5-15-2020

Elucidation of Radical Cation Trapping Chemistry: Using Electrochemical and Photochemical Techniques to Qualitatively Assess the Kinetics behind Anodic Oxidative Cyclizations

Luisalberto Gonzalez
Washington University in St. Louis

WASHINGTON UNIVERSITY IN ST. LOUIS
Department of Chemistry

Dissertation Examination Committee:
Kevin Moeller, Chair
Vladimir Birman
James Janetka
John-Stephen Taylor
Timothy Wencewicz

Elucidation of Radical Cation Trapping Chemistry: Using Electrochemical and Photochemical Techniques to Qualitatively Assess the Kinetics behind Anodic Oxidative Cyclizations

By
Luisalberto Gonzalez

A dissertation presented to
The Graduate School
of Washington University in
partial fulfillment of the
requirements for the degree
of Doctor of Philosophy

May 2020
St. Louis, Missouri

Table of Contents

Acknowledgements

Financial support for this research was provided by the National Science Foundation, grant CHE-1764449. I also express thanks to the quality research facilities at Washington University in St. Louis, including the High Resolution NMR Facility and the NIH NCRR Biomedical Mass Spectrometry Resource.

I am incredibly grateful to my research advisor, Dr. Kevin Moeller, who has been crucial in my development as a chemist and as a professional. Through his teaching and guidance, I have grown both intellectually and personally, and his impact has been felt within the past years and certainly going forward in my life.

I would also like to acknowledge my family and all my friends I have made while living in St. Louis. I am certain I would not have made it to this point without their support.

Luisalberto Gonzalez

Washington University in St. Louis

May 2020

Dedicated to my mother, Julia Claudia Gonzalez Baldizon, who was not able to see me become the man I am today.

te extraño

Abstract

Elucidation of Radical Cation Trapping Chemistry: Using Electrochemical and Photochemical Techniques to Qualitatively Assess the Kinetics behind Anodic Oxidative Cyclizations

by

Luisalberto Gonzalez

Doctor of Philosophy in Chemistry

Washington University in St. Louis, 2019

Professor Kevin D. Moeller, Chair

While the field of organic chemistry has grown throughout the decades, its primary concern has always been on the generation, conversion, and study of molecular structures. Within that philosophy, the development of new reactions affords chemists the ability to overcome previous synthetic barriers or develop more elegant and simple synthetic routes to difficult-to-construct molecules. Within that realm, electrochemistry is seeing increased attention due its ability to generate highly reactive intermediates, recycle chemical reagents, and reverse the polarity of known functional groups. One example of such an application is the use of electrochemistry to form radical cations. While radical cations have a relatively small history of use within organic chemistry, they are central to our understanding of the oxidation reactions that allow us to increase the functionality of a molecule, and how we can take maximum advantage of them. Accordingly, this dissertation examines the mechanistic pathways through which radical cation initiated reactions proceed.

Chapter 2 begins with competition studies that were initially used to probe the mechanism of radical cation trapping between two nucleophiles. By tethering two nucleophilic trappings

groups to an electron rich olefin, we were able to deduce the relative reactivity of various trapping groups, which included sulfonamides, alcohols, enol ethers, and allyl silanes, toward a ketene dithioacetal derived radical cation (a commonly used synthetic intermediate in our group). The use of cyclic voltammetry aided our efforts in understanding the rate of the initial cyclization and in so doing the larger mechanistic paramaters at play.

Chapter 3 explores the relationship between electrochemical and photochemical methods for the generation of radical cations. While both methods generate radical cation intermediates, they differ in the number of electrons removed from the substrate. Hence, the downstream chemistry is significantly different. We hoped to use the studies to show the generality of the conclusions reached using electrochemical competition studies. Instead, we found that the complimentary methods were both important for getting a complete picture of the reactions. This surprising result is shaping current efforts aimed toward the development of new, synthetically relevant oxidative cyclization reactions.

Chapter 1

Introduction: Anodic Cyclization Reactions

Radical cation intermediates are receiving significant attention from the synthetic organic community because they open up entirely new reaction pathways for synthesis. This is accomplished by utilizing the highly reactive intermediates to access new mechanistic pathways that are typically available using more traditional methods. For example, consider the pair of generic reactions highlighted in Scheme 1. In both reactions, an electron-rich olefin bearing the groups X and Y undergo a coupling reaction where R is also an electron-donating group. In the first case, the substrate **1** is treated with acid leading to a more traditional acid catalyzed cyclization product **2**. This reaction is expected to lead to a 6-membered ring product resulting from initial protonation of the olefin bearing the two donors to form a cationic intermediate stabilized by substituents X and Y. Contrast this with the electrochemical reaction of substrate **3** shown in the second equation that proceeds through a radical cation intermediate. In this case, trapping of the radical cation would lead to the formation of a five membered ring product **4**, a scenario that essentially reverses the polarity of the original electron-rich double bond[1].

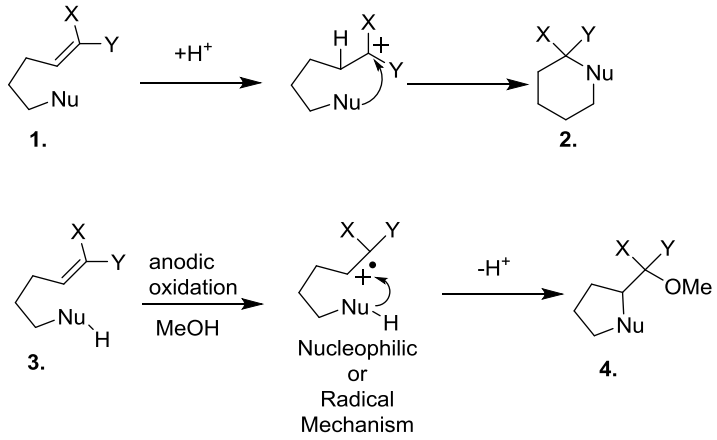

Scheme 1. Acid catalyzed cyclization versus anodic oxidation cyclization.

What is clear from the scheme is that the use of the electrochemical reaction allows the initial electron-rich double bond to be used in more than one way, and that affords synthetic opportunities for the construction of more complex molecules**.** [2-23]

The use of radical cation intermediates in synthesis has been an ongoing theme in our group. The earliest group endeavors into radical cation reactions involved the oxidation of amides

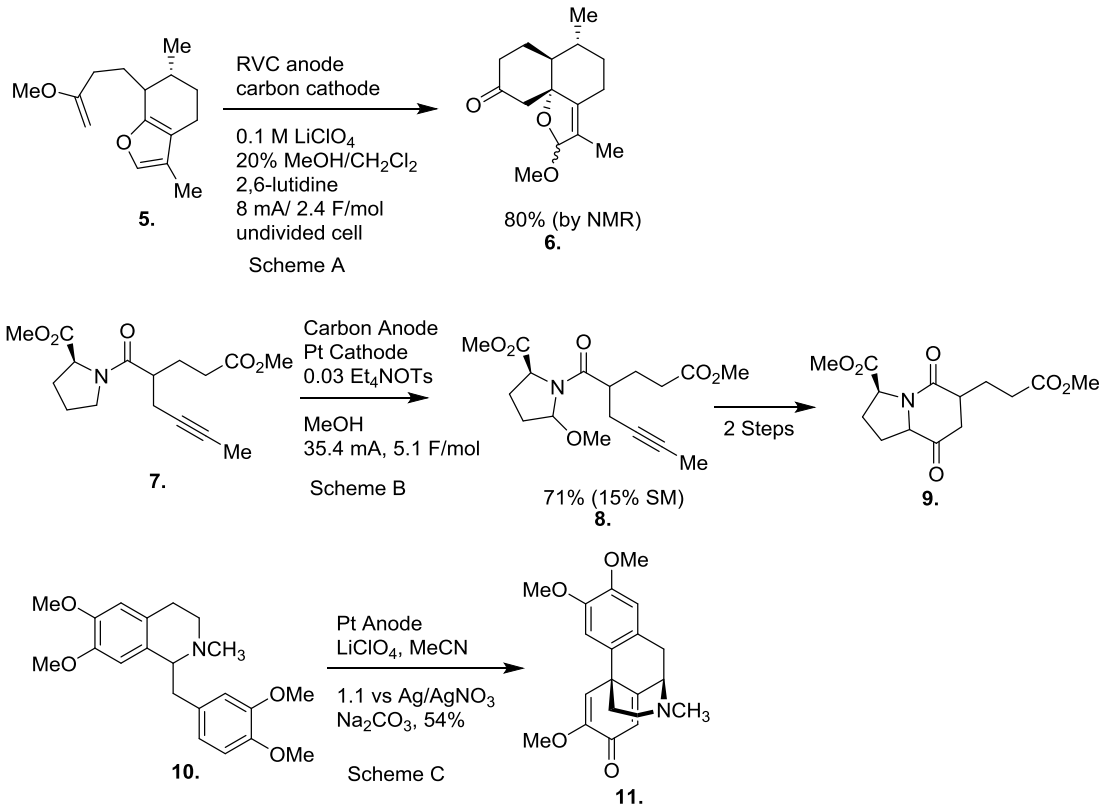

Figure 1. Total Syntheses accomplished via an electrochemical oxidation.

and electron rich olefins. The oxidation of amides led to elimination reactions from the nitrogen radical cation, the generation of N-acyliminium ion intermediates, and the formation of bicyclic ring skeletons. The oxidation of the electron rich olefins led to radical cation intermediates that triggered interesting new umpolung reactions in an effort to exploit the idea forwarded in Scheme 1. Both routes led to successful total synthesis efforts. (Figure 1). [23-25]

The chemistry outlined below will build on the olefin coupling part of this background. The take away lesson from that early work was that the direct electrochemical oxidation of electron rich olefins allows for the coupling of two nucleophilic groups by generating an incredibly reactive radical cation intermediate. The work that was done and the work that is outlined below has as its goal to provide a demonstration of how synthetic chemists can approach and think about new electrochemical transformations, and how those reaction can serve as a starting point for new retrosynthetic analyses.

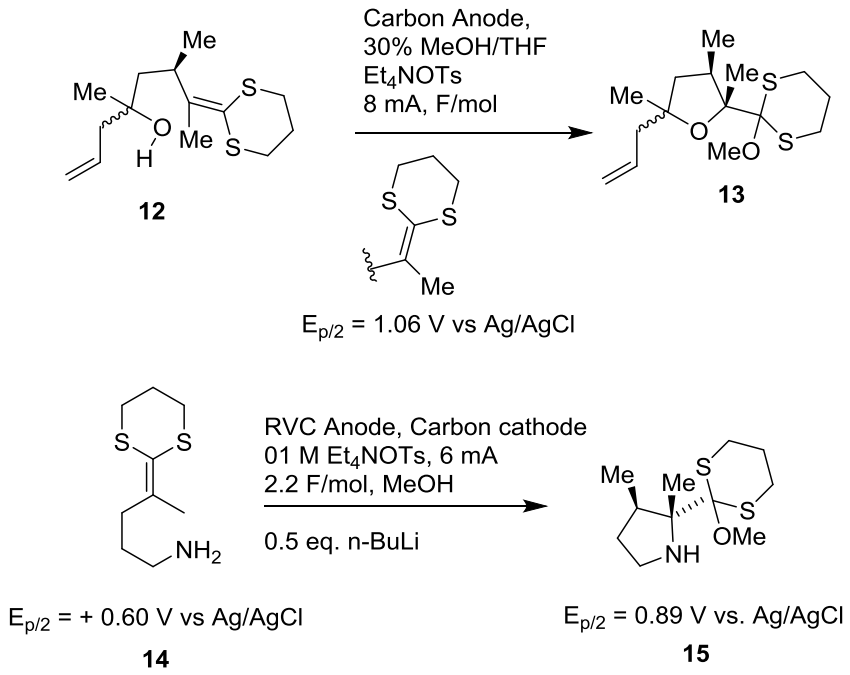

Figure 2. Chemical Oxidant vs. Electrochemical Oxidation. Oxidation potentials are represented by the $E_{p/2}$ values attached. Substrates with lower oxidation potential will be oxidized before substrates with higher potentials. In this particular example, a chemical oxidant that would facilitate the top reaction would oxidize both the initial substrate and the resulting product to give over-oxidized material.

Of course, key to any such effort is understanding the nature and reactivity of the intermediates involved in the reactions, and key to gaining that insight is another frequently overlooked advantage that electrochemistry offers that is frequently overlooked. That advantage has to do with the highly selective nature of electrochemical reactions. Traditional chemical oxidations can suffer for multiple reasons but one of the most troublesome aspects in regard to exploring the chemistry of a reactive intermediate is finding a family of oxidants that will all

selectively oxidize a particular family of functional groups without oxidizing other functional groups present on the molecule or the product from the oxidation. Without such a family of oxidants, it is difficult conduct the structure activity relationships necessary for exploring the chemistry of the reactive intermediate. The examples shown in Figure 2 highlight this issue. A chemical oxidant that would facilitate the transformation of the ketene dithioacetal **12** to the tetrahydrofuran product **13** requires an oxidative potential of at least +1.06 V vs Ag/AgCl. Compare this to the oxidative cyclization of the amine substrate **14** and its electrolysis product **15** that have oxidation potentials of +0.60 V and +0.89 V vs. Ag/AgCl, respectively. A chemical oxidant used to make the tetrahydrofuran product would over-oxidize the amine and, inversely, a chemical oxidant that would give the desired oxidized amine would not be able to oxidize conversion to tetrahydrofuran product. [26-27] The electrochemical oxidations shown had no such difficulty.

The ability for an electrochemical reaction to selectively oxidize functional groups in a truly general manner stems from the very nature of the electron-transfer itself. To understand this, let's start by pointing out that there are two types of electrochemical reactions: constant voltage and constant current. As seen in Figure 3 constant voltage reactions work by setting the working potential of the reaction relative to a reference electrode. The potential remains there throughout the course of the reaction. If a reaction has two substrates, A and B, where substrate A has an oxidation potential below or at the working potential set for the electrode and B has an oxidation potential above the working potential, then only substrate A will be oxidized. As the reaction runs out of substrate A, the current will fall of exponentially. Hence, a reaction run in this fashion is highly selective but has difficulty going to completion.

A constant current electrolysis takes the opposite approach. In a constant current electrolysis, the current pushed through the reaction is held constant and the working potential at the electrodes is allowed to float. Accordingly, the working potential at the electrode automatically adjusts to whatever substrates are in reaction. In a similar reaction to that mentioned in the previous paragraph, when the current is turned on, the working potential at the anode will climb until it matches that of substrate A. The working potential at the anode will then remain at that value until there is not enough of substrate remaining in solution to satisfy the current that needs to be passed through the cell. At that point, the working potential will begin to climb again until it matches that of substrate B. In the end, the constant current reaction is very selective until one runs out of the initial substrate. By keeping the current density for the reaction low, most of substrate A can be

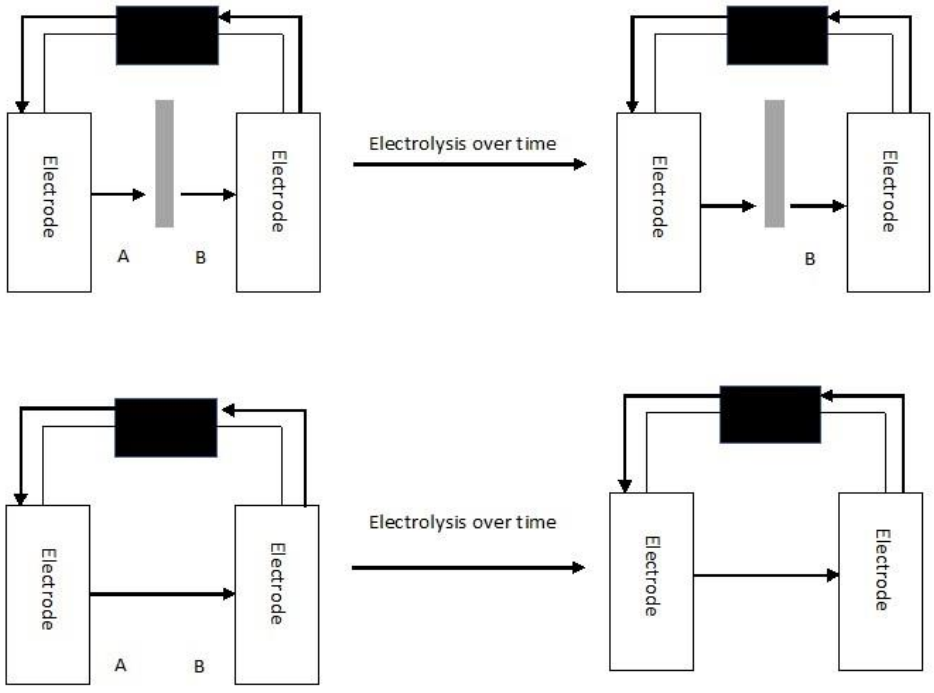

Figure 3. Constant Voltage (top) versus Constant Current (bottom). Controlling the voltage of the reaction is a method of controlling the selectivity of the reaction by oxidation potential. However, if the difference in oxidation potentials of two substrates is wide enough, then selectivity on oxidation potential can be accomplished with a constant current reaction as well.

consumed before the selectivity is lost. However, as in the constant potential reaction the transformation can be difficult to push all of the way to completion, especially if the potential needed to oxidize A and the potential needed to oxidize B are not very different.

Of the two methods, the constant current reaction is operationally easier. It does not require the use of a reference electrode, and hence any power supply from batteries to photovoltaics can be used to drive the reactions as will be seen in figure 6. Of course, commercial power supplies offer a more consistent, reproducible method for accomplishing the reactions.[28]

The other advantage of a constant current electrolysis is that it will adjust to any substrate in solution without any need to set a potential for the reactions. For example, each of the radical cations shown in Figure 4 has been generated under nearly identical conditions with a constant current electrolysis. The ability to generate all three radical cations using similar reaction conditions allowed for comparisons between their reactivity. For that reason, they are included in the figure from left to right based on the polarity of the radical cations. They were organized that way because the polarity of the reactive intermediate has been shown to control the chemoselectivity of the radical cation. Empirical evidence has shown that less polar radical cations like the ketene dithioacetal favor heteroatom trapping and the more polar radical cations like the ketene N,O-

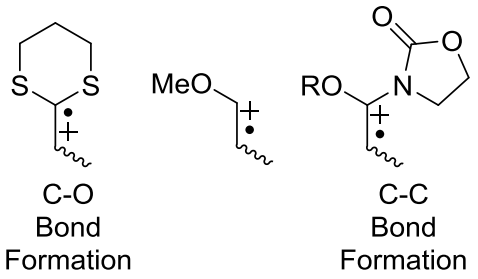

Figure 4. Polarity effects on radical cations. Empirical data has shown that polar radical cations favor carbon-carbon trapping and non-polar radical cations favor heteroatom coupling (C-N or C-O, etc.)

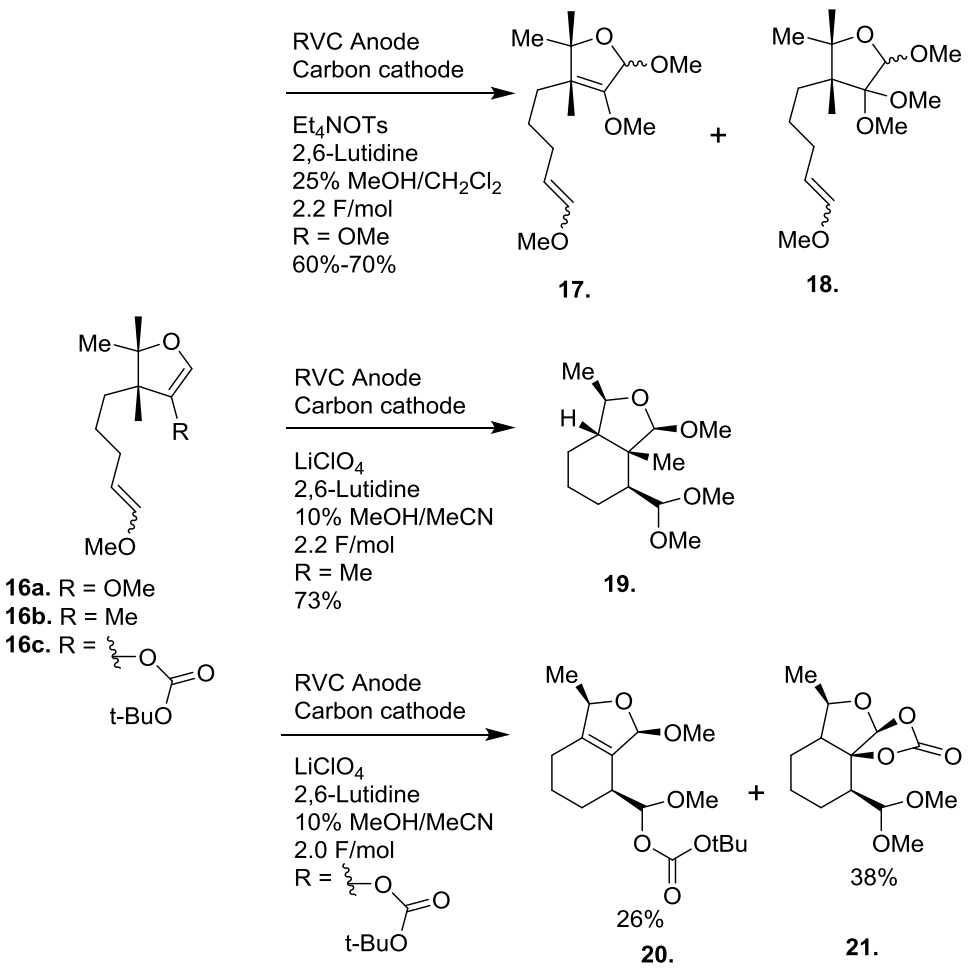

Figure 5. Exploring the effects of electron density vs. polarity on radical cation cyclizations. Initial attempts (top) at cyclization with the electron rich ene-diol were unsuccessful. A second attempt (middle) at cyclization using a simple enol ether was successful which suggests that the polarity of a radical cation affects reactivity more than the electron density. A third successful cyclization (bottom) with an electron neutral ester supports that hypothesis.

acetal favor carbon-carbon trapping. This model was directly tested with the ene-diol ether type substrates shown in Figure 5. [29] The non-polar ene-diol ether radical cation resulting from the oxidation of **16a** led to only elimination or solvent trapping products **17** and **18** and no carbon carbon bond formation. When this group was replaced with a simple enol ether **16b** the substrate cyclized well leading to a new carbon-carbon bond in product **19**. Another substrate was synthesized with an ester substituent **16c** replacing the second ether group. The ester in this situation is an electron neutral substituent. This led to a more

polar radical cation and led to a cyclization reaction products **20** and **21**. (Figure 5). These results were interesting because they showed that the generation of the carbon-carbon bond was not dependent upon the electron-richness of the radical cation but only the polarity.

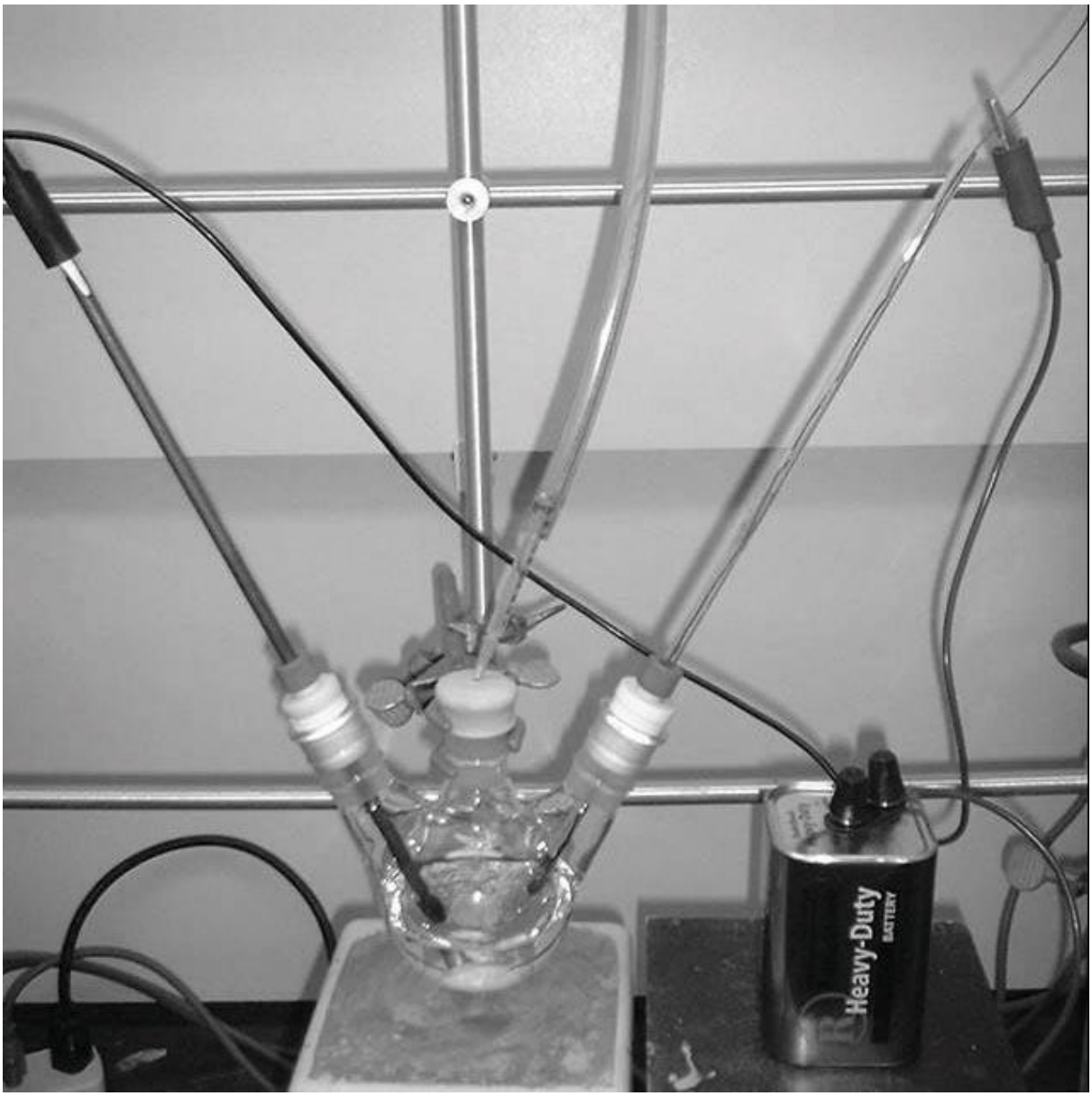

Figure 6. General Electrochemical reaction set-up. Electrical source is a heavy duty 6 volt battery. This is connected to 2 electrodes which can be made of various metals or reticulated vitreous carbon (RVC). In this set-up, A combo platinum cathode and RVC electrode are used to run a current through the chemical portion of the reaction. A combination of electrochemical substrate, electrolyte, and solvent system make up this part.

The physical parameters of an electrolysis reaction can also play a significant role in determining product formation. Hence, a brief discussion of those parameters are warranted before examining the thesis that follows. See figure 6 for representation of the physical components of an electrolysis. Key to the reactions are the electrodes used, the electrolyte employed, the presence of a base, and the solvent needed to complete the reactions proposed.

The Waldvgogel group has been exploring the role electrode material can play in defining the nature of the product obtained from an electrolysis. For example, they have developed boron doped diamond electrodes for conducting preparative electrolysis and have demonstrated their utility for a series of oxidation and reduction reactions.[31] For our part, we have also seen the role electrode materials can play. For example, many of the early anodic olefin coupling reactions were conducted on Pt-anodes. However, when we eventually moved to cyclizations that employed allylsilane groups as the trapping group for the radical cations being generated, it was determined that the reactions would benefit from a much faster second oxidation step. With this in mind, we shifted to carbon anodes, and in particular high surface area reticulated vitreous carbon anodes, that we know to aid two electron processes. This switch in electrode material greatly improved a number of the reactions we were studying. It is also important to note that the solvent used for the reaction can play a big role in the outcome of a reactions. For example, the Waldvogel group has made heavy usage of hexafluoroisopropane as a solvent for electrochemical reactions. [32] The solvent has shown excellent compatibility with the formation and generation of radical cation intermediates.

Once again, our group has also played with solvent conditions and examined their role in determining the nature of the products generated in a reaction. We have found that solvent system can play a small role in the helping optimize reactions. For example, reaction yield can be improved by adjusting the polarity of the solvent as seen in Figure 7. Reducing the concentration of methanol with a co-solvent such as tetrahydrofuran improved the yield of the reaction involving the transformation of **22** to **23**. Mechanistically, the decreased concentration of methanol slows methanol trapping of the radical cation which provides more time for the cyclization. [32-33] Contrast that to an example where switching the solvent system to methanol neat drastically improved the transformation of **24** to **25**. Here the methanol can more easily reach the anode surface. These examples show that solvent can have a weak effect on the reaction, but the effect should be considered when attempting optimization. The solvent system of a reaction typically works synergistically with the electrolyte.

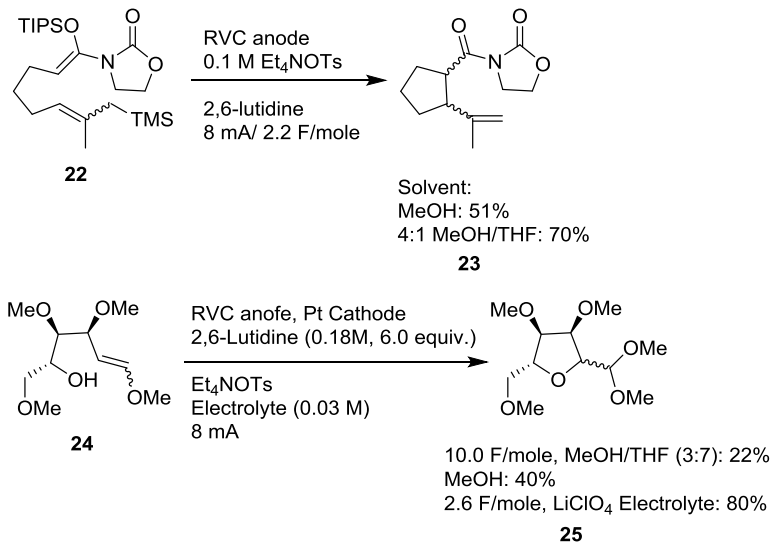

Figure 7. Solvent effects taken to optimize reactions. The top reaction shows an increased yield from introducing polar character to the solvent system. Electrochemical reactions can also be improved from changing to opposite conditions where the solvent system is less polar.

Similar to our optimizations with solvent, electrolyte and electrolyte concentration changes can lead to significant differences in reaction outcome. Once again, and example from our labs provides a nice backdrop for illustrating this effect (Figure 8). In this case, the use of a "greasier"

electrolyte in high concentration dramatically improved a reaction. For an example see: "Anodic Coupling Reactions: Exploring the Generality of Curtin-Hammett Controlled Reactions. [34] To provide a basis for the explanation of the observation, it is helpful to think about the role electrolyte plays in the reactions. In an electrolysis, the electrolyte serves two purposes; first to allow current to pass through the cell and minimize the resistance of the cell to that current and second to create an electrolyte double layer that surrounds the electrode surface. In terms of the first effect, remember that an electrochemical reaction is always the result of two half reactions, the oxidation at the anode and the reduction at the cathode. At each of the electrode, the electron transfer introduced ions into the solution, cations at the anode and anions at the cathode. As one might imagine, as the reaction proceeds the reaction medium would become more and more resistant to introducing more cations into the solution by the anode and more anions to the solution by the cathode. To counters this effect, the electrolyte provides counterions for the ions being generated at the electrodes. This neutralizes the charge buildup at the electrodes and minimizes the resistance to the current flowing through the cell.

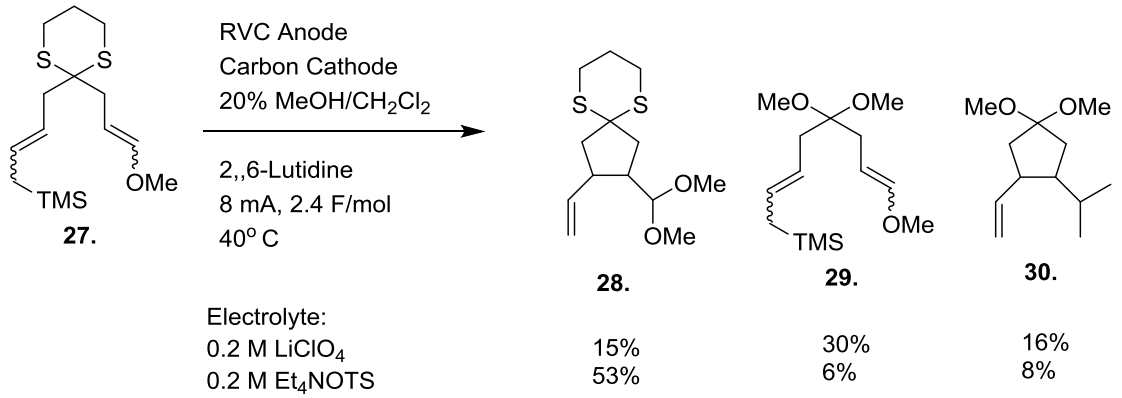

Figure 8. Electrolyte can change the outcome of the reaction. Lithium perchlorate (top) when used with an enol ether radical cation shows poor to moderate yields, 31% of desired cyclized product and it's hydrolyzed byproduct and 30% of the uncyclized product.. By changing to tetra ethyl ammonium tosylate, the reaction was improved to yields of 53% cyclized product, and small amount of hydrolyzed byproduct and uncyclized product.

A natural consequence of doing this is the double layer that forms at the electrodes. Simply put a positively charged anode attracts a coating of negative ions in the electrolyte solution. The new negative surface then attracts a layer of positive ions. These two layers make up the double layer at the surface of the anode. An equal, but opposite, double layer forms on the cathode. This double layer serves to protect reactive intermediates generated at the electrodes by providing an ordered solution that cuts down on the diffusion of species close to the electrode. Hence, a radical cation generated in the double layer is protected from dimerization (slow diffusion to find another radical cation) and solvent trapping (reduced mobility of the solvent in the double layer). In addition, the nature of the double layer can selectively exclude some solvents from the surface of the electrode. For example, a greasy electrolyte can exclude polar solvents like methanol from the anode surface. This is the case for the reaction illustrated in Figure. 8. In this case, a higher concentration of tetraethyl ammonium tosylate electrolyte excludes methanol from the surface of the anode. In the reaction highlighted, two processes competed with each other: one a desired anodic cyclization reaction leading to product **28** and second methanol trapping of a sulfur based radical cation leading to cleavage of the cyclic dithioketal and products **29** and **30**. By excluding methanol from the surface of the anode, the undesired methanol trapping reaction was slowed (relative to a reaction using a more polar lithium perchlorate electrolyte) buying more time for the desired cyclization.

It is important to note the base added to this and almost every anodic olefin coupling reaction. Electrochemical reactions remain at the pH they are initially set at because for every proton generated at an anode and equivalent of base is generated at the cathode. For the olefin coupling reactions shown above, the cathodic reaction involves the reduction of two equivalents of methanol to from hydrogen gas and two equivalents of methoxide. However, a net neutral

reaction does not mean the environment surrounding the anode does not become acidic. This can be problematic for the oxidation of an acid sensitive substrate at the anode. Hence, a base is added as a proton shuttle to neutralize the acid at the anode. The main requirement for this base is that it does not interfere with the electrolysis. To that end, sterically bulky bases like 2,6-lutidine are ideal.

This knowledge of electrochemical reactions led to the study of a number of olefin coupling reactions and the assembly of an array of empirical results. However, little was done to quantify those empirical results so that they could be effectively disseminated to the community.

For this reason, when I joined the group an effort to understand the relative reactivity of groups for a radical cation intermediate was underway. The chemistry started with a look at reactions that employed sulfonamide trapping groups, and it was focused on the possibility for the reactions proceeding through a Curtin-Hammett type mechanism.[34] The question was being probed with a competition study that examined the efficiency of different groups and their ability to trap a ketene dithioacetal derived radical cation (Figure 9). In these reactions, there is a rate constant k_1 that corresponds to the cyclization step and a rate constant k_2 that corresponds with a second oxidation of the newly cyclized radical cation. Before this study, we had mainly concerned ourselves with the cyclization step

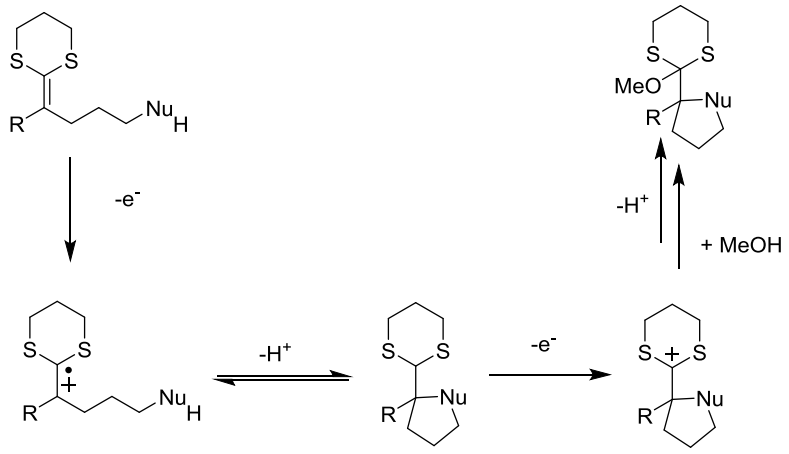

Figure 9. Proposed Mechanism for anodic oxidation cyclizations. Initial oxidation of the substrate leads to a radical cation. Cyclization occurs between the radical cation. Here a deprotonation during the cyclization. This trapping event is followed by a second oxidation to give a cation. Solvent then traps the cation to give cyclized product.

and had often ignored the second oxidation step. Certainly, we knew that the second oxidation could alter the kinetic vs. thermodynamic control of the reaction, but little concern for the effect of the reaction on the overall yield of the process was expressed. As we shall see below, this was a mistake.

The work in this thesis examines carbon-carbon bond forming reactions and the relative reactivity of different trapping groups for the dithioketene acetal radical cations. The work described in Chapter 2 reviews a series of competition studies that defined the relative reactivities of enol ether and allylsilane trapping groups in comparison to the alcohol and sulfonamide trapping groups studies previously. The chemistry described in Chapter 3 looks at a combination of the electrochemical studies with the use of one electron transfer based photocatalytic systems. The goal was to show that the electrochemical reactions described in Chapter 2 could be used to make predictions about the related photoelectron transfer reactions. What we got instead was a surprise that demonstrated how the use of electrochemical and photoelectron transfer reactions in combination can shed new light into the mechanism of oxidative cyclization reactions.

[1] Little, R.D.; Moeller, K. D.; Organic Electochemistry as a Tool for Synthesis: Umpolung Reactions, Reactive Intermediates, and the Design of New Synthetic Methods. *The Electrochemical Society – Interface* **2002**, *11*, 36

[2] Tang, F.; Chen, C.; Moeller, K.D.; Electrochemistry and Umpolung Reactions: New Tools for Solving Synthetic Challenges of Structure and Location. *Synthesis* **2007**, 3411.

[3] Miller, A. K.; Hughes, C. C.; Kennedy-Smith, J. J.; Gradl, S. N.; Trauner, D.; Total synthesis of (−)-heptemerone B and (−)-guanacastepene E. *J. Am. Chem. Soc.* **2006**, *128*, 17057.

[4] Ding, H.; DeRoy, P. L.; Perreault, C.; Larivee, A.; Siddiqui, A.; Caldwell, C. G.; Harran, S.; Harran, P. G.; Electrolytic macro- cyclizations: Scalable synthesis of a diazonamide-based drug development candidate. *Angew. Chem., Int. Ed.* **2015**, *54*, 4818.

[5] Badalyan, A.; Stahl, S. S.; Cooperative Electrocatalytic Alcohol Oxidation with Electron-Proton-Transfer Mediators. *Nature* **2016**, *535*, 406.

[6] Rafiee, M.; Miles, K. C.; Stahl, S. S.; Electrocatalytic alcohol oxidation with TEMPO and bicyclic nitroxyl derivatives: Driving force trumps steric effects. *J. Am. Chem. Soc.* **2015**, *137*, 14751.

[7] Wheeldon, I.; Minteer, S.D.; Banta, S.; Barton, C.; Atanassov, P.; Sigman, M.; Substrate channeling as an approach to cascade reactions. *Nature Chemistry* **2016**, *8*, 299.

[8] Hickey, D.P.; Schiedler, D.; Matanovic, I.; Doan, P.; Atanassov, P.; Minteer S.D.; Sigman, M.; Predicting Electrocatalytic Properties: Modeling Structure-Activity Relationships of Nitroxyl Radicals. *J. Am. Chem. Soc.* **2015**, *137*, 16179.

[9] Sevov, C. S.; Hickey, D. P.; Cook, M. E.; Robinson, S. G.; Barnett, S.; Minteer, S. D.; Sigman, M. S.; Sanford, M. S.; Physical Organic Approach to Persistent, Cyclable, Low-Potential Electrolytes for Flow Battery Applications. *J. Am. Chem. Soc*. **2017**, *139*, 2924.

[10] Kawamata, Y.; Yan, M.; Liu, Z.; Bao, D-H.; Chen, J.; Starr, J.T.; Baran, P.S.; Scalable, Electrochemical Oxidation of Unactivated C-H Bonds**.** *J. Am. Chem. Soc.* **2017**, *139*, 7448.

[11] Horn, E. J.; Rosen, B. R.; Chen, Y.; Tang, J.; Chen, K.; Eastgate, M. D.; Baran, P. S.; Scalable and sustainable electrochemical allylic C− H oxidation. *Nature* **2016**, *533*, 77.

[12] Rosen, B. R.; Werner, E. W.; O'Brien, A. G.; Baran, P. S.; Total synthesis of dixiamycin B by electrochemical oxidation. *J. Am. Chem. Soc.* **2014**, *136*, 5571.

[13] O'Brien, A. G.; Maruyama, A.; Inokuma, Y.; Fujita, M.; Baran, P. S.; Blackmond, D. G.; Radical C−H functionalization of heteroarenes under electrochemical control. *Angew. Chem., Int. Ed.* **2014**, *53*, 11868.

[14] Zhao, H.-B.; Liu, Z.-J.; Song, J.; Xu, H.-C.; Reagent-Free C–H/N–H Cross-Coupling: Regioselective Synthesis of *N*-Heteroaromatics from Biaryl Aldehydes and NH_3**.** *Angew. Chem. Int. Ed.* **2017**, *56*, 12732.

[15] Hou, Z.-W.; Mao, Z.-Y.; Song, J.; Xu, H.-C.; Electrochemical Synthesis of Polycyclic N-Heteroaromatics through Cascade Radical Cyclization of Diynes. *ACS Catal.* **2017**, *7*, 5810.

[16] Wu, Z.-J.; Xu, H.-C.; Synthesis of C3-Fluorinated Oxindoles Through Reagent-Free Cross Dehydrogenative-Coupling**.** *Angew. Chem. Int. Ed.* **2017**, *56*, 4734.

[17] Xiong, P., Xu, H.-H. and Xu, H.-C. Metal- and Reagent-Free Intramolecular Oxidative Amination of Tri- and Tetrasubstituted Alkenes. *J. Am. Chem. Soc.* **2017**, *139*, 2956.

[18] Zhao, H.-B.; Hou, Z.-W; Liu, Z.-J.; Zhou, Z.-F.; Song, J.; Xu, H.-C.; Amidinyl Radical Formation by Anodic N–H Bond Cleavage and Its Application in Aromatic C–H Bond Functionalization. *Angew. Chem. Int. Ed*. **2017**, *56*, 587.

[19] Fu, N.; Sauer, G. S.; Saha, A.; Loo, A; Lin, S.; Metal-catalyzed electrochemical diazidation of alkenes. *Science* **2017**, *357*, 575.

[20] Moeller, K.D.; Intramolecular Carbon-Carbon Bond Forming Reactions at the Anode. Moeller, K. D. *Topics in Current Chemistry* **1997**, *185*, 49.

[21] Moeller, K.D.; Synthetic Applications of Anodic Electrochemistry. *Tetrahedron* **2000**, *56*, 9527.

[22] Sperry, J. B.; Wright, D. L.; The Application of Cathodic Reductions and Anodic Oxidations in the Synthesis of Complex Molecules. *Chem. Soc. Rev.* **2006**, *35*, 605.

[23] Yoshida, J.; Kataoka, K.; Horcajada, R.; Nagaki, A.; Modern Strategies in Electroorganic Synthesis. *Chem. Rev.* **2008**, *108*, 2265.

[24] Wu, H.; Moeller, K.D.; Anodic coupling reactions: a sequential cyclization route to the arteannuin ring skeleton. *Org. Lett.* **2007**, *9*, 4599.

[25] Miller, L. L.; Stermitz, F. R.; Flack, J. R.; Electrooxidative cyclization of 1-benzyltetrahydroisoquinolines. Novel nonphenol coupling reaction. *J. Am. Chem. Soc.* **1973**, *95*, 2651.

[26] Liu, B.; Duan, S.; Sutterer, A.C.; Moeller, K.D. *J. Am. Chem. Soc.* **2002,** *124*, 10101,

[27] Hai-Chao Xu and Kevin D. Moeller *Angew. Chem. Int. Ed. Eng.* **2010**, *49*. 8004.

[28] IKA. (2019) ElectraSyn 2.0

[29] Tang, F.; Moeller, K.D.; Anodic oxidations and polarity: exploring the chemistry of olefinic radical cations. *Tetrahedron* **2009,** *65*, 10863.

[30] Lips, S.; Waldvogel, S.R.; Use of Boron-Doped Diamond Electrodes in Electro-Organic Synthesis. *Chem Electro Chem* **2019,** *6*, 1649.

[31] Schulz, L.; Waldvogel, S.R.; Solvent Control in Electro-Organic Synthesis. *Synlett* **2019**, *30*, 275.

[32] Huang, Y.; Moeller, K.D.; Anodic cyclization reactions: probing the chemistry of N,O-ketene acetal derived radical cations. *Tetrahedron* **2006**, *62*, 6536.

[33] Xu, G.; Moeller, K.D.; Anodic Coupling Reactions and the Synthesis of C-Glycosides. *Organic Letters* **2010,** *12*, 2590.

[34] Redden, A.; Moeller, K.D.; Anodic Coupling Reactions: Exploring the Generality of Curtin-Hammett Controlled Reactions. *Org. Lett.* **2011**, *13*, 1678.

Chapter 2: Competition Studies

Introduction:

Early work to quantify mechanistic aspects of the radical cation trapping reactions being explored by our group began with a series of competition studies completed by Drs. John Campbell

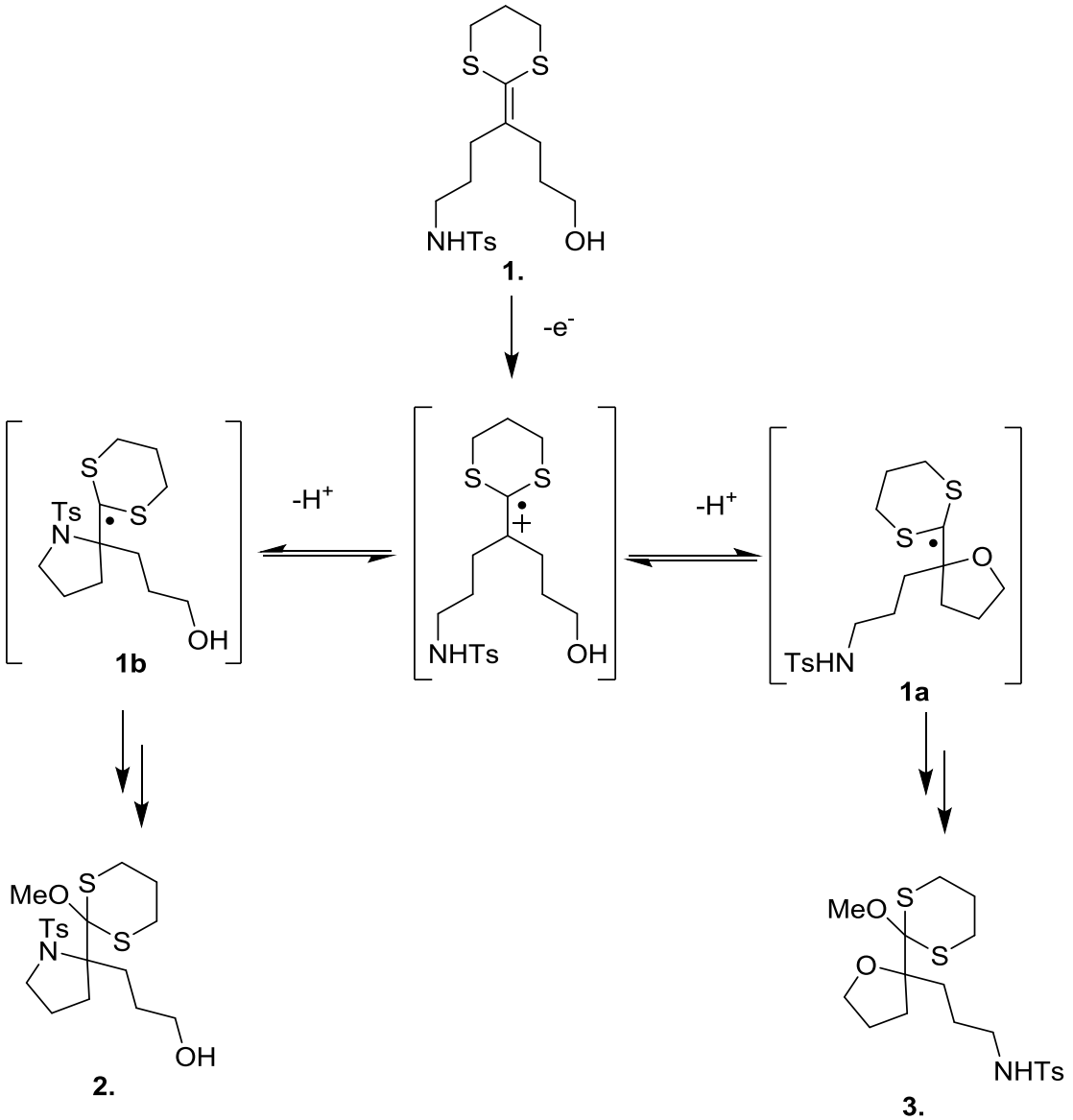

Figure 1. Proposed Pathways for the Competition Study Between Sulfonamide and Alcohol Trapping. Note how this figure does not show the follow up oxidation. Our initial assumption was that the reaction was controlled by the cyclization/radical cation trapping event.

and Haichao Xu[1-2]. While the original goal of the competition study was to examine the formation and trapping of a radical cation with a deprotonated sulfonamide, the reactions proved to be the first in a series of experiments that took a more general look at the trapping of dithioketene

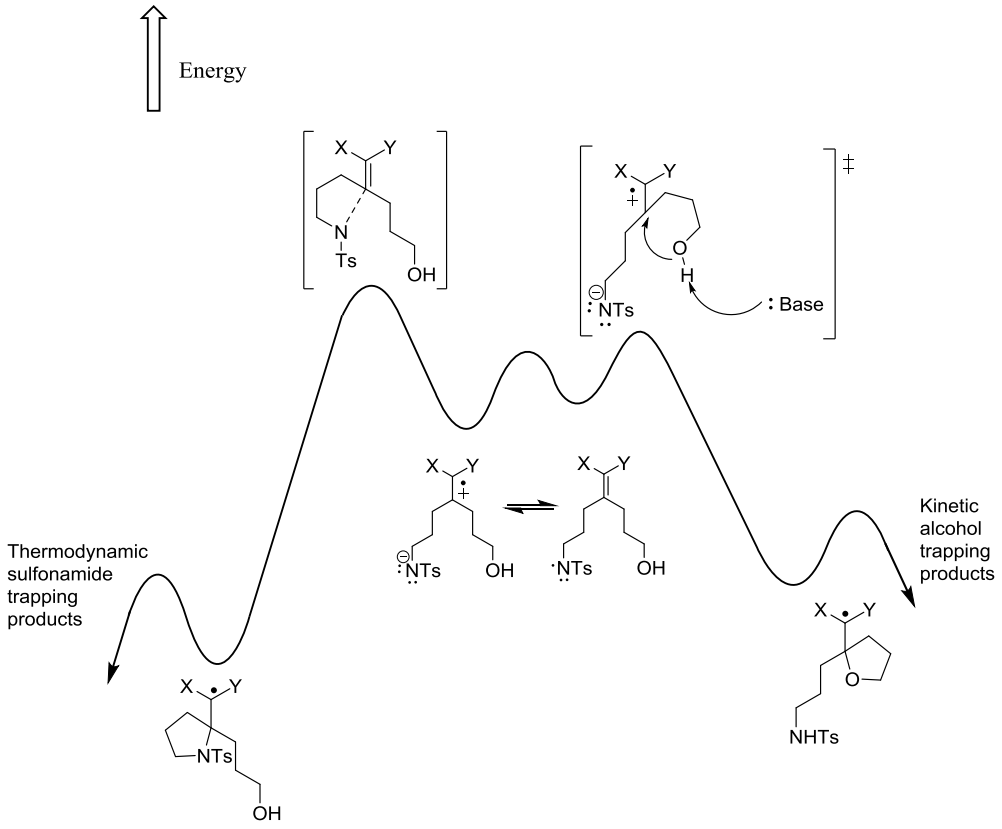

Figure 2. Energy Diagram for the Sulfonamide vs. Alcohol Competition Study. It was shown that alcohol trapping can be controlled via the conditions of the reaction. Kinetic conditions (high current, low temperature) favored alcohol trapping while thermodynamic conditions (low current, room to high temperature) favored sulfonamide trapping.

acetal derived radical cations with various groups. The initial case (Figure 1, Substrate **1**) compared the trapping of the radical cation with both nitrogen and oxygen based nucleophiles. A logical extension of this work was to utilize a similar competition study approach to gain a better understanding of the synthetically useful carbon-carbon bond forming reactions utilized in many synthetic efforts. With this in mind, it is important to take a more careful look at the initial competition studies and what was learned from them. For these studies, two trapping groups, a

sulfonamide and an alcohol, were tethered to an electron rich olefin that served as the site for generation of the radical cation being studied. The reactions showed that the nature of the trapping pathway could be controlled by changing the temperature and current density used for the reaction. If alcohol trapping pathway **1a** was desired, then a comparatively low temperature and high current density was used. These conditions led to formation of the kinetic product which proved to be the product derived from alcohol trapping of the radical cation. Higher temperatures and lower current (thermodynamic reaction conditions) allowed the reaction to proceed through the sulfonamide trapping pathway **1b** which gave the thermodynamic product. [1]

This difference can be summarized by an energy diagram (Figure 2).[1] This work initially examined the oxidation to form a N-based radical (the sulfonamide anion oxidizes at a potential lower than the ketene dithioacetal) followed by an intramolecular electron transfer to form the radical cation. The fact that both alcohol and sulfonamide trapping products could be observed provided clear evidence for the electron transfer. Computational studies were conducted by Dr. John Campbell in the group to determine potential energy barriers for the transformations resulting from the initial oxidation intermediates. [2] The lowest barrier from the initial radical cation was associated with trapping of the ketene dithioacetal derived radical cation by the oxygen nucleophile. Under kinetic conditions, the cyclization is not reversible and the reaction is trapped as the ether product. The key to conducting the reaction under kinetic conditions is slowing the reverse reaction by keeping the reaction cold and increasing the rate of the second oxidation reaction by increasing the current flow in the electrolysis.

When the reaction was run at lower current and warmer temperature, the alcohol based cyclization has time to reverse. The result is a chance for a competitive sulfonamide trapping reaction that either arises from trapping of the olefin radical cation by a sulfonamide anion or by a

cyclization between a N-based radical and the ketene dithioacetal. This leads to the most stable, thermodynamic product.

The ability to control the reversibility of alcohol trapping proved to be a useful tool for probing the reactivity of additional trapping groups for the radical cation. Since we know the conditions that lead to kinetic trapping of the radical cation by the alcohol, we can determine if a second nucleophile is faster or slower than the alcohol trapping of the radical cation (which would not reopen). In other words, the alcohol serves as a baseline reaction. Using this approach, a qualitative measurement of the relative kinetics associated with different carbon-based trapping groups can be made. With this in mind, the structure of the original alcohol/sulfonamide was changed to include either an enol ether **4** or allyl silane **5** trapping group as the second nucleophile (Figure 3).

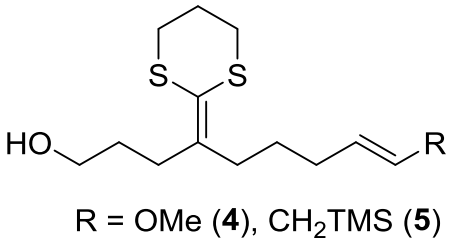

Figure 3. Electrolysis substrate designed to compare carbon-based trapping groups to alcohol which serves as a qualitative handle for radical cation trapping.

Results and Discussion

The synthetic route towards the enol ether substrate started with generating an alkyl lithium from a protected bromo-alcohol chain. On generation of the anion, the solution was added to the valerolactone to give the ring-opened ketone in modest yield. A swern oxidation converted the deprotected alcohol to aldehyde with little trouble in generous yield. This was followed by a wittig reaction to replace the aldehyde with the enol ether. Dr. John Campbell noted that there is a small amount of ketone conversion if too much phosphine is used. A standard TBAF deprotection affords the alcohol. A dithioketene acetal conversion and deprotection were attempted but the best method

is to separate the two steps into individual reactions. The synthesis of the enol ether substrate was carried out primarily by Dr. Campbell.

An attempt to adapt the synthetic route of the enol substrate towards the allyl silane proved troublesome with the first step. In an unconventional Grignard reaction, the side chain added to butyrolactone to give the alcohol, but the synthesis was eventually switched to generating a weinreb amide from a dimethyl hydroxy amine salt. Washing the salt with benzene to remove and moisture substantially helps the reaction during the work-up step. Treating the reaction with saturated sodium potassium tartrate solution overnight further helps with improving the yield of this step. Yields are excellent even on multi gram scale. Before addition of the second side chain, the alcohol requires protection using standard TBS protection procedures. Work up of this reaction with hexane helped crash imidazole out of solution to purify product. The second side chain was added via a Grignard procedure. 5-Bromo-1-pentene was treated with Mg metal to give a Grignard reagent that typically ranged between 1.2-1.5 M in concentration. This Grignard was added to the weinreb amide to accomplish the conversion to the ketone in yields above that of the unconventional method. This reaction was not optimized, but recent efforts by visiting student Alex to optimize a different version give hope that the yield can be improved. A standard Grubb's metathesis installed the allyl silane group at the end of the second chain. To achieve the dithioketene acetal, the ketone was treated with 2-trimethylsilyl-1,3-dithiane via Peterson olefination conditions. Finally, a TBAF deprotection affords the alcohol in good yield and purity.

With the substrates in hand, the anodic oxidation was conducted to examine the reactivity of the allylsilane and enol ether groups relative to the alcohol trapping group (Figure 4). Reaction

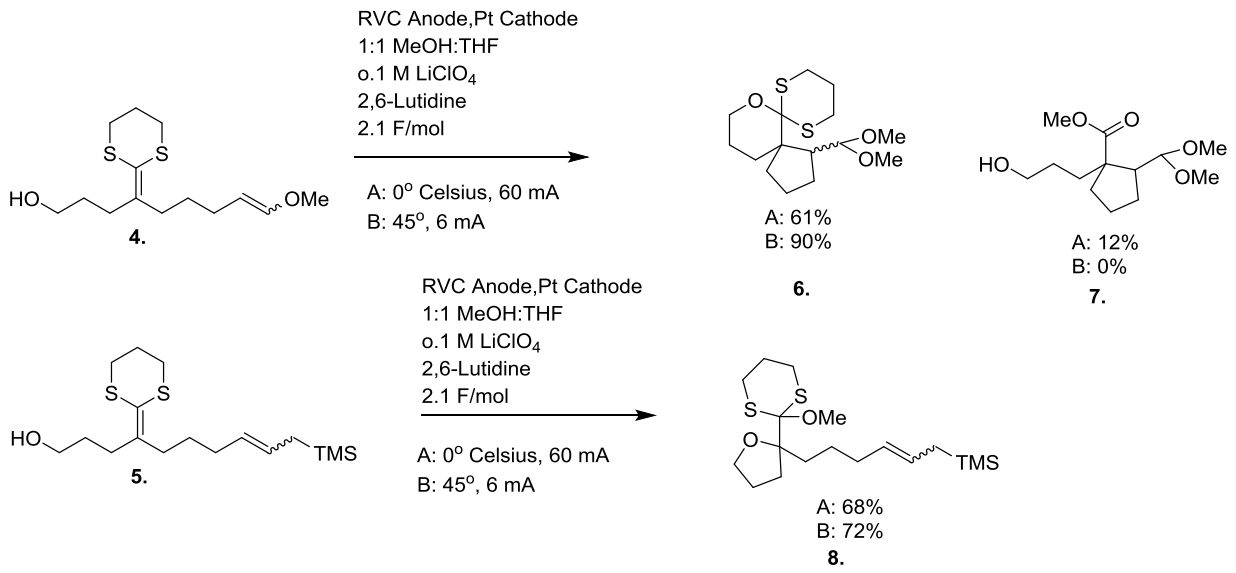

Figure 4. Electrolysis of enol ether and allyl silane reactions. The products from the enol ether competition were a spiro[2.5] decane system (**6**) and simpler 5-ring product with an acetal group derived from the original enol ether and an ester group derived from hydrolyzation of the dithiane group (**7**). Product from the allyl silane competition was solely cyclized ether (**8**).

conditions for the electrolysis involved 3 important factors: Solvent system that allows for methanol trapping, a base to neutralize acid generated at the cathode surface, and electrolyte to both facilitate current and stabilize the radical cation generated. The cosolvent used for the electrolysis was dichloromethane although tetrahydrofuran and acetonitrile have been used. We settled on 2,6-lutidine for base as it was used in previous reactions. The electrolyte, $LiClO_4$, and concentration were also based on previous reaction conditions.

The products obtained from the electrolysis indicated that under both kinetic and thermodynamic conditions, the enol ether trapping product is favored when in competition to the

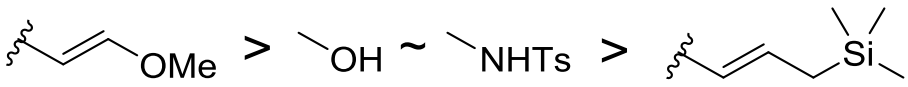

Figure 5. Heteroatom and carbon-based trapping groups ranked by reactivity.

alcohol. In contrast, the alcohol trapping product is favored under both thermodynamic and kinetic conditions when in competition to the allyl silane.

It is important to note that both the enol ether based and the allylsilane based reactions did not lead to a mixture of products. The olefinic trapping group either completely dominated the alcohol nucleophile or was completely dominated by the alcohol nucleophile. These results did allow us to provide a qualitative ranking for the relative ranking of the carbon-based trapping groups (Figure 5). [3]

While the competition experiment gave us a fast picture of the relative reactivity of a radical cation trapping group, we began to wonder if things were as simple as they appeared. Because trapping of the radical cation by an alcohol turned out to be reversible, we wondered if that situation might also be governing the chemistry observed with the less reactive allylsilane trapping group. Was the allyl silane trapping reaction really slow or was it fast but reversible so

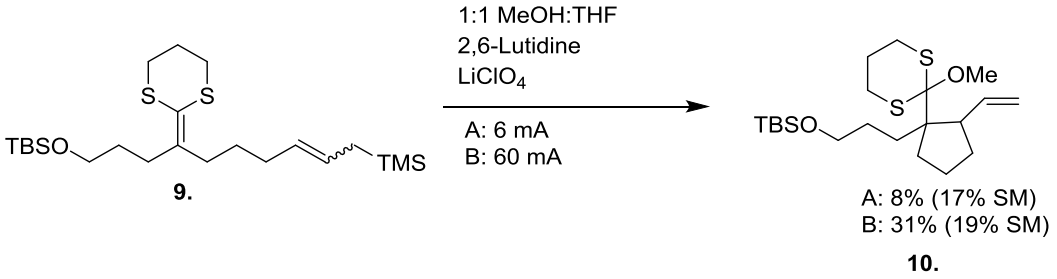

Figure 6. Electrolysis of allylsilane with protected alcohol. Contrast this to the results from Figure 4, Substate **8**.

that it led to a product derived from a thermodynamic reaction. With this is mind, a new competition study was proposed that examined trapping of the ketene dithioacetal derived radical cation by an allylsilane in the presence of TBS-protected alcohol trapping. (Figure 6, Substrate **9**) In this example, the electrolysis of the allyl silane substrate successfully gave the cyclized material. The successful cyclization implied that the alcohol was outperforming the allyl silane from a preparative standpoint, but the result still did not provide any definitive insight into the kinetics of the allyl silane trapping reaction. It was still possible that the allylsilane cyclized quickly but that the reaction was reversible leading back to starting material. To probe the initial cyclization, a CV

study was devised that would look at the oxidative potential of a series of substrates: a parent substrate without any trapping group, an enol ether substrate, and an allyl silane substrate. Understanding the Nernst equation is key to understanding this study.

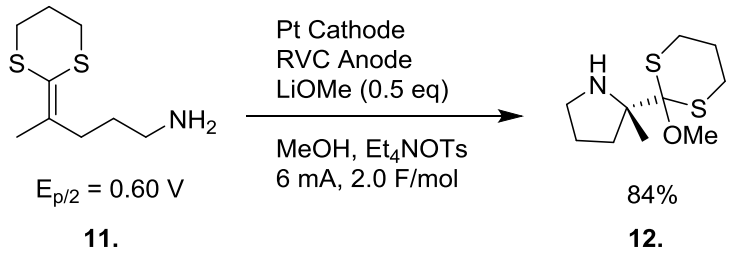

Figure 7. Amine Trapping. Note the oxidation potential of substrate **11**. When in the presence of an amine trapping group, the oxidation potential of the dithioketene acetal drops from the oxidation potential seen in Figure 9.

The Nernst equation is used to determine changes in oxidative potentials in non-standard electrochemical conditions. It accomplishes this by relating the potential measured for an electron transfer to the equilibrium established at the electrode between the starting material and the reactive intermediate generated (normally a radical cation or radical cation). If something in a

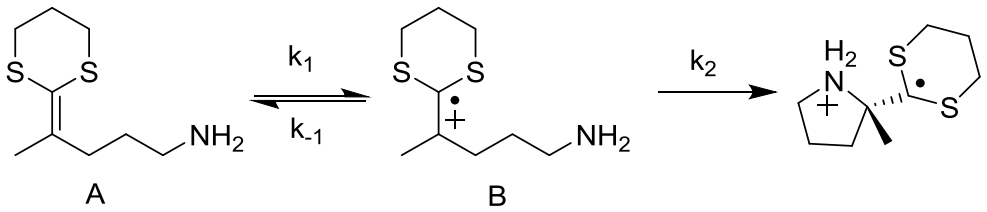

$$[B] = \frac{k_1[A]}{k_{-1}+k_2} \qquad \text{Eq. 1}$$

$$E = E_o - \left(\frac{RT}{nF}\right)\ln Q = E_o - \left(\frac{RT}{nF}\right)\ln\frac{[A]}{[B]} = E_o - \left(\frac{RT}{nF}\right)\ln\frac{k_{-1}+k_2}{k_1} \qquad \text{Eq. 2.}$$

Figure 8. Mechanism of Amine Trapping with derivation of Nernst equation at steady-state. When the steady-state assumption is taken into account, the Nernst equation can include the k values to show how the relative rates affect the speed of oxidation. Note how the larger the values of k_2 and k_{-1} become, the large the drop in oxidation potential becomes.

reaction changes the position of the equilibrium, then the potential measured is shifted. The "something" in the case of the anodic cyclizations being studied is the cyclization reaction itself.

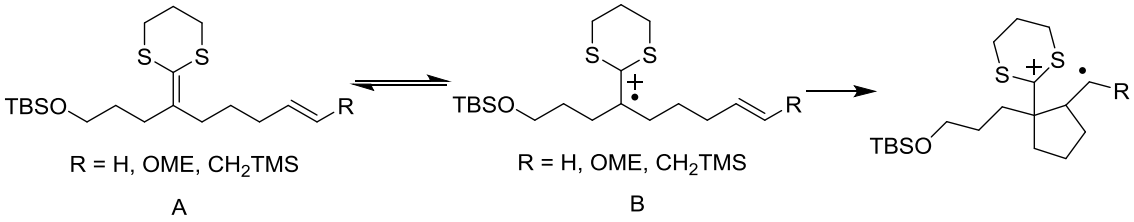

$$E = E_o - \left(\frac{RT}{nF}\right) \ln Q = E_o - \left(\frac{RT}{nF}\right) \ln \frac{A}{B} \qquad \text{Eq. 3}$$

Scheme 1. Qualitatively analyzing the speed of carbon-based trapping groups using CV. The Nernst equation is included to show how the speed of the cyclization affects the oxidation potential of the parent molecule at the electrode surface. A fast cyclization "pulls" the equilibrium between the parent substrate and radical cation towards radical cation formation and makes oxidation of the parent substrate easier.

In the past, we have shown that the cyclization reactions occur at or near the electrode surface and are fast enough to alter the position of the equilibrium at the electrode surface. The faster a reaction occurs, the more it drains the radical cation away from the anode and the more it lowers the potential measured for the transformation. For example, consider the reaction shown in Figure 7 and 8.[4] An isolated dithioketene acetal has an $E_{p/2}$ value of 1.06 V vs Ag/AgCl. When tethered to an amine nucleophile, the $E_{p/2}$ value of the substrates drops to 0.60 V vs Ag/AgCl. At 460 mV, this drop in potential can be explained with steady state kinetics and the Nernst equation.

With this in mind, let's examine the data obtained for the experiment outlined in Scheme 1 (Figures 7 and 8). The first thing that we noted was that with the protecting group on the alcohol, the reaction using the allylsilane trapping group did lead to product (Figure 5). However, like previous reactions utilizing the allylsilane trapping group, the reaction with the ketene dithioacetal based radical cation struggled to make the product in a decent yield.

As mentioned earlier, allylsilanes are not outstanding trapping groups for radical cation intermediates, especially when those radical cation intermediates are non-polar and favor heteroatom trapping reactions. The chemistry did provide a hint that the second oxidation reaction

in the mechanism might be problematic when the reaction was conducted under conditions that would optimize kinetic trapping of the radical cation. The colder temperature and higher oxidation rate (higher current) led to a significant improvement in the yield of the reaction, although it was still low from a synthetic standpoint.

With the results of the preparative electrolysis in place, the next step was to probe the cyclization using cyclic voltammetry. As mentioned above, three separate substrates were synthesized; a parent substrate with a simple olefin **13** that would allow us to assess the potential for the ketene dithioacetal group in the absence of a cyclization, a substrate containing the enol ether **14** known to trap exceptionally well, and a substrate with the allyl silane trapping group **15**. The protected alcohol sidechain was included on the substrates so that the results could be directly compared to the competition studies.

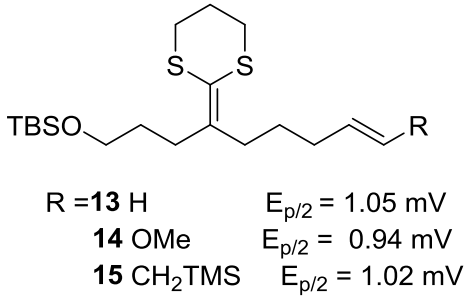

Figure 9. Results of the CV studies with carbon based trapping groups. Compare these to oxidation potential to previous results shown in Figures 4 (Products 1B and 1C) and Figure 6. Note how the enol ether shows a drastic drop in oxidation potential.

The parent substrate **13** gave an Ep/2 value of +1.05 V vs Ag/AgCl while the enol ether **14** substrate gave an Ep/2 value of +0.94 V vs. Ag/AgCl. The cyclization caused a drop in potential of 110 mV. In comparison to the enol ether, the allyl silane **15** gave an Ep/2 value of +1.02 V vs. Ag/AgCl for a much smaller 30 mV drop in potential relative to the parent ketene dithioacetal. While the drop in potential is smaller for the allylsilane trapping group and the indication is that the reaction is slower than the enol ether based cyclization, it is important to note that the reaction does show the drop in potential. This means that the cyclization is still fast enough to occur at or near the surface of the electrode. So slower than the enol ether did not mean slow.

Conclusions

This data helps to differentiate between two possible explanations for the inability of the allyl silane to cyclize efficiently with the dithio ketene acetal relative to the alcohol trapping group in the competition study. Either the competitive alcohol cyclization was very fast (k_4) and channeled the electrolysis toward the alcohol product ($k_4 >> k_1$) or the allyl silane is trapping the radical cation in a reversible fashion and the second oxidation reaction is slower than the cyclization to form the alcohol trapping product (the rate of k_{-1} plus k_3 is faster than k_2).

The CV study suggests that second scenario may be the correct one. Certainly, the allylsilane traps quickly. Hence, the poor yields for the preparative cyclizations shown in Figure 5 would suggest a slow second oxidation; a suggestion that was supported by the improved yield of product at higher current. This would be consistent with a fast, reversible trapping reaction with the allylsilane (a reaction that would still lower the effective concentration of the radical cation at the anode and shift the potential measured) followed by a slow second oxidation that failed to drive the competition study toward the product of C-C bond formation.

Of course, it is still possible in the competition study that the alcohol trapping is faster than the allylsilane trapping reaction and that the observations made by CV and in the chemistry highlighted in Figure 5 are mute points for a competitive reaction. However, at this point we had the information we needed. The alcohol trapping group wins the competition, and if one wants to improve the allylsilaned trapping reaction, then the second oxidation needs attention because the initial trapping reaction is fast enough to occur at the electrode surface. It is this later observation that is currently being pursued.

Experimental

The synthesis of enol ether substrate was carried out by Dr. John Campbell. This section is a summary of his synthetic route. For the full synthesis and characterization information, please see the supporting information associated with the referenced paper.

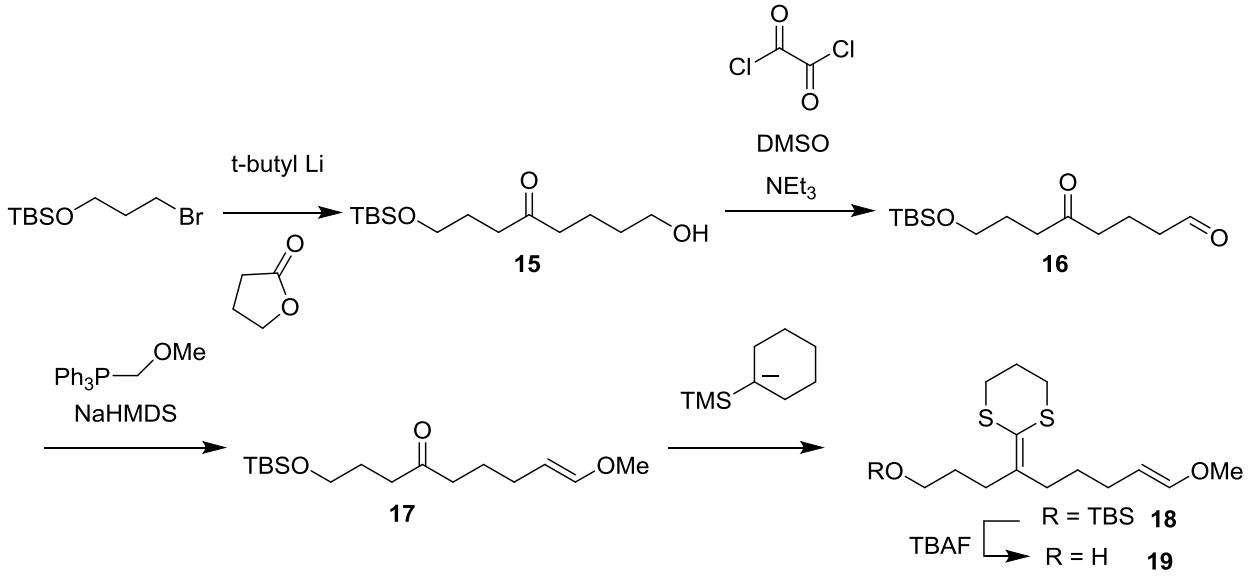

Synthesis of 19. Bromo-alcohol was dissolved in tetrahydrofuran and treated with 2 equivalents of t-butyl lithium. Solution was stirred for approximately 1 hour before being added to a solution with 1 equivalent of valerolactone in tetrahydrofuran. Reaction quenched with water. Bottom aqueous layer was separated from organic layer via separation funnel. Aqueous layer was washed with diethyl ether two more times and organic layers were collected. Product was concentrated down via rotary evaporator.

Free alcohol **15** was converted to aldehyde via swern oxidation. 2.1 equiv. of oxalyl chloride was dissolved in THF, cooled to -78^{o} Celsius, and treated with 1.1 amount of dimethyl sulfoxide. Alcohol was added to mixture. After stirring for 5 minutes, triethylamine was added to solution. White precipitate formed. After 30 minutes solution was diluted with diethyl ether and white

precipitate was filtered via filter paper. Product **16** was concentrated down via rotary evaporator. Product was purified with 5:1 mixture of Hexane and ethyl acetate. Yield was 56%.

1.1 equivalents of phosphine was suspended in tetrahydrofuran and treated with 1.05 NaHMDS. Solution was added to a second flask with aldehyde dissolved in tetrahydrofuran. Reaction diluted with diethyl ether and quenched with water. Top organic layer was extracted 3 times via separation funnel. Product **17** was concentrated down via rotary evaporator. Product was purified via column and 2:1 Hexane and dichloromethane.

1.1 equivalents of 2-trimethylsilyl-1,3-dithiane were dissolved in tetrahydrofuran and treated with 1.1 n-butyl lithium at -78^{o} Celsius. Anion was transferred over to a solution of ketone **17** dissolved in tetrahydrofuran. Reaction was diluted with diethyl ether and quenched with water. After being concentrated on rotary evaporator. Product was purified with 2:1 hexane in ethyl acetate.

After conversion to the dithioketene acetal, product **18** was dissolved in THF and treated with 5 equivalents of TBAF to give the alcohol **19** in 54% yield.

The following synthetic products represent my contributions to the project.

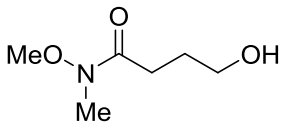

Synthesis of 20. In an open flask, N,O-dimethyl hyrdoxyl amine hydrochloride salt (1.510g, 15.4 mmol) was suspended The salt was suspended in tetrahydrofuran (25mL) and stirred in dry ice and acetone bath for 30 minutes. Diisobutyl aluminum hydride (1 eq., 1M in Hexane, 15.4mL) was added dropwise. After stirring for 1 hour, γ-valerolactone (0.9 eq., 1.20g, 1.06mL) was added dropwise to the container. Reaction ran for 3 hours at room temperature to give a clear yellow solution. The reaction was quenched with 3N HCl (4.6mL) solution to give a two phase solution.

Top layer was decanted off and bottom layer was washed with hexane twice. Collected layers were dried over magnesium sulfate and concentrated down using rotary evaporator. H^1 NMR showed a mixture of product and starting material (1: 0.3 Starting material and product) but was carried on to the next reaction.

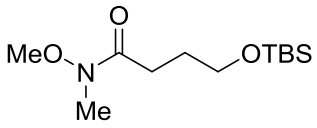

Synthesis of 21. Weinreb amide **S2-3** (0.563g, 3.83 mmol) was dissolved in tetrahydrofuran (10mL) under argon atmosphere. In a second flask with addition funnel, imidazole (2.5 equivalents, 0.652g) was suspended in THF (2mL) under argon atmosphere. The **S3-2** solution was added via syringe to the imidazole suspension. Tert-butylsilyl chloride (1.1 equivalents, 0.635g) was added to the addition funnel and dissolved with 3mL THF. The TBSCl solution was dripped into reaction flask over a period of 10 minutes. The reaction was monitored via TLC and upon completion, it was quenched with water. Layers were separated by decanting off the top layer. Bottom layer was washed with hexane 2 more times. Top layers were collected and dried over magnesium sulfate. Collected layers were concentrated on rotary evaporator. Material was purified by column chromatography using 1:1 mixture of ethyl acetate to hexane as the mobile phase. H^1NMR and C^{13}NMR matched previously reported data.

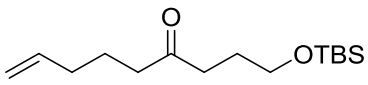

Synthesis of 24. In a flame dried flask flushed with argon, 5-bromo-1-pentence was dissolved in 15mL tetrahydrofuran. The mixture was sonicated to kickstarted the reaction which reacted

violently (vigorous bubbling, appearance of reflux) until completion. The concentration of the Grignard reagent was checked via menthol (0.2389g menthol, 1.53 mmol) titration with 1,10-phenanthroline in tetrahydrofuran. Concentration of the Grignard was determined to be approximately 1.53M 0in hexane. Once the Grignard was generated, amide **S3-3** was dissolved in THF(10mL) under argon. Solution was stirred for 30 minutes in ice bath. Typical concentrations ranged between 1.4-1.7 M of active Grignard reagent that are stable for storage in freezer. **S2-3** solution was treated with 2 equivalents of Grignard reagent. Reaction was monitored by TLC. Reaction quenched with water and diluted with diethyl ether. Acid was added slowly to a pH of 7-8. Mixture was stirred for 30 minutes. Top layer was decanted off and aqueous layer was washed 3 times with hexane. Collected layers were concentrated down via rotary evaporator.

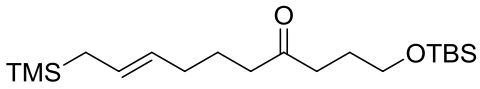

Synthesis of 25. 0.7887 (3.028mmol) grams of ketone **S2-4** were dissolved in dichloromethane (10mL) under argon. To this solution was added 4 equivalents of trimethyl allyl silane (1.384g, 1.925 mL). The mixture was sonicated for 1 minute before being fitted with a reflux condenser and placed on heating mantle. The reaction was refluxed (Setting 30%) and monitored by TLC. On completion, reaction was allowed to cool to room temperature and then flushed through a plug of silica gel with dichloromethane to remove catalyst. Filtrate was concentrated down using rotary evaporator and then carried onto the next reaction.

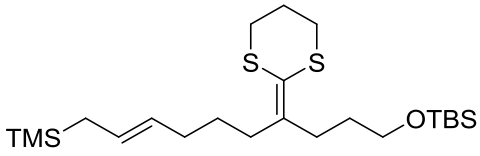

Synthesis of 26. The ketone with allylsilane in place (.187g, .525mmol) was dissolved in THF (10mL) under argon. In a separate flask, 1.2 equivalents of 2-trimethylsilyl-1,3-dithiane (0.121g,

0.120mL) was dissolved in THF and set to stir in dry ice/acetone bath. n-butyl Lithium (1.6 M in hexane, 0.393mL) was added slowly to dithiane solution. On complete addition, the solution was taken out of the dry ice/acetone bath, allowed to warm to room temperature, and stirred for 1 hour. The solution was then cooled down again using dry ice/acetone bath. The ketone solution previously prepared was added to this dithiane solution. The reaction was stirred overnight and before being quenched with water to give a two phase solution. The layers were separated by decanting off the top layer. The bottom layer was washed twice with hexane neat. Top layers were collected and dried over magnesium sulfate. Collected layers were concentrated down using rotary evaporator. Purification was accomplished using column chromatography and a 30:1 hexane:diethyl ether solution as the mobile phase.

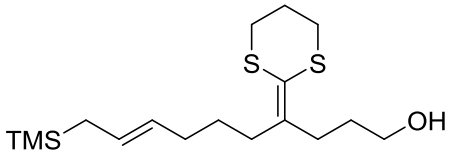

Synthesis of 27. Protected alcohol was dissolved in THF under argon. 1.1 equivalents of TBAF were added to stirring solution. Reaction monitored via TLC. On complete deprotection, reaction was quenched with water. Organic layer was decanted off. Aqueous layer was washed with three times with hexane. Organic layers were concentrated down using rotary evaporator. Purification was accomplished via LC with 20% diethyl ether in hexane mobile phase.

Electrolysis of 27. A three-necked round bottom flask was flame dried and flushed with argon. To this flask, electrolyte $LiClO_4$ (0.1M desried concentration, 10.6 mg), was dissolved in a 20% methanol in THF solvent system. To this mixture was added 2,6-lutidine base (1.1 eq.) via syringe. The electrolysis substrate **S2-7** was then added to give a 0.40 M concentration of the substrate in the electrolyte solution. Pt cathode and RVC anodes were connected to glassware via standard thermometer adaptors. A current was between 6 or 60 mA was passed through the cell. The

reaction showed visible bubbling at the cathode and anode and was monitored by TLC. On completion, product was concentrated down and washed with diethyl ether. Organic layers were collected and concentrated down using rotary evaprorator.

Reference List

[1] Campbell, J. 2013 ‘Anodic Olefin Coupling Reactions: Experimental and Computational Methods for Investigating the Intramolecular Cyclization Reactions of Electrooxidatively-Generated Radicals and Radical Cations’ PhD Thesis, Washington University in St. Louis, St. Louis.

[2] Campbell. J.M.; Xu, H.;Moeller, K.D.; Investigating the Reactivity of Radical Cations: Experimental and Computational Insights into the Reactions of Radical Cations with Alcohol and p-Toluene Sulfonamide Nucleophiles. *J. Am. Chem. Soc.* **2012**, *134*, 18338.

[3] Campbell, J.M.; Smith, J.A.; Gonzalez, L.; Moeller, K.D. Competition studies and the relative reactivity of enol ether and allylsilane coupling partners toward ketene dithioacetal derived radical cations. *Tetrahedron Letters,* **2015,** *56*, 3595.

[4] Xu, H-C.; Moeller, K.D.; Intramolecular Anodic Olefin Coupling Reactions: Use of the Reaction Rate to Control Substrate/Product Selectivity. *Angew. Chem. Int. Ed.* **2010,** *49*, 8004.

Chapter 3 Electrochemistry and Photochemistry

Introduction:

Photoelectron transfer reactions provide a useful means for accessing new methods that involve radical cation and radical anion reaction pathways. For example, oxidative photochemical reactions proceed through a radical cation mechanism that is facilitated by an excited state photocatalyst. An example is highlighted in Figure 1 in which a photoinduced electron transfer between Ruthenium-based photocatalyst and substrate modal **1** would trigger a radical cation based cyclization to product **2**. The reaction is complementary to the electrochemical based cyclizations reported earlier in that it involves the oxidation and then a back electron-transfer once the cyclic product is made. The reaction is thus redox neutral as opposed to the two electron

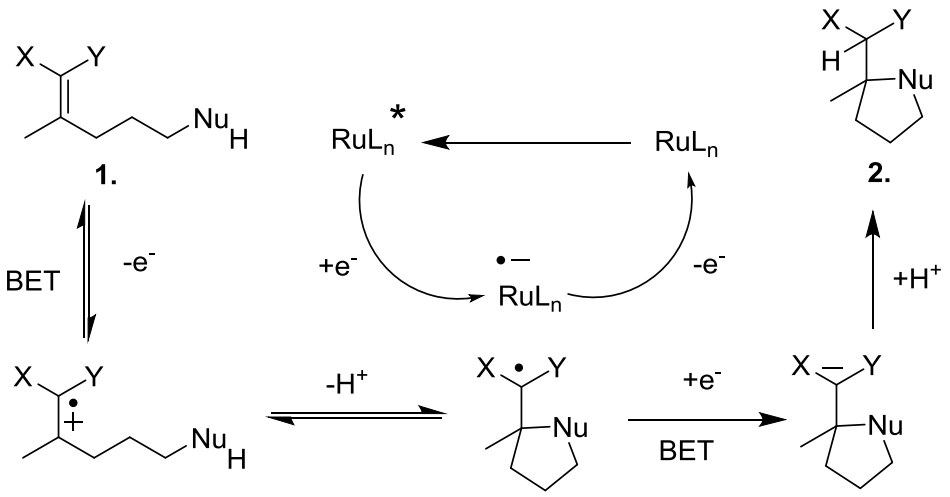

Figure 1. Proposed mechanism of a photochemically generated radical cation cyclization. Not immediately noticeable from the figure is that the two radical ions interact intimately during the reaction. They electron transfer occurs while the two radical ions are ionically bonded together.

oxidations described in the previous chapter, and the two processes can be thought of as being complementary. One can add a co-oxidant to the reactions to attempt a two electron process as well. With this in mind, Dr. Matt Graaf in our group began a study aimed at examining the

relationship between the electrochemical and photoelectron transfer derived methods. [1] Since both involved a central radical cation intermediate, we questioned if the method used for generating a radical cation had any impact on the overall course of the reaction. Put another way, could our knowledge of electrochemical reactions help predict photochemical outcomes?

With this in mind, the proposed mechanism for the photoelectron transfer reactions begins with a photocatalyst that is excited by 450nm wavelength light, typically LED range. The catalyst in its excited state then oxidizes the substrate to give a radical cation – radical anion pair. The radical cation goes through a cyclization similar to the initial step of the electrochemical mechanism. At the cyclized intermediate, instead of a second oxidation to give a dication, the photocatalyst returns an electron to the radical cation through a Back Electron Trasnfer (BET) to regenerate the ground state catalyst and an anionic intermediate. The anionic intermediate is protonated to give cyclized product. The photocatalyst is free to repeat the cycle.

An important distinction between the photoelectron-transfer reaction and the electrochemical reaction involves where in the reaction medium/flask the cyclization occurs. In the electrochemical reaction, the initial oxidation, cyclization, and second oxidation all occur at the electrode surface and within an electrolyte double layer that dictates the local environment. The double layer protects the reactive intermediates generated during the electrolysis from solvent trapping, dimerization, etc. In the photochemical reaction, the cyclization occurs following the

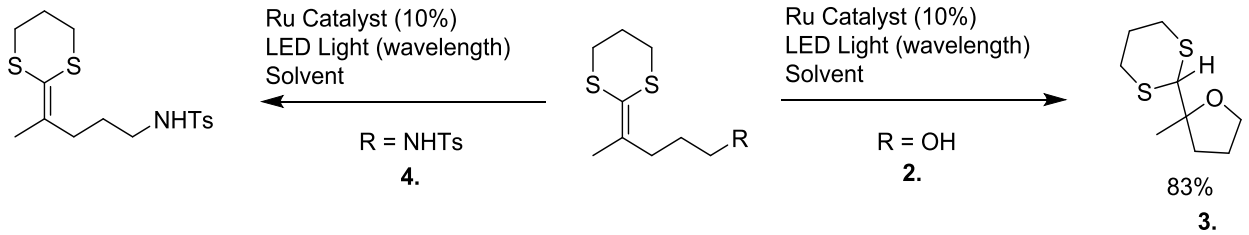

Figure 2. General results of photochemically driven cyclizations with sulfonamide and alcohol. These results were further explored under oxygen rich environment to probe the mechanism of the cyclization.

electron-transfer step when the radical cation is paired with the radical anion of the photocatalyst. Because of the intimate nature of the ionic bond formed in the photochemical reaction, a BET may occur after the initial oxidation if the cyclization is slow. No such possibility exists for the electrochemical reaction unless the radical cation is stable enough to migrate across the reaction cell to the cathode. Hence, the electrochemical reaction is much less likely to involve a re-reduction of the radical cation and much more likely to undergo a second oxidation step since the cyclization occurs near the surface of the anode.

Dr. Matt Graaf was the first in our labs to examine the photocatalytic coupling of an alcohol nucleophile with a ketene dithioacetal derived radical cation (Figure 2., Substrate **2**). He found that the reaction afforded the cyclic product **3** with little issue leading to excellent yield of cyclized product. Surprisingly, under the same conditions the coupling of a sulfonamide nucleophile with the ketene dithioacetal derived radical cation (Figure 2, Substrate **4)** led to recovered starting material and no evidence of product formation. When the reactions were run in the presence of oxygen, the reaction using the alcohol nucleophile again proceeded well, although it did lead to the product in a slightly reduced yield. The reaction utilizing the sulfonamide trapping group, afforded a ketone product that was derived from trapping of the initial radical cation with oxygen.

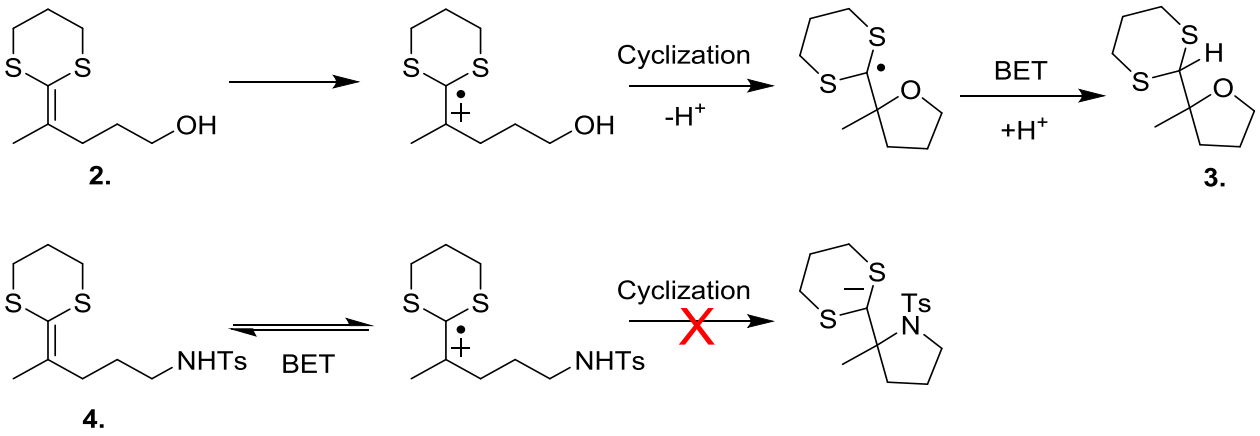

Figure 3. General results of the photochemical cyclizations. A back-electron transfer is emphasized here to show that while the alcohol can outcompete the BET to give cyclized product, the BET is faster than the sulfonamide

The proposed mechanisms of the general reaction and the oxidative cleavage reaction are shown in Figures 3 and 4, respectively.

The general mechanism for the reactions without oxygen is illustrated in Figure 3. Upon generating the radical cation, there are two mechanistic pathways available: cyclization or back electron transfer. The alcohol proceeds to product because it traps the radical cation fast enough to beat the BET. Under inert atmosphere, the sulfonamide returns starting material. This result implies that the sulfonamide is not cyclizing fast enough to compete with the BET. The sulfonamide's speed (or lack of) is further emphasized when the reaction proceeds under oxygen. With these conditions (Figure 4), after the initial radical cation is generated an oxygen radical anion, generated from being reduced by the photocatalyst, can trap the radical cation and the subsequent ketone formed by a retro [2+2]-cycloaddition. Alternatively, the radical cation could trap the oxygen directly followed by the back electron-transfer leading to the same key four-

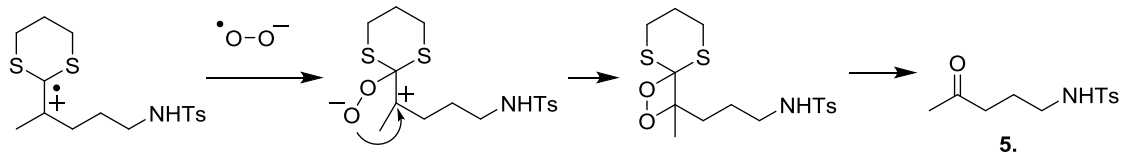

Figure 4. Ketene dithioacetal cleavage mechanism. Note the generation of the superoxide formed by electron transfer from the photocatalyst.

membered ring intermediate. The bottom line for both sets of conditions is that the alcohol traps the ketene dithioacetal derived radical cation quickly and the sulfonamide does not. This finding is completely consistent with the electrochemical competition study discussed in the last chapter that demonstrated the relative rates of the trapping groups for the reactive intermediate. Recall that alcohol trapping of the radical cation led to the kinetic product and sulfonamide trapping of the intermediate led to the thermodynamic product.

This use of an electrochemical competition study to explain the outcome of photoelectron transfer based study suggested that other electrochemical competition studies might serve as predictive tools for the photoelectron transfer reactions. We decided to test this idea with carbon-based trapping groups seen in figure 5..

Results and Discussion

For this study, we chose to examine photoelectron transfer initiated cyclizations between the ketene dithioacetal derived radical cation and enol ether and allylsilane trapping groups. The enol ether was chosen because it is an excellent radical cation trapping group that when competing with an alcohol provides both the kinetic and the thermodynamic product. Hence, we expected it to perform just as well under photochemical conditions. The allylsilane trapping group was known to be a worse trapping group than even the sulfonamide group used above. Hence, we proposed that the enol ether

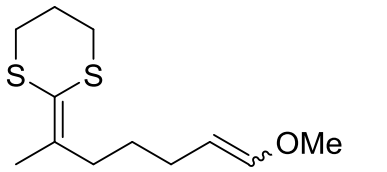

7.

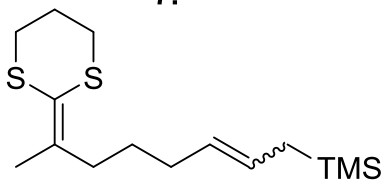

8.

Figure 5. Substrates for photolysis. Substrates use the radical cation trapping groups from previous electrochemical studies.

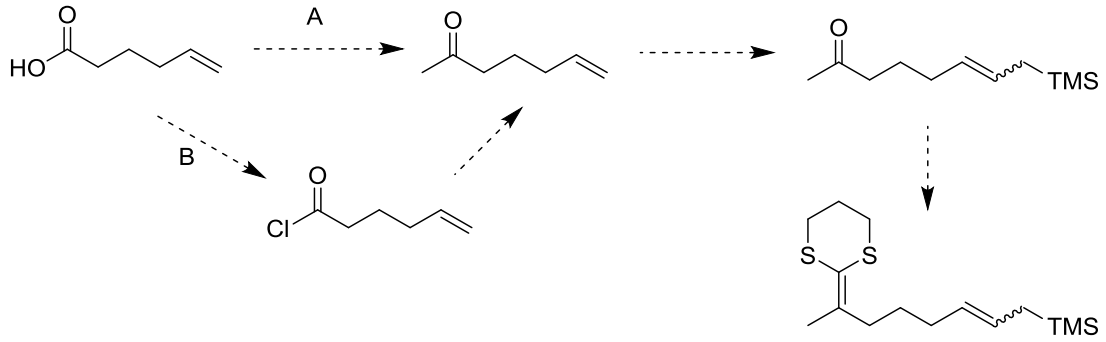

Scheme 1. Synthetic efforts towards the allylsilane substrate.
Reaction conditions:
A. MeLi (1.6 M in Hexane)
B. $SOCl_2$, DMF

trapping group would serve will in the photoelectron transfer reactions and the allylsilane trapping group would not.

To test this idea, the synthesis of subtrates **7** and **8** was undertaken. Synthetic efforts towards these substrates began with attempts to generate the allyl silane from either an acyl chloride or carboxylic acid as seen in **Scheme 1**. The route intended to generate the simple methyl ketone **9** then attach the allyl silane via a Grubbs cross- metathesis reaction before converting the ketone to the ketene dithioacetal. Hexanoic acid was initially used as starting point. Initial attempts at the conversion from carboxylic acid to ketone used 2 equivalents of methyl lithium added directly to a stirring solution of the acid in THF in dry ice/acetone bath. Attempts using this method were unsuccessful as the methyl lithium used would lead to double addition. Conversion to the acyl halide with thionyl chloride was unsuccessful as well. An alternative route was explored with acetyl chloride. With a similar intention with the acyl halide, the idea was to introduce the olefin sidechain with a copper mediated nucleophilic addition as shown in scheme 2. The copper iodide used for the reaction was purified using a purification method developed by Kauffman and Fang. [2] Conversion to the ketone **2** was successful, but this route was plagued by low yields and difficulty with purification as seen with the yield of dithioketene acetal **10**. While working on this chemistry, it became clear that a second approach that would allow for both the enol ether and the allylsilane substrates might be a superior choice. The retrosynthetic route is shown in Scheme 3.

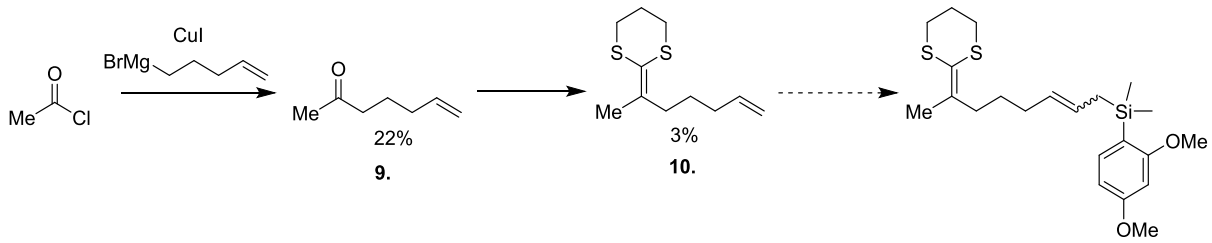

Scheme 2. Unsuccessful route towards electron rich allyl silane substrate.

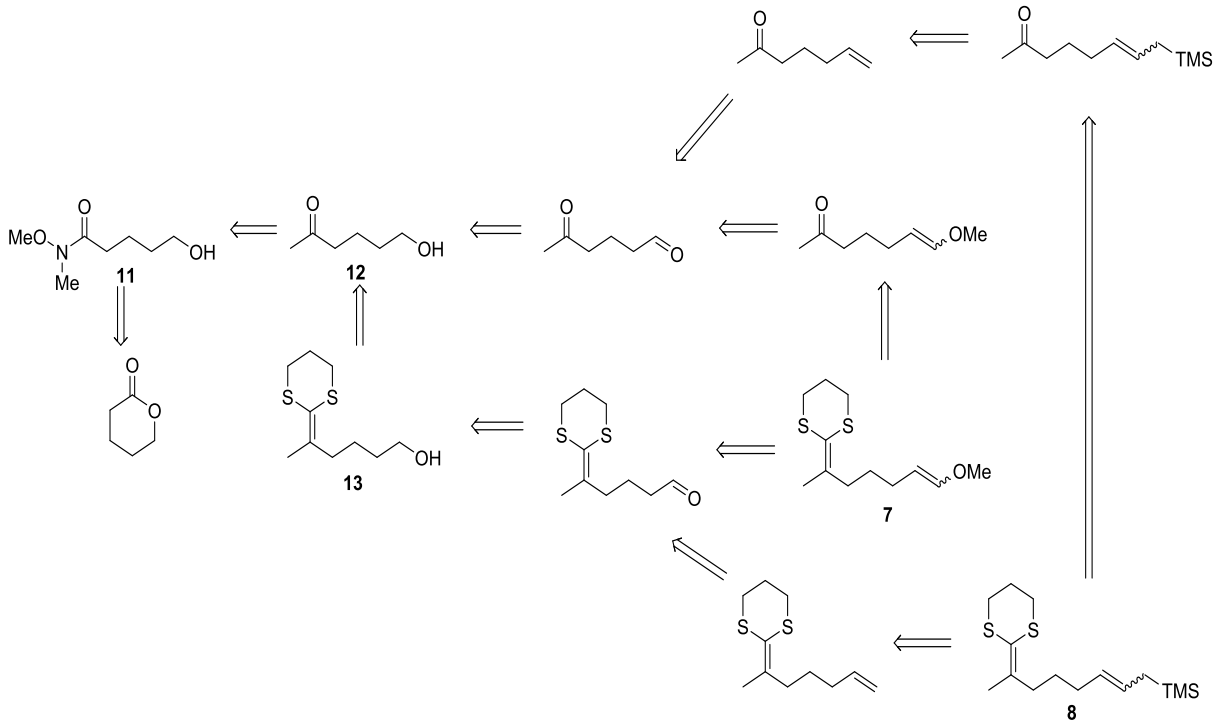

Scheme 3. Restrosynthetic Map for the synthesis of the allyl silane **(A**) and enol ether (**B**) substrates.

The route would build off the chemistry developed in the previous chapter, another positive aspect of making the change. The key idea was to convert a Weinreb amide **11** generated from a lactone starting point to the methyl ketone **12**. Weinreb amides were developed for solving mono-addition challenges to carboxylic acid derivatives like the one we were encountering. In this case, generation of the methyl ketone from the lactone would also lead to an alcohol on the other end of the molecule that could be used to develop the trapping group for the eventual ketene dithioacetal derived radical cation. This could be done by introducing the ketene dithioacetal to give substrate **13** and then introducing the other coupling partner for the oxidation by taking the opposite approach and first introducing the coupling partner for the ketene dithioacetal. This approach was particularly attractive because of the numerous contingency paths that could be followed if any one reaction proved unreliable. For example, when attempting several methods to purify the ketene dithioacetal enol ether substrate following a Wittig reaction to put the enol ether in place, an alternative route was proposed where the enol ether portion would be introduced before the ketene

dithioacetal so that purification from triphenylphosphine oxide could be accomplished more easily before incorporation of the more sensitive ketene acetal derivative.

With this in mind, the Weinreb amide **11** was generated from γ- butyrolactone. This reaction was previously used in the competition studies but with a δ-valerolactone. When we started with this reaction, it was problematic because it led to inconsistent yields of the product. At most, the reaction conditions adopted from Dr. John Campbell's synthesis would give 30%-

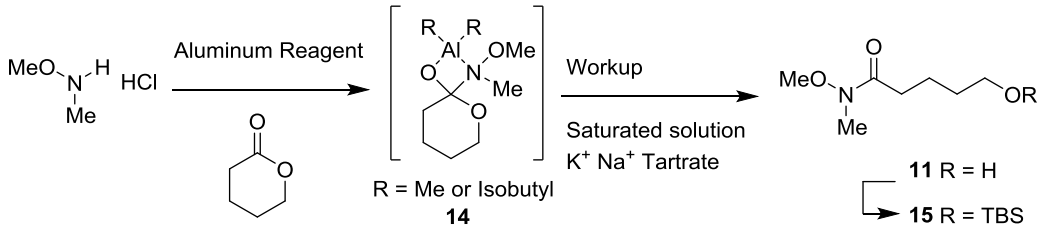

Scheme 4. Generation of the weinreb amide and protection with TBSCl.

40% of the Weinreb amide. The chemistry utilized the lactone, the methoxy amine nucleophile, and diisobutylammonium hydride as reagent to activate the amine. Initial attempts to improve the reaction involved the use of trimethyl aluminum, a more reactive aluminum reagent. The hope was that generating more of the tetrahedral intermediate from the initial addition would improve the reaction overall. However, the change led to the Weinreb amide in yields comparable to the reactions run with DIBAL. So, increasing the reactivity of the aluminum species was ruled out as a means for reaction optimization. This led us to examine the purity of the reagents used for the reaction. Accordingly, the hydroxy dimethyl amine salt was dried with benezene under rotary evaporator. This improved the reaction leading to a yield of the Weinreb amide on the order of 50%. With the starting materials in place, we then focused on the chemistry associated with the intermediate **14** that is central to the success of the reaction. The final step of this mechanism is the collapse of the tetrahedral intermediate to eliminate an alcohol. This occurs upon water workup, a scenario that is important for eliminating the chance for any type of over addition reaction or

alternative decomposition event. While a traditional organic-water solvent extraction type workup does afford product, it is possible that the product generated can act as a ligand for the aluminum species with both (or either) the amide end or the alcohol binding to the aluminum. This would take the product into the water layer or an emulsion leading to less recovery of the desired material. With this in mind, a saturated sodium potassium tartrate (Rochelle's salt) in water solution was employed in the workup to complex the aluminum and solubilize any emulsions in analogy to other workup procedures following aluminum hydride reductions of carbonyls. At first, this change did not improve the yield of product, but this turned out to be a result of rushing through the process. When the workup was allowed to stir overnight following the addition of the Rochelle's salt, the workup solution eventually separated into two distinct phases. Separation of the layers and then isolation of the product **11** led to a greater than 90% yield of the product on a gram scale.

Subsequent alcohol protection with TBS went smoothly to give protected alcohol **15**. The reaction afforded the silyl ether and silyl alcohol biproducts derived from the use of a slight excess of the silylating agent. Both were readily separated by flushing the product through a plug of silica

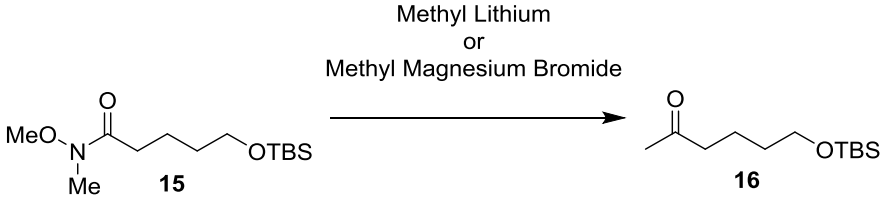

Scheme 6. Synthesis of the methyl ketone. Note: Methyl magnesium bromide leads to incomplete addition. Using methyl lithium completely converts the amide to ketone.

gel with with diethyl ether as the eluant. The only other impurity was imidazole that could be separated by crystallization from hexane followed by a paper filtration.

Protection of the alcohol allowed the Weinreb amide to be converted to the ketone **16** using methyl lithium or methyl magnesium bromide. Methyl magnesium bromide was used initially

because it directly paralleled the Grignard reagent used in the competition substrate synthesis. When using the methyl magnesium bromide reagent, yields would typically max out at 50%. To optimize this step, methyl lithium was tested. At first, yields were similar to the methyl magnesium bromide reaction. At this point, we worried about the purity of the methyl lithium reagent and if our THF contained a proton source. To address this, freshly distilled THF and brand new methyl lithium were used. This change led to a 91% yield of the desired product.

At this point, we worried about the chemoselectivity of the reactions needed to place the enol ether and dithioketene acetal coupling partners into the oxidation substrate. A route that deprotected the TBS ether and introduced the enol ether trapping group for the radical cation prior

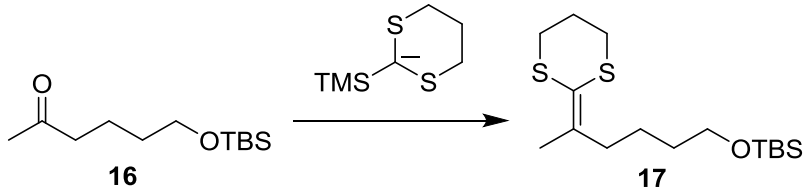

Scheme 7. Ketone conversion to Ketene dithioacetal using Peterson olefination.

to incorporation of the very sensitive ketene dithioacetal would require the Wittig reaction to make the enol ether to occur selectively at an aldehyde without interference from the ketone. Hence, we decided to avoid this route and examine the stability of the ketene dithioacetal group to a TBS ether deprotection, an oxidation reaction to form an aldehyde, and a subsequent Wittig reaction. To this end, the methyl ketone **16** was first converted to the ketene dithioacetal **17** (Scheme 7). The chemistry proceeded smoothly and needed no real optimization effort. Purification of the product was a small concern because of the sensitivity of the ketene dithioacetal to acid. We preferred to not use chromatography because of the slight acidity of silica gel. Initial purification attempted to use kugelrohr distillation. This was partially successful, but it was difficult to completely separate the starting dithiane from the product. Eventually, we settled on liquid

chromatography using silica gel as the solid support and 1:3:13 Dichloromethylene:Ethyl Acetate:Hexane mobile phase. Note: neat hexane will also give a separation but the length of the column will allow more time for product degradation. The progress of the column was monitored by TLC using potassium permanganate as a stain because it served as a good indicator of both the product and the starting dithiane. The separation worked well with the dithiane moving quickly, an rf value of almost 0.9, and the product moving more slowly with an rf value closer to 0.5. This allowed for a rapid chromatography that minimized the time that the acid sensitive product was on the silica gel. Using this method a 70-89% yield of the desired product was obtained.

With the ketene dithioacetal in place, the next step was deprotection of the TBS ether to afford the alcohol. Previously, we used a procedure that involved a stirring solution of potassium bisulfate at room temperature to remove the TBS ether. This procedure was lengthy, and it led to

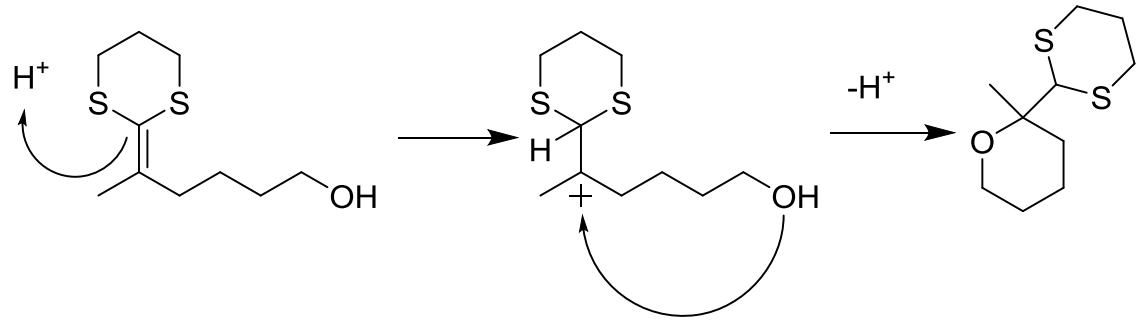

Figure 6. A possible side reaction that can occur at the deprotection step is an acid catalyzed intramolecular cyclization.

some protonation of the ketene dithioacetal and the loss of product associated with that reaction. As an alternative, treatment of the TBS ether with TBAF easily gave the alcohol in modest yield (50%) with no evidence for the formation of a side product or degradation of the ketene dithioacetal. Purification of the product involved column chromatography through silica gel eluent from the previous step.

Surprisingly, the alcohol product was more stable than predicted, but we still found it best to convert the alcohol to the enol ether or an alternate olefin as quickly as possible. Residual acid from the chromatography column did catalyze cyclization reactions involving the alcohol and ketene dithioacetal as illustrated in Figure 6. To avoid this problem, the alcohol was converted to an aldehyde using a Swern oxidation. The reaction was successful, but the aldehyde product was unstable. An NMR of the freshly generated aldehyde confirmed that it was formed cleanly with only a single peak evident in the aldehyde region. This changed rapidly overnight, and we found that the product could not be isolated or purified without it quickly degrading. To overcome this barrier, a procedure completed by Haichao Xu was used. This procedure was initially developed to accomplish a double conversion from a diol to a bis enol ether.[3] The procedure calls for conversion of the alcohol to the enol ether without any isolation of the intermediate aldehyde. To this end, the Swern oxidation is run in THF, the solids formed removed by filtration, and then the crude aldehyde solution directly added to a stirring solution of the ylide needed for the Wittig reaction. The ylide was generated by treating the corresponding triphenylphosphonium salt with sec-butyl lithium. The use of n-butyl lithium does form the desired ylide, but when making an enol ether it also leads to some exchange of the methoxy group with the butyl lithium and then formation an olefin side-product containing that butyl group. This phenomenon had previously been seen but not reported. Using sec-butyl lithium instead of n-butyl lithium gave no exchange product, and therefore the s-butyl lithium was used here. This two step sequence with our alcohol substrate afforded the enol ether in low yield. (6%-10%- yield after removing the triphenylphosphine oxide side product. Removal of the triphenylphosphine proved very problematic. Attempts to purify the product by column chromatography ultimately led to complete loss of the product. The triphenyl phosphine oxide both moved with the solvent front and streaked

down the entire length of the column. If the chromatography was accelerated to get the product without complete decomposition, then enough triphenyl phosphine oxide remained in the product to ruin the electrolysis. This scenario was easy to identify because triphenylphosphine is electroactive at an anode affording a stable radical cation. That radical cation will migrate to the cathode and get reduced to regenerate the original triphenylphosphine. In this way, the trace impurity "steals" all of the current and the desired substrate is recovered from the reaction. This problem became increasingly burdensome because of the product being generated was the result of a multistep synthesis. Hence, the purification could only be attempted when enough enol ether was available, and having enough enol ether available was difficult.

Eventually, a change was attempted to the overall approach. If we could not separate the triphenyl phosphine from the product without destroying the ketene dithioacetal, then maybe we needed to solve the chemoselectivity problem described above and get rid of the triphenylphosphine before generating the ketene dithioacetal. Unfortunately, this attempt proved unsuccessful, and the combined losses associated with the chemoselectivity issues, separation of the triphenylphosphine and stability of the enol ether to formation of the dithioketene acetal did not provide the desired improvement in the overall product yield.

Facing the reality that the triphenyl phosphine would have to be dealt with near the end of the synthesis, we continued with a variety of changes to the purification and workup procedure at the end of the initial route. The triphenyl phosphine oxide impurity is noticeably less soluble in hexane than in diethyl ether so the organic solvent used on workup was changed to hexane. When hexane is added directly to dilute the reaction, an orange precipitate crashes out of solution. The liquid phase is easily decanted off and concentrated down to around 5-10 mL of product solution. A cold silica plug is prepared by wrapping a paper towel around a filter plug filled with silica gel.

The paper towel is wet with diethyl ether. The evaporating diethyl ether cools the silica plug which helps further crash out any triphenyl phosphine from the product solution. The product solution is washed with hexane and the collected wash is further concentrated down. NMR at this point shows a significant reduction in the size of the triphenylphosphine peak. The residual triphenylphosphine can be removed via a simple column chromatography and 1% diethyl ether in hexane. The best yield from this reaction and purification was 20%.

At that point, we could undertake the electrochemical and photoelectron transfer studies that were initially planned. Remember, that our goal was to show that the more efficient enol ether trapping group would cyclize using the photoelectron transfer conditions in a manner analogous

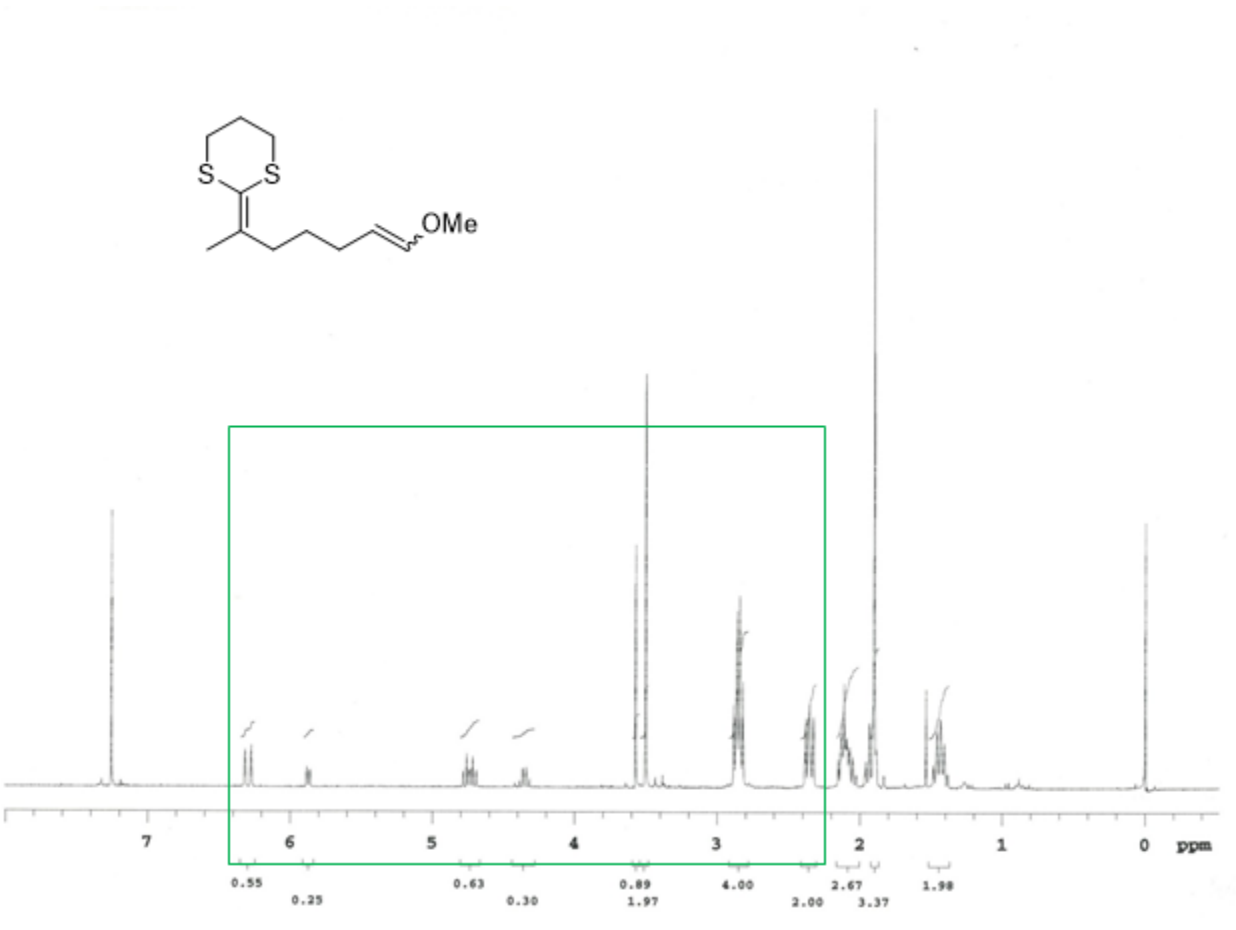

Figure 7. Enol Ether Starting Material **7**

to the alcohol trapping group based upon the electrochemical competition studies that showed the enol ether to trap a ketene dithioacetal radical cation faster than the alcohol.

To our surprise, this was not the case. Employing the same photoelectron transfer conditions utilized above with the alcohol trapping group, the use of an enol ether in place of that alcohol led to very little of the cyclized product. In fact, the photochemical reaction afforded mostly a polymer product. Key to this polymer was that its formation consumed both the starting ketene dithioacetal and the enol ether. In the past, we have found that such reactions do undergo the cyclization reaction, but then have trouble with the second oxidation step. This is a problem that would never hinder an electrochemical reaction involving an enol ether trapping group

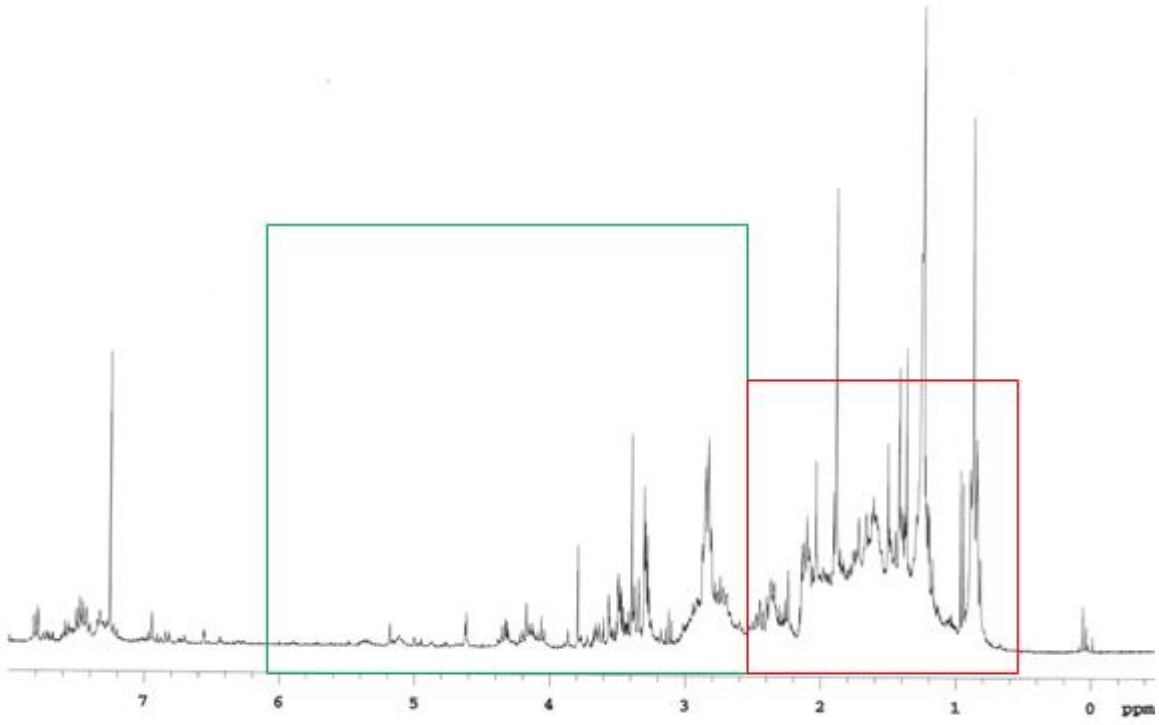

Figure 8. Photolysis of Enol Ether Starting Material

because this second oxidation reaction would occur very quickly at an anode surface. In order to improve the photoelectron-transfer reaction, the catalyst loading was increased to help the speed of the BET and maybe circumvent the polymerization. However, the result of the reaction was again the formation of a polymer. Once again, both ends of the coupling reaction were being consumed. This was visible in the proton NMR of the crude material where we noticed the peaks for the dithio ketene acetal and the enol ether were missing. The key regions of the NMR are shown in Figures 7 and 8. Note the olefin region marked in green that disappears in the proton NMR of the crude reaction, and the evidence for polymerization seen in the region marked in red in spectrum for the crude product.

The peak assignment for the starting material was simple. The doublets at 6.3 ppm (trans) and 5.9 ppm (cis) along with the doublet of triplets at 4.7ppm (trans) and 4.4ppm (cis) correspond to the trans and cis isomers of the enol ether. Singlets in the 3.5 to 3.6 region were assigned to the methoxy group on the enol ether because of their ppm value and their integration compared to the doublets and doublet of triplets previously assigned. The triplets at 2.8 (Sulfur adjacent) and 2.4 (middle) were assigned to the methylene peaks of the ketene dithio acetal next to the sulfurs. The triplet at 2.1 ppm and 1.9 ppm correspond to the methylene and methyl group immediately adjacent to the ketene dithioacetal because these two peaks appear when the methyl ketone is introduced and shift upfield when the ketone is converted to the ketene dithioacetal. The final peak at 1.4 ppm was assigned to the remaining methylene peak on the sidechain. Note how in the photolysis crude NMR that both the peaks for the enol ether isomers and the ketene dithio acetal group disappeared. Both groups were involved in the reaction.

As suggested above, when an electrochemical reaction generates a polymer while consuming both the initiating and terminating ends for the cyclization the problem has historically

been caused by a slow second oxidation step following the cyclization. [4] Such issues have typically been associated with poor trapping groups like the allylsilane or cyclization reactions that lead to stable radicals.[5] Of course, a second oxidation step in the reaction cannot occur during the photoelectron-transfer reactions that involve one electron processes. Hence, the failure of the enol ether group to trap the radical cation cleanly in the photoelectron transfer reaction suggested that maybe the second oxidation step is important for all of the reactions that lead to carbon-carbon bond formation, even reactions that utilize the best trapping groups available. After all, the use of the enol ether in the related electrochemical cyclization that can readily undergo the second oxidation step leads to cleaner formation of the product (71.2% yield by NMR) that separates out to either non-hydrolyzed or hydrolyzed products as seen in figures 9 and 10**.** In this case, the

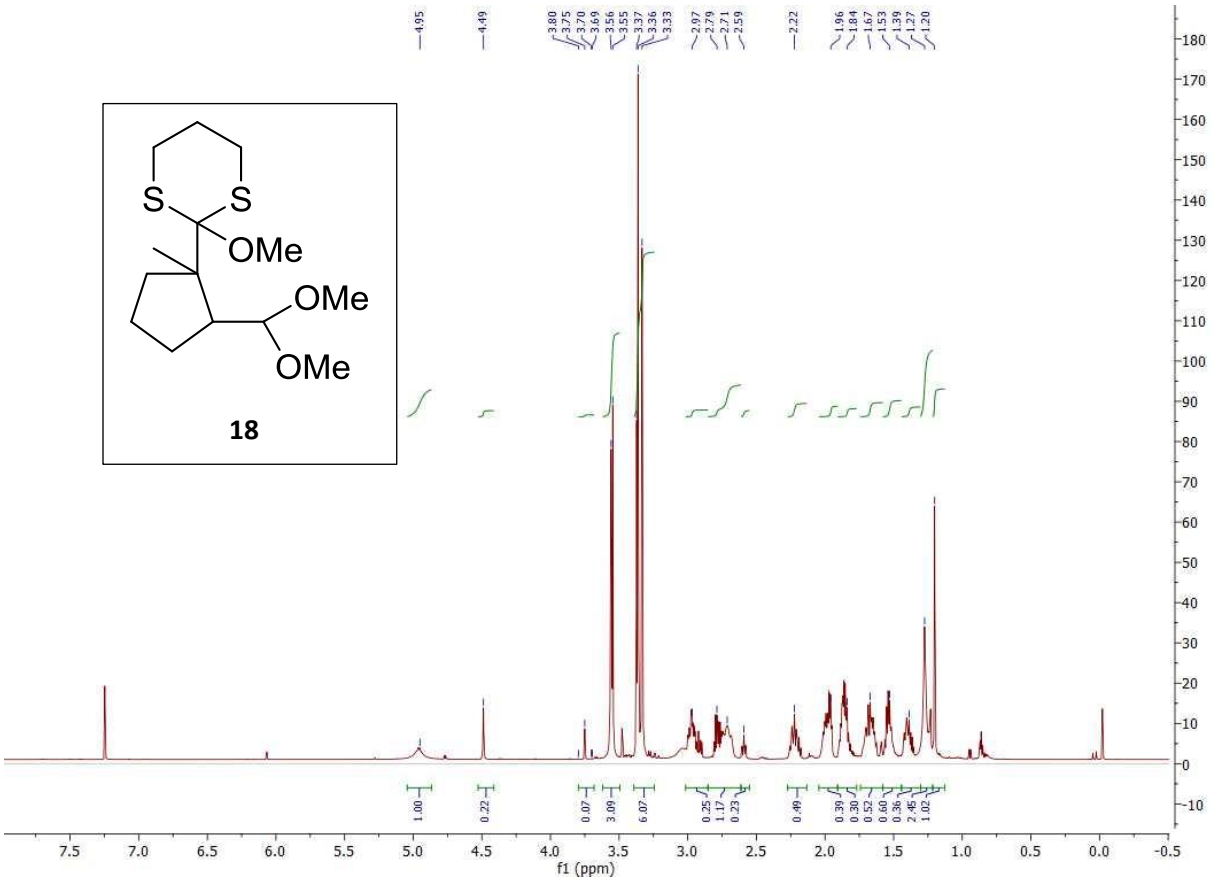

Figure 9. NMR of purified electrolysis product **18**.

cyclization product contained two types of product; one with dithiane remaining intact and another where the dithiane had hydrolyzed. The structure of these two types of products was confirmed via NOESY and COSY (Figure 11 and 12). It should be noted that both products contained more than one stereochemical isomer.

The proton NMR for the non-hydrolyzed material is shown below. Note the 2 important peaks at 4.5 (sharp) and 5.0 (broad) ppm. These peaks correspond to the single proton of the acetal. For clarity, cis- and trans- nomenclature will refer to the positioning of the larger dithio group and the acetal group. The cis-acetal product would have less free rotation because of steric hindrance from the dithio group. The lack of free rotation would cause a singlet seen at 5.0 ppm to broaden. The trans-acetal would have less steric hindrance and explains the sharper singlet. Peaks within

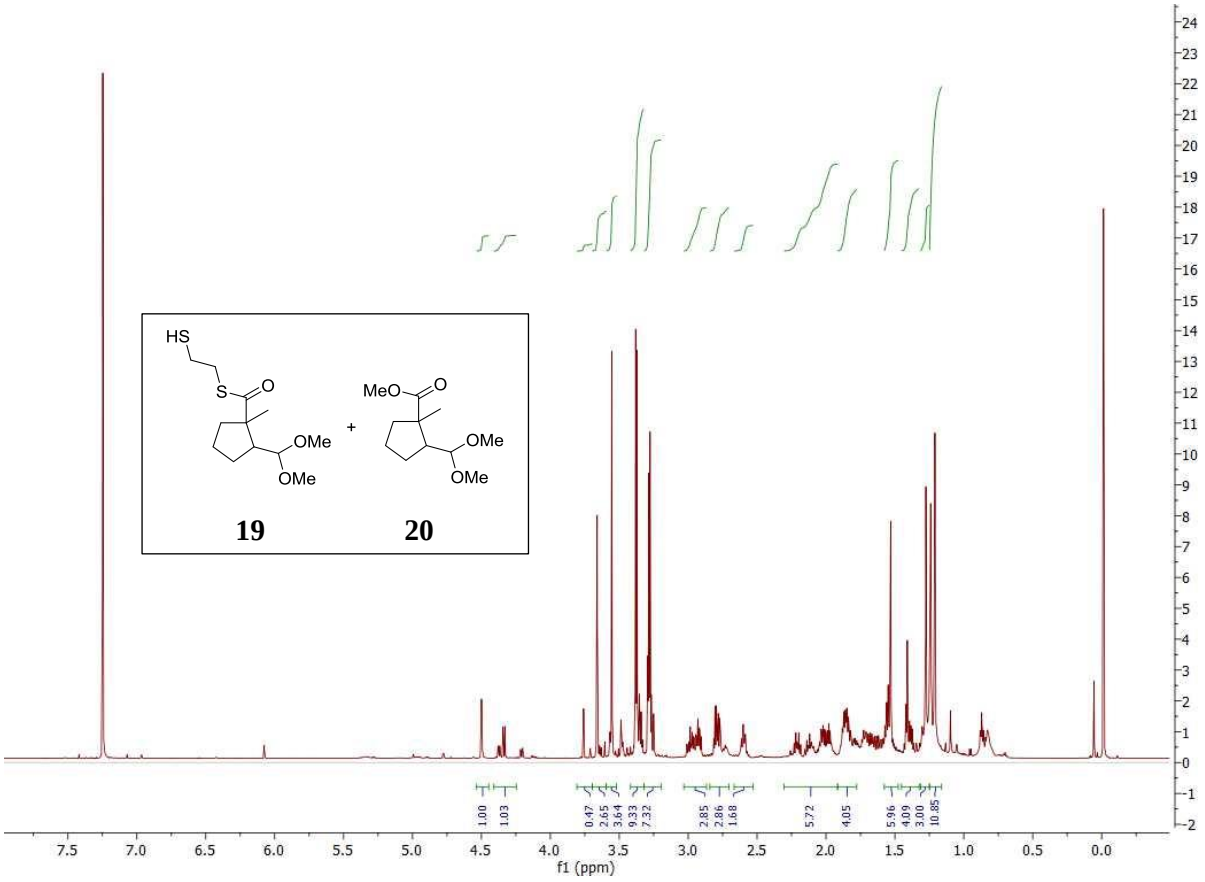

Figure 10. Hydrolyzed electrolysis products from enol ether substrate.

the 3.0 – 3.6 region correspond to the methoxy peaks found on the acetal and the dithiane, again because of integration compared to the singlets found at 4.5 and 5.0 ppm. Peaks within the 2.5 – 3.0 region were assigned to methylene peaks of the dithio group and protons next to the quaternary center. Similar to the starting material, sulfur adjacent protons saw a downfield shift from the typical methylene region. The quaternary center generated acts as an electron donor group and causes the protons on carbons adjacent to it to shift slightly less downfield. That is why the methylene region for this molecule extends from 1.3 out to 2.3. The second set of important peaks are the two singlets around 1.3 that are assigned to the methyl group next to the quaternary center.

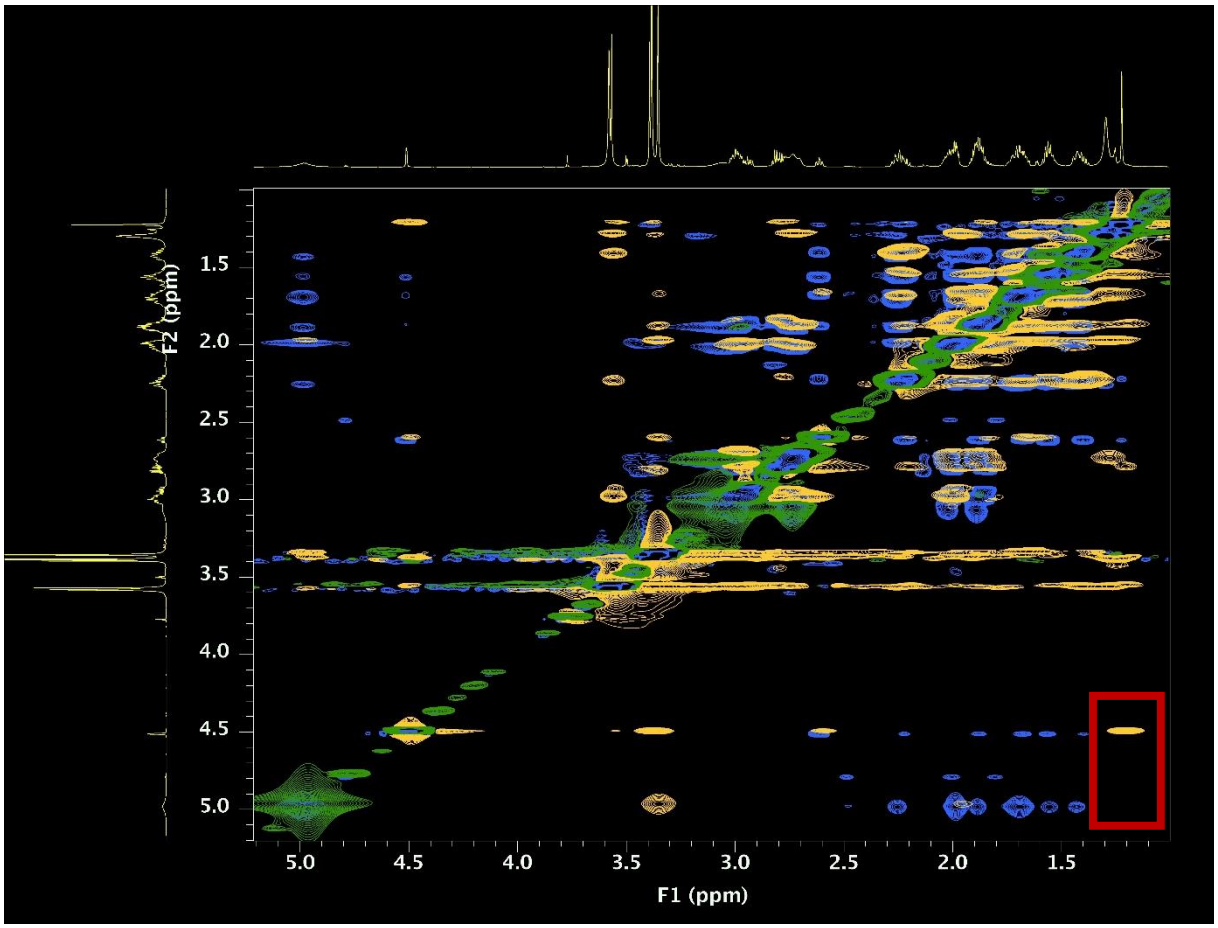

Figure 11. NOESY(yellow) and COSY(blue) of product **18.**

The non-hydrolyzed product **18** was isolated along with hydrolyzed products **19** and **20**. The proton NMR of the hydrolyzed material is shown in Figure 10. Peak assignment is similar to that of the previous H NMR. Note the number of methoxy peaks in the 3.3 – 3.8 region. There is evidence for multiple products in that there are more methoxy peaks than expected from 1 single set of isomers. This is further supported by the multiple singlets attributed to the methyl group centered around 1.3 ppm. Compared to the set of isomers in the first proton NMR, there should only be 2 singlets, but the appearance of a third singlet implies at least a second product. The peaks in the 2.5- 3.0 region were assigned to the methylene peaks of the hydrolyzed dithiane. Peaks within the 1.7 – 2.3 region were associated with the methylene peaks of the ring. With this

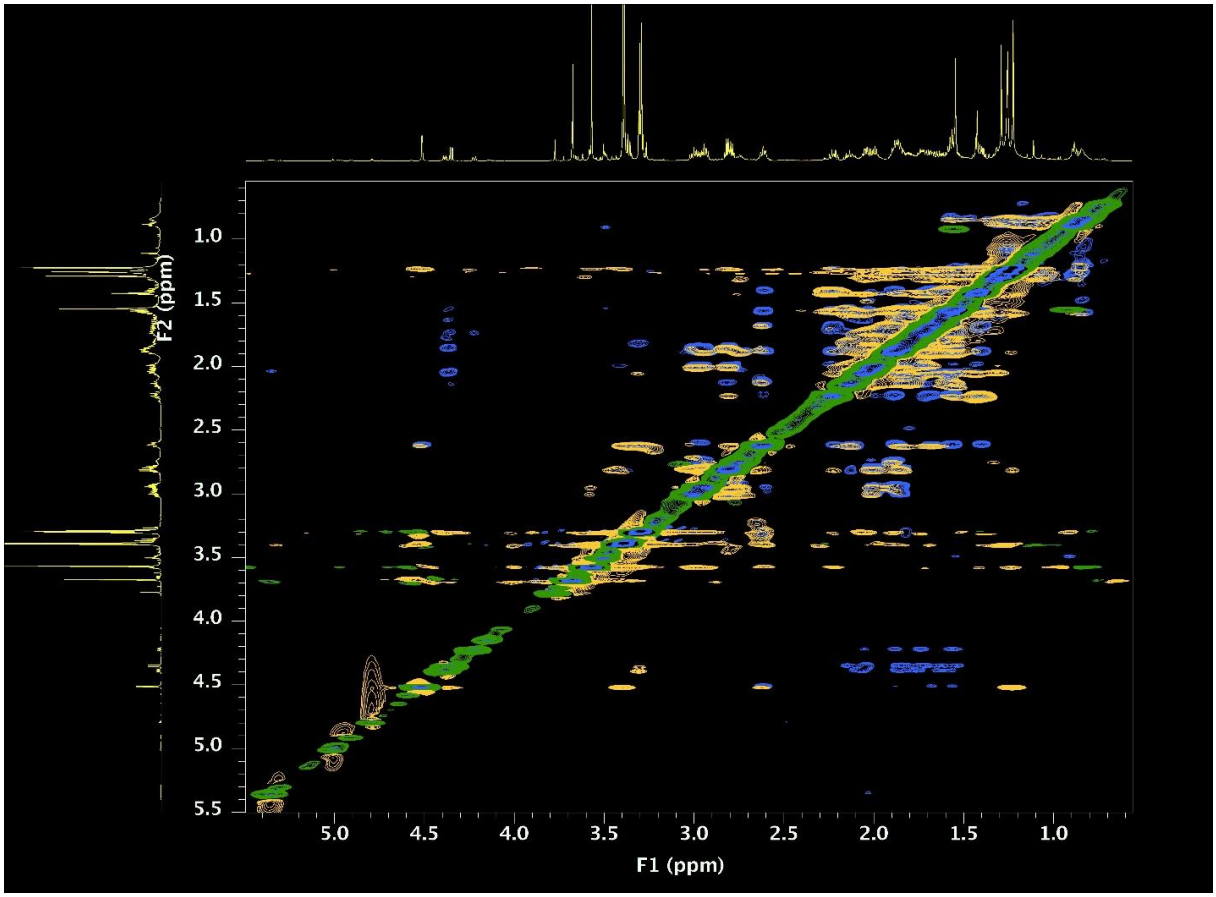

Figure 12. NOESY(yellow) and COSY(blue) of products **19** and **20**.

information, we were able to differentiate which peaks belong to which isomers using 2D NMR techniques.

As previously stated, the key interaction centers around the doublet at 4.5 ppm. Note the difference between the hydrolyzed and non-hydrolyzed material that would indicate a mix of isomers is a missing NOESY interaction between the broad peak at 5.0 ppm and the singlet at 1.2 ppm (highlighted with the red box). It is predicted that proton of the acetal that is normally at 4.5 is slightly downfield at 5.0 ppm either because it is being shared between the acetal and the dithiane or because the acetal has eliminated one of the methoxy peaks and the cation is stabilized by the nearby dithiane. With this evidence, we were able to show that there is a mixture of the cis and trans isomers. Further evidence for degradation to either the thioester or methyl ester is seen with the lone peak at 180 ppm.

If one considers the mechanism for this electrochemical cyclization (Figure 13), one can see that with the enol ether substrate the cyclization leads to a new radical that is perfectly set up for the second oxidation and the formation of a stable cation. The photoelectron transfer reaction indicates that this is a critical element for the oxidative cyclization that aids the fast cyclization reaction (observed using the CV data cited in Chapter 2). Interestingly, without the combination of the electrochemical and photoelectron transfer reactions, this detail in the mechanism would not be clear. So, we set out to show that the electrochemical competition studies could shed light on

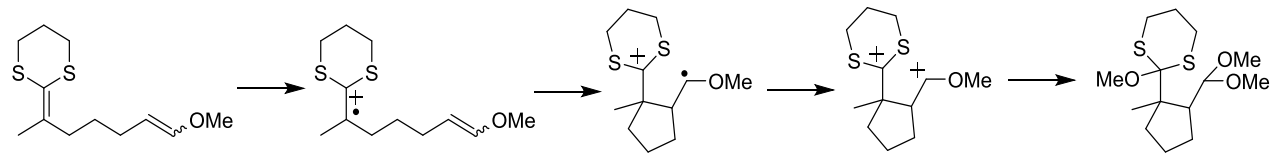

Figure 13. Electrolysis Mechanism

photoelectron transfer reactions and wound up showing that the use of both methods in concert provided new insights into radical cation mediated oxidative cyclizations.

To further test whether this observation was general, we turned our attention to a second C-C bond forming reaction. Initially, our goal was to use the allylsilane substrate. However with the more reactive enol ether failing as a trapping group in the photoelectron-transfer reaction, the initial plan of showing that the competition studies would predict success with the enol ether and failure with the allylsilane fell apart. Instead the question arose as to whether any of the carbon-carbon bond forming reactions would work with the photoelectron transfer conditions, or did they all require a second oxidation step. With that question in hand, we turned our attention to the use of a furan ring as a radical cation trapping group. From a purely synthetic standpoint, furan rings have been among the most successful radical cation trapping groups used to date as seen in Scheme 8. For this reason, they have been used in several total synthesis efforts by our group and others.[6] While to date these reactions had involved the trapping of enol ether derived radical cations, we figured that the electrochemical cyclizations would also occur easily with the ketene dithioacetal derived intermediates because the second oxidation step again appeared to be ideal (Figure 14). In other words, we anticipated behavior similar to that of the enol ether trapping group that proved to be the most successful trapping group for the ketene dithioacetal derived radical cations.

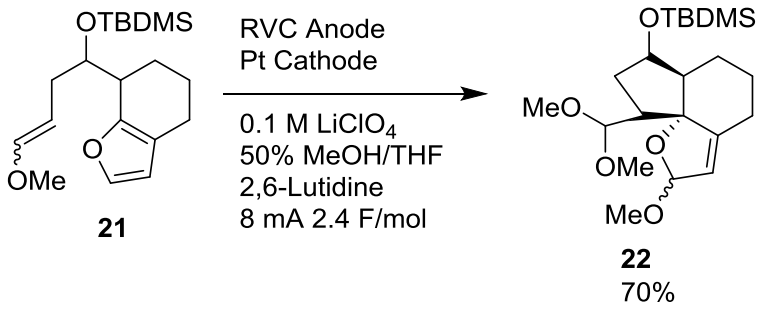

Scheme 8. Total synthesis using furan group.

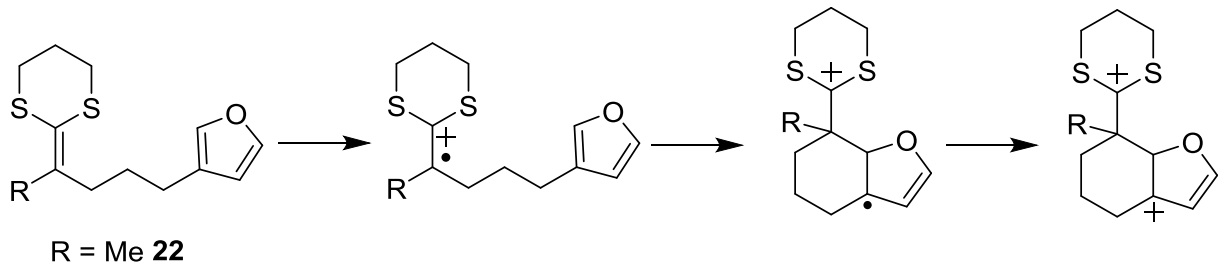

Figure 14. Mechanism of furan trapping.

Tthe synthesis of the furan substrate **22** was designed to take advantage of the previously developed route. Once again, the route was developed for its versatility. In the previous case, the lactone starting material was opened to form a Weinreb amide that was then treated with a methyl group. The resulting ketone was transformed into the ketene dithioacetal and the alcohol into the enol ether. For the current synthesis, the route can be adapted to add the furan coupling partner and associated tether as the lithium anion instead of the methyl lithium. Similar nucleophiles have been employed by our group for the construction of furan based substrates. In place of the lactone for this synthesis, methyl acetate was used. However, one could imagine a synthesis starting from the lactone as well; a reaction that would result in substrate for a competition study between the furan and the alcohol. Such a substrate could be used to probe the reactivity of the furan ring in a competitions study in order to assess its reactivity toward a radical cation intermediate relative to the enol ether, alcohol, sulfonamide, and allylsilane nucleophiles previously studied.

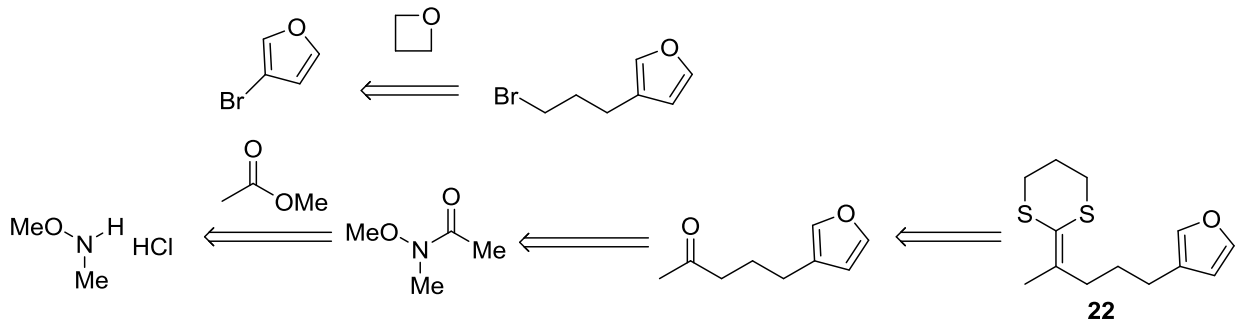

Scheme 9. Retrosynthetic route to furan substrate **22**.

But first, we wanted to test the simpler substrate in connection with the photoelectron-transfer reaction and the conclusion that the second oxidation reaction was important. For the reaction, the Weinreb-amide was generated from the methyl acetate using the same synthetic conditions described above. The amine was converted into an aluminum-based nucleophile with the use of DIBAL, the methyl ester was introduced, and the reaction workup utilized Rochelle's salt as in the previous transformation. It is important to note that the simple Weinreb-amide generated in this synthesis is volatile under vacuum. Care must be taken or the product will be can be lost, even on a rotary evaporator.

The second part of the synthesis required construction of a Grignard reagent from the known bromofuran.[7] The first step of this synthesis was accomplished via metal-halogen exchange using 3-bromofuran in dry ice/acetone bath with n-butyl lithium. The anionic solution was then treated with trimethylene oxide and boron trifluoride etherate at -78^{o} C. It is important to keep this reaction cold in order to avoid a deprotonation reaction that leads to anion equilibration and the addition of two trimethylene oxide molecules to one furan. The purity of the boron trifluoride etherate will also affect the reaction. If the color of the boron etherate species is anything but clear, the reactions suffers from the generation of a polymer that that is difficult to remove from the product. The product can be purified nicely by chromatography through silica gel using a 1:1 mixture of ethyl acetate and hexane. This leads to the product alcohol **23** in 55-70% yield on a gram scale.

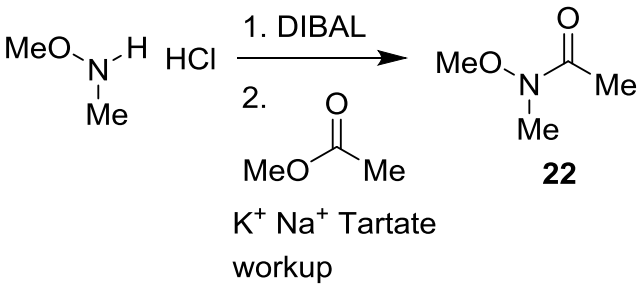

Scheme 10. Synthesis of weinreb amide **22**.

The alcohol was converted to a bromide with standard Appel conditions. Unfortunately, an attempt at generating a Grignard reagent from the bromide gave no reliable anion. Initially, this was thought to be residual water in the solvent. However, even after drying the THF through distillation, it was found that the anion could not be reliably generated. An examination by proton

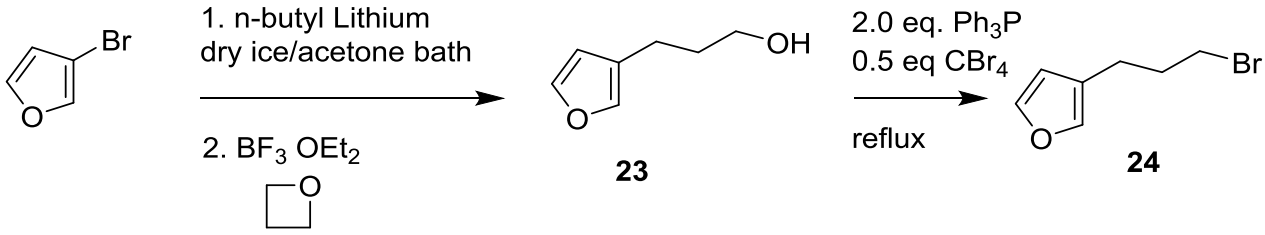

Scheme 11. Generation of the bromide **24.**

NMR showed no impurity in the brominated furan. TLC analysis of the starting bromide did indicate the presence of a second compound. Using UV light as an indicator, a TLC taken for the bromide starting material showed both the expected bromide and tetrabromomethane. The tetrabromomethane was identified by co-spotting the bromide starting material for the Grignard reagent with the known tetrabromomethane. Based on this observation, the reaction used to make bromide **24** was conducted with less tetrabromomethane and the product was purified by chromatography using neat hexane as the eluant. These conditions successfully afforded bromide in a level of purity that allowed formation of the desired Grignard reagent with only gentle heating. It is also important to note that converstion of bromide to the Grignard reagent must be done quickly because the bromide is unstable to visible light and quickly leads to a black liquid that is difficult to purify.

Even with the more pure bromide, generation of the Grignard reagent can be

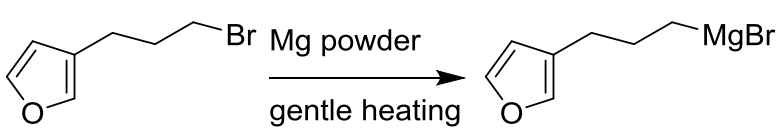

difficult. A number of attempts were made to form the Grignard in consistently high yield. Magnesium chips were initially used for the reaction, but the chemistry was not successful. With that we turned to the magnesium ribbon source of the metal that had previously proven successful with difficult cases. The ribbon was especially successful when it was sanded down to remove the magnesium oxide top layer. This approach again proved unsuccessful with the current reaction. The last attempt at generating the Grignard reagent used magnesium powder. Even with this very activated source of magnesium, the conversion required mild heating and the use of iodine to help jumpstart the electron-transfer process. This approach provided the only reliable method of generating the required Grignard solution. No further attempts at optimization of the reaction were taken due to time constraints.

At this point, the ketone **25** could be made via simple 1:1 addition of the Grignard reagent to the Weinreb-amide in THF solvent at 0 ^{o}C. The yield of the reaction was typically around 50%. Optimization of this reaction is certainly possible if it is deemed worthwhile to revisit the overall process (a statement that should become clear from the discussion below). Once available, the ketone was converted to the ketene dithio acetal *via* a Peterson olefination reaction utilizing the 2-trimethylsilyl-1,3-dithiohexane derived anion. The product was purified using a kugelrohr distillation. With the substrate in hand, we examined the

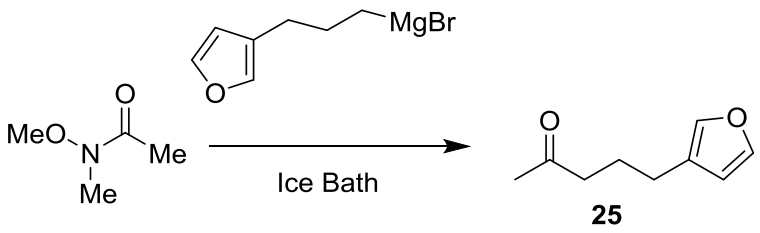

25

oxidation reaction. The initial experiment attempted used the electrolysis conditions previously employed for substrated containing a furan ring. These conditions utilized an RVC anode, a Pt cathode, 20% MeOH in dichloromethane as solvent, 0.1M concentration of $LiClO_4$ electrolyte, 2,6-lutidine, 2.1 F/mol of charge, and 6mA of current. To our surprise, this first attempt at the cyclization led to a polymer as can be seen from the proton NMR of the crude reaction mixture and very little if any of the desired product. (Figure 15) This result was a surprise because the electrolysis using the enol ether trapping group had gone so well, and as mentioned above the furan

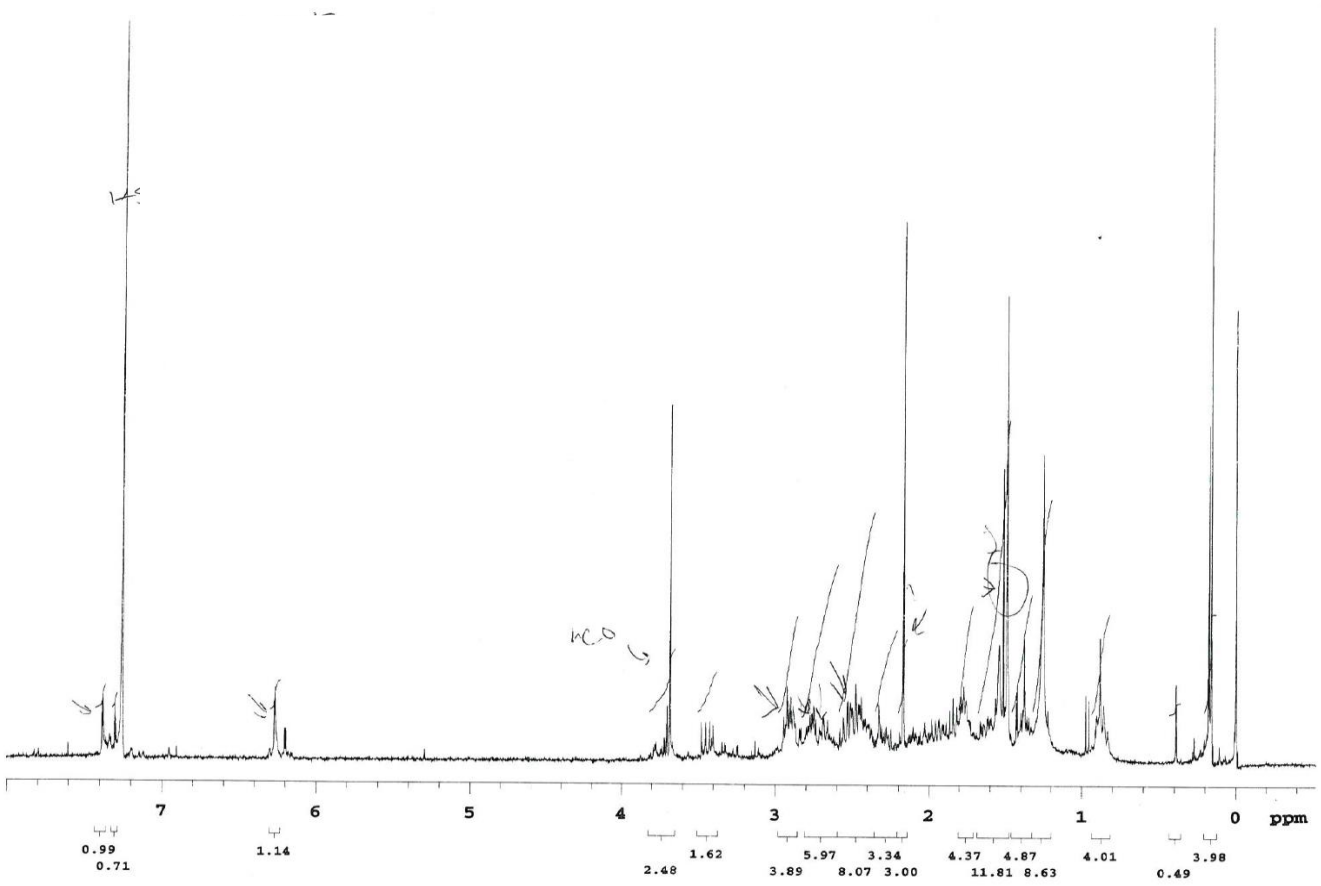

Figure 15. Proton NMR of Furan Electrolysis Crude

trapping group was thought to be one of the best, perhaps even better than the enol ether. Clearly, it is not.

When reconsidering the reaction, the outcome was not all that surprising. In previous work, we had correlated the polarity of the radical cation with the chemoselectivity of a trapping reaction. More polar radical cations led to C-C bond formation through radical-type processes, presumably due to stabilization of the cation nature of the radical cation by donating groups. Less polar radical cations favored trapping by heteroatoms, presumably due to trapping of the cationic nature of the radical cation by the heteroatom. With this backdrop, it appeared that the aromatic furan ring behaved more like a radical acceptor that struggled to trap the less polar radical cation. In other words, it behaved like the less nucleophilic C-C bond forming trapping groups like the allylsilane than it did a nucleophilic heteroatom. The enol ether, to no big surprise, does both well. The end result is that the furan ring did not trap the less polar ketene dithioacetal derived radical cation nearly as well as it trapped the more polar enol ether radical cations used in earlier studies.

Within that context, the formation of the polymer in the current reaction did hint at a slow second oxidation as well so several methods for improving the second oxidation step in the reaction were pursued as well. These methods involve a change in the electrolyte for the reaction, a change in the electrolyte concentration, and/or an increase in the current/current density used for the reaction. These changes target mechanistic observations that we have made about the reactions in the past.

A change in electrolyte can prevent methanol from interrupting the reaction too quickly at the electrode surface. Less polar electrolytes exclude methanol from the electrode surface slowing intermolecular trapping of the reactive intermediates generated. This can allow the cyclized radical time to oxidize and prevent reopening of the ring, an event that can lead to polymerization of the

uncyclized radical. At the same time, changes in the concentration of the electrolyte helps stabilize the radical cation and the dication intermediate following the second oxidation. The stabilization of the dication lowers the oxidation potential needed for the second oxidation. Finally, increasing the amount of current that is passed through the reaction helps funnel the reaction pathway down the dicationic pathway by effectively increasing the concentration of the oxidant used. The initial reaction conditions used for the furan based cyclizations mimicked previously optimized furan cyclizations with the more polar enol ether derived radical cation intermediates and were employed without consideration of any of these factors.

The initial change made to these conditions involved increasing the electrolyte concentration from 0.1M to 1M $LiClO_4$. This successfully increased the yield of the desired cyclized product to 19%. In further efforts to optimize the reaction, electrolyte and solvent were changed. A change from $LiClO_4$ to Et_4NOTs electrolyte led to no substantial improvement. The solvent was then changed from 20% methanol in dichloromethane to 10% methanol in dichloromethane to further decrease the amount of methanol available for trapping the radical cation intermediate generated at the anode. A yield of 21% was obtained for the desired cyclized product, a result that showed the modification had no real effect of the cyclization. A second change to solvent included using hexafluorinated propanol that has seen extensive use in the Waldvogel group for radical cation reactions (citations). Unfortunately, the use of these conditions led to polymer formation and none of the desired product.

At this point, we utilized the optimal solvent and electrolyte conditions (1 M $LiClO_4$ and 10% methanol in dichloromethane) along with an increase in the current used for the transformation (60 mA relative to the 6 mA used previously). This change increased the yield of the reaction to 31% yield of the hydrolyzed product. It was clear that the second oxidation reaction

was important, but it was not enough to overcome problem with the initial trapping reaction associated with the non-polar radical cation. The use of an aromatic trapping group required the more polar radical cation for obtaining a synthetically useful yield.

Conclusions:

While the poor yield of cyclized product obtained from the use of an enol ether trapping group in a photoelectron transfer reaction was surprising, it demonstrate how effective the combination of an electrochemical study with a one electron process could be for elucidating the mechanism of radical cation initiated cyclizations. The combination of the two techniques showed us that even cyclizations that utilize the best radical cation trapping groups available depend greatly on the success of the second oxidation step required by the reaction. Specifically, the enol ether trapping group, the best trapping group studied to date, completely failed to afford a cyclized product when employed in a one electron, photocatalytic reaction. The corresponding electrochemical reaction with the same substrate led to high yields of the product. Clearly, the reaction utilizing the enol ether trapping group required the second oxidation to be successful. While the furan cyclization reaction struggled because of the non-polar radical cation used in the current cases, the reaction also showed clear evidence for the importance of the second oxidation reaction with efforts to raise the yield of product formation directly tied to methods known to improve that step of the mechanism. This last result implied that the enol ether trapping group is a very special one for oxidative cyclization reactions because it clear traps both polar and non-polar radical cations with a rate of success not seen with any other trapping group. Previously, we had placed furan rings into the same category, a status that has turned out to not be warranted.

As mentioned above, our original hypothesis was to see if electrochemical principles could be used to guide our understanding of photochemistry. What we learned instead is that photoelectron transfer chemistry and electrochemistry can best be used in conjunction to provide a better understanding of the mechanistic pathways that underpin radical cation initiated cyclization reactions. It is only the use of the two techniques together that allowed us to get an accurate understand of just how special enol ether trapping groups are for radical cations and why. The enol ether is the one group we have studied that combines the ability to both trap cations and radicals well with the generation of a cyclized product perfectly setup for the second oxidation reaction.

This conclusion does suggest that an allylsilane group might be able to join this elite company if it is made more electron-rich in a way that accelerates a slow second oxidation reaction. CV data shows that its trapping of the less polar radical cation is not slow, so a fast second oxidation reaction that made this reaction synthetically viable would allow it to serve as an excellent trapping group for the non-polar radical cation. It already works well with the more polar radical cations. Efforts to test this hypothesis are underway.

Experimental

Synthesis of Enol Ether Substrate

Tetrahydrofuran used in the following reactions was distilled over sodium metal and benzopehenone. Dichlormethane used in the following reactions was distilled over calcium hydride. Triethylamine used in the following reactions was distilled over calcium hydride. Proton and carbon NMR spectra were obtained via a Varian 300 MHz and 500 MHz machine. Mass spec were obtained via the following method: samples were dissolved in 200 µL MeOH + 0.1% Formic acid and directly infused to an ESI source at 3 µL/min. High-mass-resolving power (60,000) ESI-MS was conducted in the FTMS positive-ion mode on a LTQ Orbitrap XL from Thermo Scientific. m/z was measured between 50 – 400 mass range.

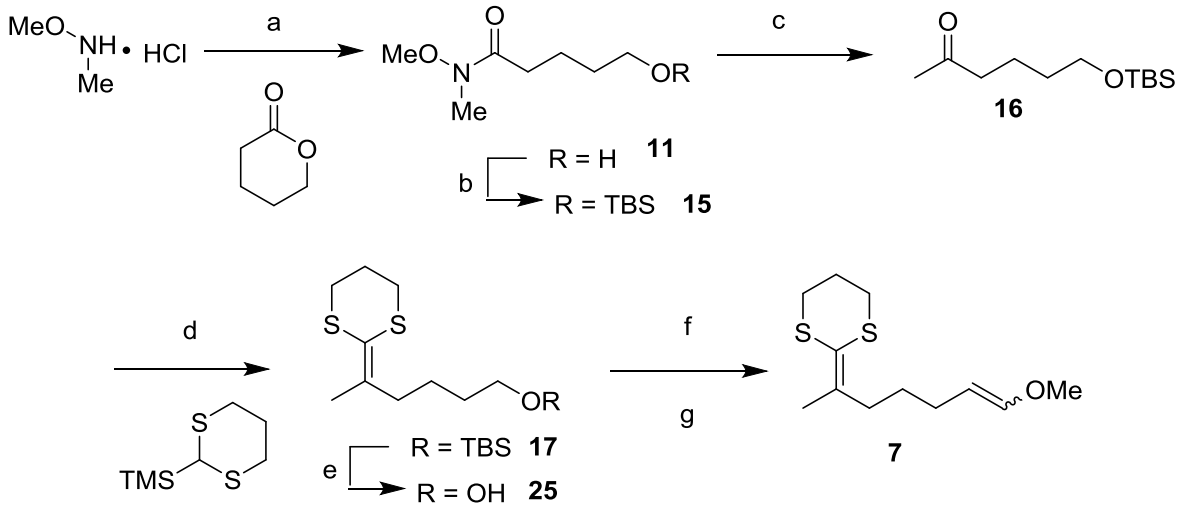

Figure 17. Conditions a) diisobutyl aluminum hydride, γ-valerolactone, saturated potassium sodium tartrate solution, b) imidazole, tertbutyl silyl chloride, c) methyl lithium, d) 2-trimethylsilyl-1,3-dithiane, n-butyl lithium, e) tetrabutyl ammonium fluoride, f) oxalyl chloride, dimethyl sulfoxide, triethylamine, g) (methoxymethyl)triphenyl phosphonium chloride, sec-butyl lithium.

Synthesis of 11. N,O-Dimethylhydroxylamine hydrochloride salt (5.000 grams, 51.26mmol) was submerged in benzene in round bottom flask. Benzene was evaporated off using rotary evaporator. The flask containing the salt was flushed with argon. 15mL of tetrahydrofuran was added to suspend the amine salt. The suspension was stirred in dry ice/acetone bath for 15 minutes. Diisobutyl aluminum hydride (Concentration 1.0 M, 1 equiv., 52.00mL) was added to the suspension dropwise to prevent quick evolution of hydrogen gas. Reaction flask was taken from dry ice/acetone bath and stirred at room temperature for 1 hour to give a clear, light yellow solution. Reaction flask was returned to dry ice/acetone bath to cool for 15 minutes before valerolactone (2.50g, 2.34mL, 24.7mmol) was added via syringe and needle. Reaction was stirred in dry ice/acetone bath for 30 minutes. Mixture was removed from dry ice/acetone bath to stir at room temperature for 1-3 hours. Work-up involved cooling the solution in dry ice/acetone bath again, dilution with hexane under open atmosphere, and quenching with saturated solution of sodium potassium tartrate (10mL). The quenched reaction was stirred open to air at room temperature overnight. Reaction showed two distinct layers: a clear upper layer and a cloudy bottom layer. Top layer was decanted off 3 times and dried over magnesium sulfate. **11** product was concentrated down on rotary evaporator.

IR (neat, cm^{-1}) 3384 (broad) 2939

^1H NMR (75 MHz, $CDCl_3$) δ 3.674 (s 3H), 3.63 (t, 2H, J = 6.2 Hz), 3.17 (s, 3H), 2.46 (t, 2H, J = 7.0) 1.73 (m, 2H, J = 7.2), 1.61 (m, 2H, J = 6.6 Hz)

HRMS (ESI) m/z: $[M+Na]^+$ Calcd for $C_7H_{13}NO_3$ 161.1052; Found 162.1120

Synthesis of 15. Imidazole (2.5 equivalents to alcohol, 3.75g) was weighed into round bottom flask. Flask was vacated and flushed with argon. Tetrahydrofuran (15mL) was added to flask to suspend the imidazole. The suspension was stirred in ice bath for 15 minutes to chill. In a separate

flask, starting alcohol **11** (3.55g) was dissolved in tetrahydrofuran and transferred over to the imidazole solution. Tert-butyl silyl chloride (1.1 equivalents, 3.6g) was placed in a flask. Flask was vacated and flushed with argon. Tetrahydrofuran was added to the flask to dissolve the silyl chloride. Tert-butyl silyl chloride solution transferred dropwise to reaction solution via syringe generated a cloudy mixture. Reaction was stirred at room temperature for 3 hours before being diluted with hexane. Water was added to quench reaction and dissolve white precipitate from during reaction. Work up solution was stirred for 30 minutes to give 2 layers: clear top layer and cloudy bottom layer. Top layer was decanted into separate flask 3 times and dried over magnesium sulfate. Magnesium sulfate was removed via fluted paper filtration method. Product **15** material was concentrated under rotary evaporator. Concentrated material was treated with hexane to crash out any remaining imidazole. Remaining imidazole was filtered off using fluted paper filter. Product **15** was concentrated back down under rotary evaporator.

IR (neat, cm^{-1}) 2989, 2856

^1H NMR (300 MHz, $CDCl_3$) δ 3.66 (s, 3H), 3.62 (t, 2H, J = 6.4 Hz), 3.17 (s, 3H), 2.44 (t, 2H, J = 7.4 Hz), 1.66 (m, 2H, J = 7.4 Hz), 1.56 (m, 2 H, J = 7.2 Hz)

Synthesis of 16. A round bottom flask was flame dried and vacated of air. The round bottom flask was flushed with argon. Starting material **15** (5.35g 19.4mmol) was dissolved with tetrahydrofuran and added to the round bottom flask. Solution stirred in ice bath for 30 minutes. Methyl lithium (2.00 equivalents, 12.1 mL) was added dropwise to the stirring solution. Reaction stirred for 3 hours. Reaction was quenched with water and diluted with hexane to give two clear layers. Top layer was decanted off 3 times and dried over magnesium sulfate. Magnesium sulfate was filtered of using fluted paper method. Ketone **16** was concentrated down under rotary evaporator.

IR (neat, cm^{-1}) 2829, 2857

^1H NMR (300 MHz, $CDCl_3$) δ 3.43 (t, 2H, J = 6.6 Hz), 2.44 (t, 2H, J = 7.4 Hz), 2.13 (s, 3H), 1.64 (m, 2H, 7.7 Hz), 1.52 (m, 2H, 7.2 Hz) 0.88 (s, 9H), 0.04 (s, 6H)

HRMS ESI m/z: $[M+Na]^+$ Calcd for $C_{12}H_{26}O_2Si$ 253.1594; Found 253.1582

Synthesis of 17. Round bottom flask vacated and flushed with argon. Dithiane (1.2 equivalent, 1.99 g, 1.96 mL) added to flask and dissolved in tetrahydrofuran (15mL). Solution was cooled in dry ice/acetone bath for 30 minutes. Solution was treated with n-butyl lithium (1.1 equivalent, 1.6 M, 6.50 mL). Reaction stirred for 1 hour before being removed from dry ice/acetone bath and stirred at room temperature for 30 minutes. While dithiane solution was stirring at room temperature, methyl ketone **16** (1.99g, 8.650 mmol) was dissolved in tetrahydrofuran. Dithiane solution was cooled in dry ice/acetone bath for 15 minutes. The methyl ketone solution was added to dithiane solution dropwise. Reaction was stirred overnight while allowing it to warm to room temperature. The reaction was quenched with water and diluted with hexane. Top layer decanted off 3 times and dried over magnesium sulfate. Magnesium sulfate filtered of using fluted paper filter method and material was concentrated under rotary evaporator. Ketene dithio acetal **17** purified via LC with diethyl ether (20%) in hexane or 1:3:13 DCM:EA:Hexane.

IR (neat, cm^{-1}) 2928, 2855

^1H NMR (300 MHz, $CDCl_3$) δ 3.61 (t, 2H, J = 6.3 Hz), 2.84 (m, 4H, J = 6.0 Hz), 2.36 (t, 2H, J = 7.1 Hz) 2.11 (t, 2H, J = 6.1), 1.90 (s, 3H), 1.53 (m, 2H, J =7.0), 1.26 (m, 2H, J = 7.7), 0.9 (s, 9H), 0.16(s, 6H)

HRMS (ESI) m/z: $[M+Na]^+$ Calcd for $C_{16}H_{32}OSiS_2$ 355.1556; Found 355.1541

Synthesis of 25. Round bottom flask flushed with argon. Ketene dithio acetal **17** (2.55 g, 8.62 mmol) added to flask and dissolved in tetrahydrofuran. Tetrabutylammonium fluoride (1M, 1.1 equivalent, 9.48mL) added to the stirring solution at room temperature. Reaction monitored by thin-layer chromatography. At completion, reaction was diluted with diethyl ether. Water used to quench reaction. Top layer was decanted off 3 times and dried over magnesium sulfate. Magnesium sulfate filtered off using fluted paper filter. Purified material **25** was attained by flushing material through a short silica plug.

IR (neat, cm^{-1}) 3456, 2928, 2855

HRMS (ESI) m/z: $[M+K]^+$ Calcd for $C_{10}H_{18}S_2O$ 257.0634; Found 257.0431

Synthesis of 7. Triphenyl phosphine (4 equiv, 4.30g) was suspended benzene in 100mL round bottom flask. Suspension was condensed under rotary evaporator and then placed under vacuum. Flask was flushed with argon. Tetrahydrofuran (15mL) was added to the flask. Mixture was stirred in dry ice/acetone bath for 30 minutes. While stiring in dry ice acetone bath, n-Butyl lithium (1.6 M in Hexane,7.84mL) was added dropwise to the mixture. Reaction flask was removed from dry ice acetone bath and stirred at room temperature for 30 minutes to give a deep red solution.

Oxalyl chloride was distilled under argon using a short distillation column. In a separate flask flushed with argon, dimethyl sulfoxide (2.4 equiv. 0.533 mL) was dissolved in tetrahydrofuran. Distilled oxalyl chloride (1.2 equiv., 0.322 mL) was transferred to DMSO solution. Solution was set to stir in dry ice/acetone bath for 15 minutes. Alcohol **25**(0.6825g, 3.13mmol) was dissolved with tetrahydrofuran and added to dimiethyl sulfoxide/oxalyl chloride (swern conditions) reaction flask. Triethylamine was added after 5 minutes. Reaction was stirred at room temperature for 3 hours to give a solution with a white precipitate. Reaction was diluted with hexane and filtered

through fluted paper filter. Filtered liquid was collected and concentrated down to approximately 10-15mLs in pear flask. Material was transferred to stirring phosphine solution. Reaction stirred at room temperature overnight. Reaction was quenched and diluted with hexane. Solution was filtered through cold silica plug to collect the majority of phosphine oxide material. Remaining phosphine oxide was removed via LC with diethyl ether (1%) in hexane. Product **7** was confirmed by H1 NMR.

^{1}H NMR (300 MHz, $CDCl_3$) δ 6.77 (d, 1H, J = 12.7 Hz), 5.86 (d, 1H, J = 6.4 Hz), 4.72 (m, 1H, J = 7.3 Hz), 4.34 (m, 1H, J = 7.6 Hz), 3.57 (s, 3H), 3.50 (s, 3H), 2.86 (t, 4H, J = 2.8 Hz), 2.35 (t, 2H, J = 6.3 Hz), 2.11 (m, 4H, J = 7.9 Hz), 1.93 (s, 3H), 1.45(m, 2H, J = 7.8 Hz)

Electrolysis of 7 Conditions used called for a solution containing $LiClO_4$ electrolyte (0.1 M), 2,6-Lutidine base (1 equiv.), and enol ether substrate **7** (0.282mmole) in 1:1 THF:MeOH solvent system. Electrolyte was added to a 3-neck round bottom flask and dissolved with tetrahydrofuran. To this solution, 2,6-lutidine was added via syringe. Electrolysis substrate was dissolved with methanol and added to mixture. Solution was sonicated for 1 minute and stirred in ice bath for 10 minutes. A platinum cathode and reticulated vitreous carbon anode were connected to reaction flask. Potentiostat was set to 6 mAmp and connected to reaction flask at the electrodes. Electrolysis was ran until 57.14 C had passed (2.1 F/mole) and monitored via thin layer chromatography. On completion, solution was diluted with hexane and quenched with a small amount of water. Top layer was extracted using separation funnel and hexane three times. Material was concentrated won using rotary evaporator. An internal NMR standard of 1,3,5-Trimethoxybenzene was used to determine yield with the crude material. 71.2% yield was calculated with the NMR standard. Purification was completed on column using 5-10% Et_2O in Hexane. Two dots were isolated off

the column. Both dots correspond to cyclized material. The first dot was shown to be non-hydrolyzed material with the dithiane intact while the second product was the hydrolyzed thioester and methyl ester.

Dithiane (**18)**

^{1}H NMR (300 MHz, $CDCl_3$) δ 4.95(broad s, 1H), 4.49 (s, 1H), 3.54 (s, 3H), 3.36 (s, 3H), 3.33(s, 3H), 2.97 (t, 2H, J = 9.9 Hz), 2.75 (t, 2H, J = 5.7 Hz), 2.22 (m, 2H, J = 9.3, 7.7, 2.7 Hz), 1.97 (m, 2H, J = 5.7, 4.7, 3.6 Hz), 1.84 (m, 2H, J = 13.2, 7.4, 3.4 Hz), 1.67 (m, 2H, J = 14.3, 6.8 Hz), 1.52 (m, 2H, J = 7.4, 6.9 Hz), 1.38 (m, 2H, J = 7.6, 6.5, 4.7, 3.1 Hz), 1.26 (s, 3H) 1.18(s, 3H)

^{13} C NMR (75 MHz, $CDCl_3$) δ 110.0, 109.0, 58.1, 57.7, 55.8, 54.6, 49.8, 41.7, 31.0, 30.5, 28.7, 26.9, 25.4, 25.0

Ester and Thioester (**19** and **20)**

^{1}H NMR (300 MHz $CDCl_3$) δ 4.50 (s, 1H), 4.37 (d, J =7.9 Hz , 0.40 H), 4.34 (d, J = 7.9 Hz, 0.55), 3.66 (s, 3H), 3.55 (s, 3H) 3.38 (d, J = 5.4 Hz, 3H), 3.28 (d, J = 5.8 Hz, 3H), 2.96 (m, J = 14.5, 8.8, 5.6 Hz, 2H), 2.79 (dq, J = 14.1, 5.5 Hz, 2H), 2.59 (m, J = 7.5, 3.4 Hz, 2H), 2.21 (dt, J = 12.7,7.9 Hz, 1H), 2.12 (m, J = 12.7, 4.8, 1H), 2.01 (m, J = 7.9, 6.1 5.5 Hz, 3H), 1.85 (m, J = 7.5, 7.2, 5.2 Hz, 3H), 1.53 (s, 3H), 1.40 (s , 3H), 1.28 (s, 3H), 1.24 (s, 3H), 1.21 (s, 3H)

Synthesis of Furan Substrate

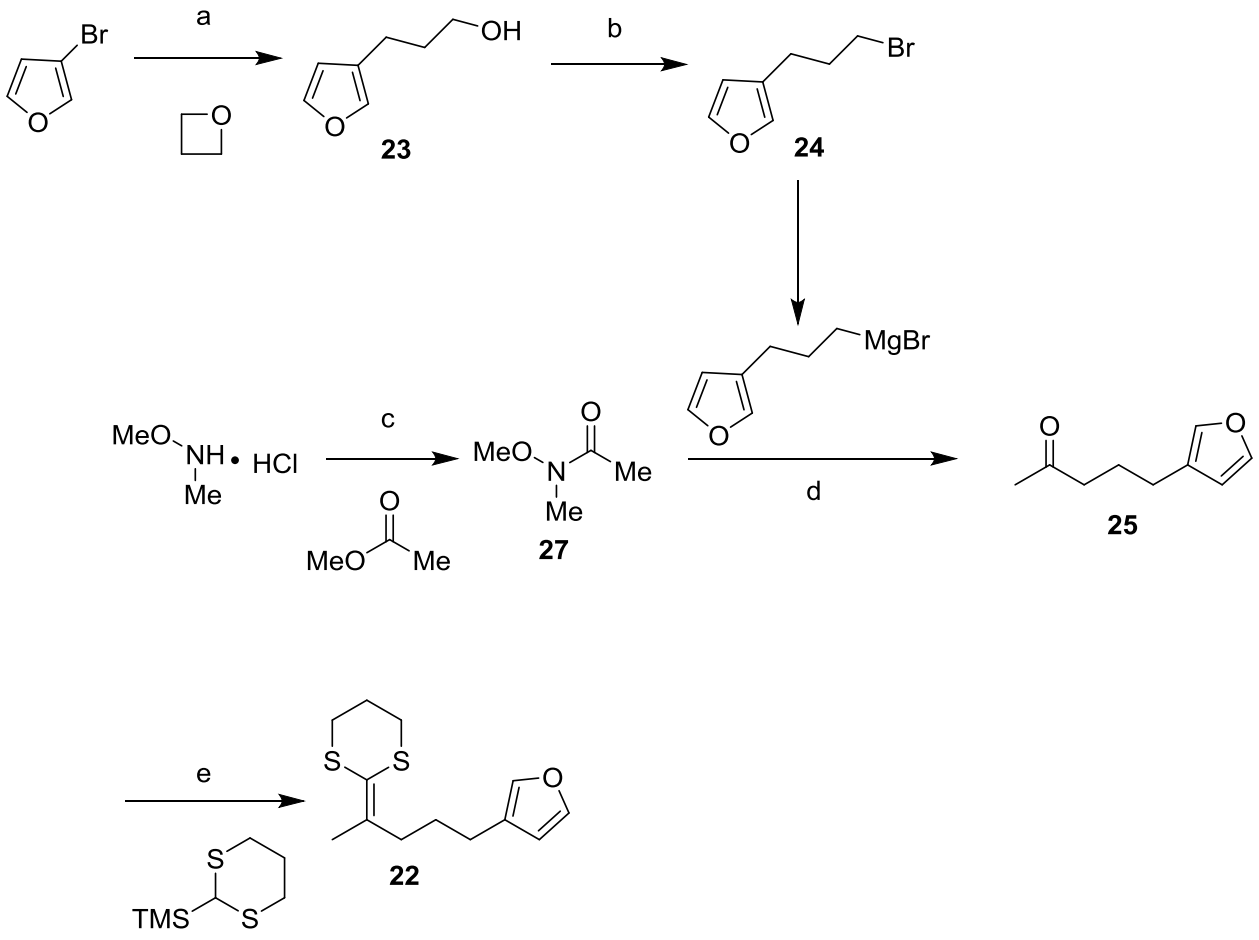

Figure 18. Conditions: a) n-butyllithium, trimethylene oxide, b) triphenyl phosphine, tetrabromomethane, c) DIBAL, Methoxymethl ester, d) Magnesium powder, I_2, e) n-butyllithium

Synthesis of 23. A round bottom flask was flame dried and flushed with argon. To this flask, 3-bromo furan (2.000g, 13.61mmol) was added. Tetrahydrofuran (15mL) was added to the flask to dissolve the bromofuran. Solution was stirred in dry ice/acetone bath in dewar for 30 minutes. n-Butyl lithium solution (1.6 M in hexane, 8.5 mL, 1.1 equivalents) was added dropwise to avoid radical polymerization and undesired deprotonation. Reaction was stirred while maintained in a dry ice ad acetone bath for 1 hour. Trimethylene oxide (1.15 equivalent, 0.910g, 1.02mL) was added dropwise. Immediately after, boron trifluoride etherate(1.25 equivalent, 2.41g, 2.10mL)

was added dropwise. Reaction stirred in dry ice acetone bath for 3 hours. Reaction was quenched with 5mL of a solution of saturated sodium bicarbonate while stirring in dry ice acetone bath. Reaction warmed to room temperature overnight.

Reaction was diluted with hexane and water. Organic layer was decanted off. Aqueous layer was washed twice with hexane. Collected material was dried over magnesium sulfate. Product **23** was concentrated under rotary evaporator. Product **23** was purified by column with ethyl acetate and hexane (1:1 mixture).

IR (neat, cm^{-1}) 3339(broad) 2936, 2861

^{1}H NMR (300 MHz, $CDCl_3$) δ 7.35 (s, 1H), 6.28(s, 1H), 3.68(t, 2H, J = 7.2 Hz), 2.52(t, 2H, J = 7.2 Hz), 1.83 (m, 2H, J = 7.2 Hz)

^{13}C NMR (75 MHz, $CDCl_3$) δ 145.5, 141.5, 127.0, 113.5, 64.9, 35.4, 23.6

HRMS (ESI) m/z: $[M]^+$ Calcd for $C_7H_{10}O_2$ 126.068; Found 126.069

Synthesis of 24. To a flame dried round bottom flask flushed with argon, Triphenyl phosphine(1.90 equiv., 2.41g) was suspended in 15mL of tetrahydrofuran. Suspension was stirred in dry ice and acetone bath for 15 minutes. Tetrabromomethane(1.40 equivalent, 2.25g) was added to the suspension and the mixture was stirred for 15 minutes. The solution was taken out of dry ice and acetone bath to warm to room temperature. Alcohol **23** was dissolved with 5mL THF and added to the stirring reaction solution. Reaction was set to reflux on heating mantle (30% power) under reflux column and argon atmosphere. Reflux continued overnight.

Reaction was diluted with hexane. A solid beige precipitate was filtered off using short silica plug and hexane. Product **24** was collected and concentrated under rotary evaporator. Purification was carried out with LC column and hexane neat.

IR (neat, cm^{-1}) 2932, 2854

^{1}H NMR (300 MHz, $CDCl_3$) δ 7.35(s,1H), 6.81 (s, 1H), 6.26(s, 1H) 3.40(t, 2H, J = 6.5 Hz), 2.59 (t, 2H, J = 7.3 Hz), 2.08 (m, 2H, J =6.7 Hz)

^{13} C NMR (75 MHz, $CDCl_3$) δ 145.6, 141.9, 113.4, 35.4, 25.7

HRMS (ESI) m/z: $[M]^+$ Calcd for C_7H_9OBr 187.98; Found 187.98

Synthesis of 27. N,O-dimethylamine hydrochloric salt (2.00 equivalents, 3.08 g 31.8 mmol) was suspended with benzene in round bottom flask. Benzene was evaporated off using rotary evaporator. The flask was then flushed with argon to give an inert atmosphere. Amine salt was suspended with 15 mL tetrahydrofuran. The suspension was then stirred in dry ice acetone bath for 30 minutes. Diisobutyl aluminum hydride was added to the amine salt suspension (2.0 equivalents, 1M in hexane, 31.8 mL) to generate the activated aluminum species. The solution was stirred, warming to room temperature, for 1 hour. The flask was then returned to the dry ice acetone bath to chill for 15 minutes. Methyl acetate (15.8 mmol, 1.17 g, 0.932 mL) was added to reaction and stirred for an additional 1 to 3 hours. The reaction was cooled in an ice bath and stirred for 20 minutes. The reaction was diluted with hexane, and then quenched with 10 mL of a saturated solution of potassium sodium tartrate. The solution was stirred open to air and overnight to give a two-phase solution. The top layer was decanted off and dried over magnesium sulfate. Process was repeated 3 times using hexane as wash. The combined layers were filtered through fluted paper funnel and then concentrated *in vacuo* with the use of a rotary evaporator. The material was carried on without further purification.

IR (neat, cm^{-1}) 3485 (broad), 2937

^{1}H NMR (300 MHz, $CDCl_3$) δ 3.65(s, 3H), 3.2 (s,3H), 2.1(s,3H)

Synthesis of 25. A flame dried flask was flushed with argon. Magnesium powder(1.0 equiv, 0.141g) was added to the flask and suspended in 2mL of tetrahydrofuran. Bromide **24** (1.08g, 5.7mmol) was dissolved with 2mL of THF and added to the magnesium suspension. Solution was sonicated approximately 5 minutes before being placed onto heating mantle (25%) to gentle reflux. Solution was refluxed until magnesium powder was completely consumed. Concentration of Grignard solution (1.4M) was checked by Watson and Eastham titration method.

In a separate flame dried flask, amide **27** was dissolved in tetrahydrofuran under argon. Solution was stirred in ice bath for 15 minutes. Grignard generated from bromide **24** was added to amide **27** solution. Reaction was stirred overnight at room temperature.

Reaction was diluted with hexane and water. Solution was stirred for 15 minutes. Top layer was decanted off and bottom layer was washed twice with hexane. Collected material was dried over magnesium sulfate. Magnesium sulfate was filtered of through fluted paper filter and concentrated under rotary evaporator.

IR (neat, cm^{-1}) 2930, 2857

^1H NMR (300 MHz, $CDCl_3$) δ 7.34 (s, 1H), 7.20 (s, 1H), 6.25 (s, 1H) 2.40(t, 2H, J = 7.1Hz), 2.15(s, 3H), 1.85(m, 2H, J = 7.3 Hz)

Synthesis of 22. Round bottom flask was flame dried and flushed with argon. 2-trimethylsilyl-1,3-dithiane (1.2 equivalent, 0.300g, 0.296mL) was added to flask and dissolved with 10mL THF. Solution was stirred in dry ice/acetone bath for 30 minutes. n-Butyl lithium solution (1.6 M in Hexane, 0.975mL, 1.2 equivalent) was added dropwise. Reaction was continued to stir in dry ice/acetone bath. After 30 minutes, dithiane solution was taken out of dry ice/acetone bath and allowed to warm to room temperature. After stirring at room temperature for 1 hour, reaction was

again placed into dry ice/acetone bath and allowed to stir for 15 minutes. Ketone **25** (0.1979g, 1.3mmol) dissolved in tetrahydrofuran and added dropwise. Reaction stirred overnight. Water was added to quench reaction. Reaction was diluted with hexane. Top layer was decanted off and aqueous layer was washed with hexane twice. Material was dried over magnesium sulfate and concentrated under rotary evaporator. Material was purified by distillation with kugelrohr distillation to give 50% yield.

^{1}H NMR (300 MHz, $CDCl_3$) δ 7.35(s, 1H), 7.23(s, 1H), 6.28(s,1H), 2.87 (t, 4H, J = 7.4) 2.41(m, 2H, J = 7.5 Hz), 2.12(t, 2H, J = 6.0 Hz), 1.91(s, 3H), 1.66(m, 2H)

^{13} C NMR (75 MHz, $CDCl_3$) δ 145.3, 141.4, 113.6, 38.3,33.7, 32.8, 30.8, 27.6, 27.2, 22.8

Electrolysis of **28**

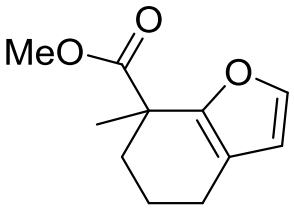

Figure 19. Electrolysis Product **28**

Optimized conditions used a solution of containing $LiClO_4$ electrolyte (1 M), 2,6-Lutidine base (1 equiv.), and substrate **22** (0.282mmole) in 20% MeOH/CH_2Cl_2 solvent system. Solution was sonicated for 1 minute and stirred in ice bath for 10 minutes. A platinum cathode and reticulated vitreous carbon anode were connected to reaction flask. Potentiostat was set to 60 mAmp and connected to reaction flask at the electrodes. Electrolysis was ran until 57.14 C had passed (2.1 F/mole). Solution was diluted with hexane and quenched with a small amount of water. Purification was conducted on column using hexane neat to give 31% of hydrolyzed methyl ester material **28**.

^{1}H NMR (300 MHz, $CDCl_3$) δ 7.30 (s,1H), 6.20(s,1H), 3.65(s,3H), 2.45(q, 2H, J = 5.34 Hz), 2.38 (m, 2H, J = 6.7 Hz), 1.8 (m, 2H, J = 2.7 Hz), 1.50(s, 3H) ppm.

^{13} C NMR (75 MHz, $CDCl_3$) δ 178.3, 153.3, 144.0, 120.6, 112.8, 54.9, 46.5, 38.6, 26.1, 24.86, 23.4 ppm

Reference List

[1] Graaf, M. 2015. "Manipulating Electron Transfer Reactions from Micro-to Preparative Scale." PhD Thesis. Washington University in St. Louis, St. Louis.

[2] Kauffman, G.; Fang, L; Purification of Copper (I) Iodide. *Inorganic Syntheses,* **1983,** *22*, 101

[3] Moeller, K.D.; Tinao, L.V; Intramolecular Anodic Olefin Coupling Reactions: The Use of Bis Enol Ether Substrates. *J. Am. Chem. Soc.,* **1992**, *114*, 1033.

[4] Feng, R.; Smith, J.A.; Moeller, K.D.; Anodic Cyclization Reactions and the Mechanistic Strategies that Enable Optimization. *Acc. Chem. Res.* **2017**, *50*, 2346.

[5] Smith, J.A.; Moeller, K.D.; Oxidative Cyclizations, the Synthesis of Aryl-Substituted C-Glycosides, and the Role of the Second Electron Transfer Step. *Organic Letters* **2013,** *15*, 5818.

[6] Wu, H.; Moeller, K.D.; Anodic Coupling Reactions: A Sequential Cyclization Route to the Arteannuin Ring Skeleton**.** *Organic Letters* **2007** *9*, 4599.

[7] Kotoku, N.;Fujioka, S.; Nakata, C.; Yamada, M.; Sumii, Y.; Kawachi, T.; Masayoshi, A.; Kobayashi, M.; Concise synthesis and structure-activity relationship of furospinosulin-1, a hypoxia-selective growth inhibitor from marine sponge. *Tetrahedron* **2011**, *67*, 6673.

[8] Schulz, L.; Waldvogel, S.R.; Solvent Control in Electro-Organic Synthesis. *Synlett* **2019,** *30*, 275.

Chapter 4: Future Directions

One of the first things that can be done to further the chemistry being developed is a study of how the use of an electron-rich allyl silane would alter the course of the reaction. At this point, the use of an allyl silane trapping group with a non-polar radical cation like the one derived from a ketene dithioacetal is not synthetically viable. Even with more polar enol ether derived radical

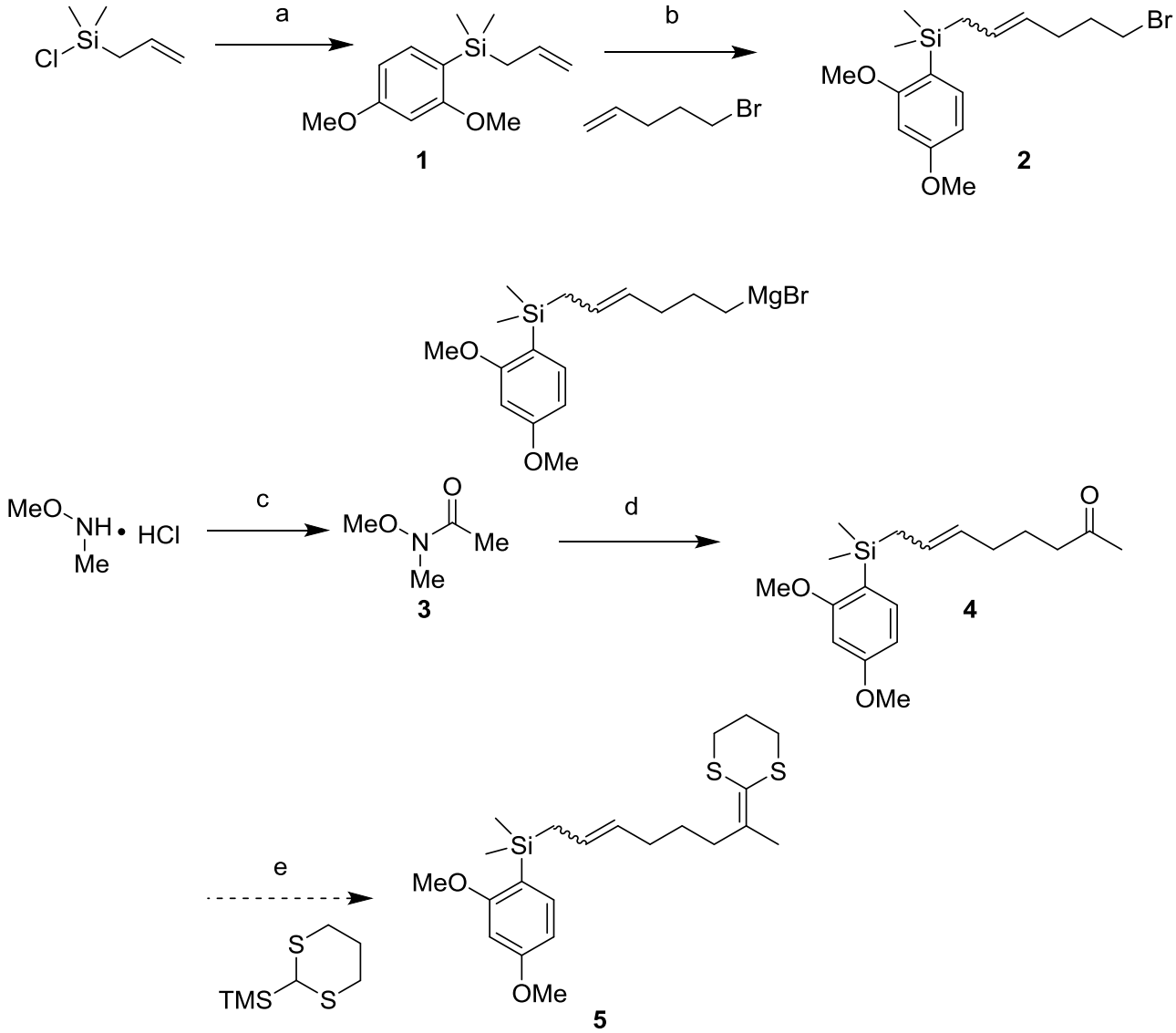

Scheme 1. Synthetic route towards electron rich allyl silane. Efforts towards this substrate have been taken over by Xi Wei in our lab.

cations, the allylsilane is not ideal. We have reached a point where we believe that we understand why this is the case in that the reactions appear to suffer from a slow second oxidation step. Chapter 2 explored the use cyclic voltammetry to ascertain the speed of the initial allyl silane cyclization. This result indicated that the initial cyclization worked well. The photochemical reactions, which never directly studied the allyl silane, exposed a similar reliance on the second oxidation for the enol ether and furan trapping groups suggesting that all oxidative cyclization reactions leading to new carbon-carbon bonds might require a fast second oxidation step. In fact, we argued that if the enol ether required the second oxidation to succeed, then the allyl silane would certainly struggle under the photoelectron transfer conditions and hence did not pursue it. Instead, an alteration to the nature of the allylsilane was suggested.

Scheme 1 shows a proposed synthesis of a substrate that would contain a variation of the allyl silane used above. In this case, the allylsilane would have an electron-donating dimethoxybenzyl group attached.[1] The increased electron density would decrease the oxidation potential of the radical generated after the first cyclization step. The expected effect would be a faster second oxidation step and hopefully an improved yield for the overall oxidative cyclzation. The reaction would be important

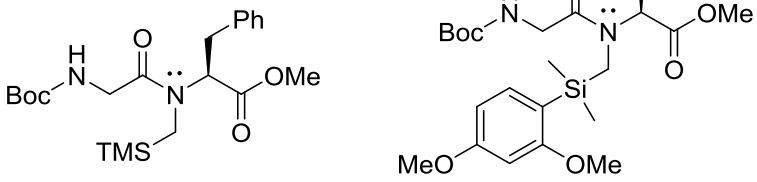

$E_{p/2}$: +1.63 V $E_{p/2}$: +1.38 V

Figure 1. Increasing electron density of allylsilane

[1] Yoshida, J.-i.; Watanabe, M.; Toshioka, H.; Imagawa, M.; Suga, S.; Selective electrochemical oxidation of heteroatom compounds having both silicon and tin on the same carbon as electroauxiliaries. J.*Electroanal. Chem*. **2001** ,507, 55.

in that it might lead to cyclized products with the efficiency of an enol ether while providing a different, very versatile synthetic handle for further development of the product. Similar chemistry has been utilized in our group before to selectively oxidize amides within a peptide chain. [2] Consider the two amides illustrated in Figure 1. Both utilize a neighboring silyl-substituent to lower the oxidation potential of the amide. Note the drastic drop in potential when changing this silyl electroauxiliary (a group that makes oxidation of a substrate more obtainable) from a trimethyl silyl group to the more electron rich moiety. The drop in potential associated with the more electron-rich allylsilane is 250 mV. If one compares the relationship between the amide lone pair and the silyl group in these examples with the position of the radical resulting from the cyclization relative to the silyl group (Figure 2), then it appears that this same ability to accelerate an oxidation step might apply to the second step of the cyclization.

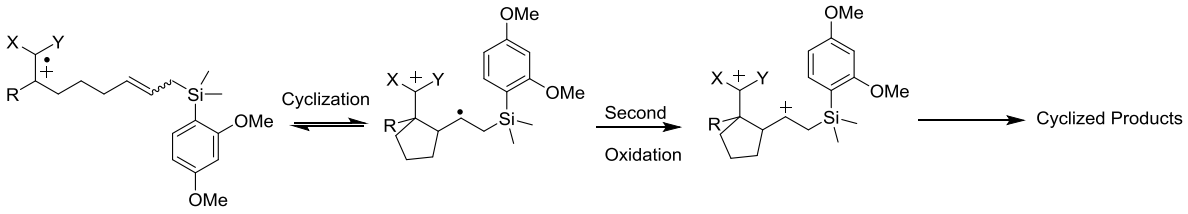

Figure 2. Electron Rich Allyl Silane. Note the similarity between the amide in Figure 1 and

With that in mind, I have been working on the synthesis of this substrate. The goal is to initially make the ketone intermediate because it can potentially be used to probe the use of the electron-rich allylsilane with a series of radical cation intermediates. Currently, the addition of the

[2] Sun, H.; Martin, C.; Kesselring, D.; Keller, R.; Moeller, K.; Building Functionalized Peptidomimetics: Use of Electroauxiliaries for Introducing N-Acyliminium Ions into Peptides. *J. Am. Chem. Soc.* **2006**, *128*, 13768.

Grignard reagent to the amide leads to a low yield, but there is hope that the reaction can be optimized or run on a large enough scale to proceed to the ketene dithio acetal. The synthesis of this material has been taken up by lab member Qiwei Jing.

Long Term Applications:

The ultimate goal of this project is to use what we learn about the mechanism of radical cation reactions and the relative reactivity of various nucleophiles toward the intermediates to develop a new approach for the synthesis of functionalized spirocyclic compounds. As can be seen from the initial competition studies in chapter 2, both end of the radical cation can be used in a synthetically productive manner.[3] Scheme 2 shows a possible route towards a spirocyclic compound that could be achieved through an anodic cyclization reaction with a sulfonamide and either enol ether or allyl silane trapping groups. Note how the mechanistic conclusions reached in Chapter 2 can be used to guide the nature of the product generated. Use of the faster trapping enol ether should lead to an initial carbon-carbon bond forming reaction relative to sulfonamide trapping. Use of the slower allylsilane group would

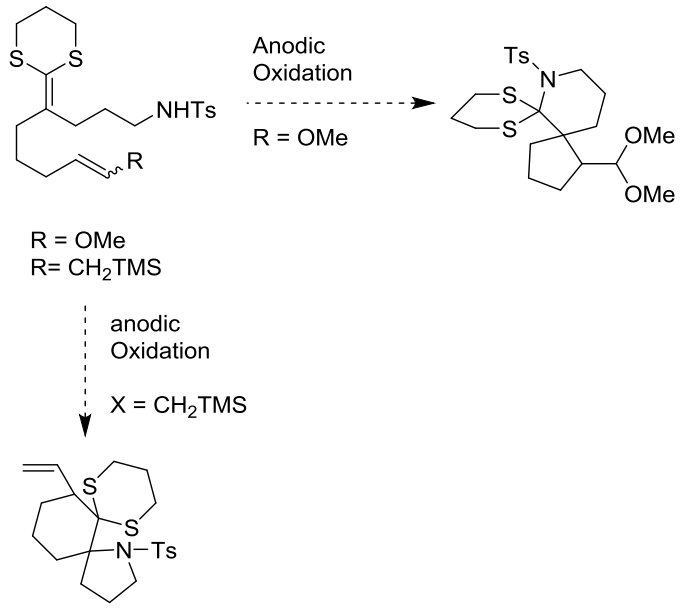

Scheme 2. Proposal for the use of electrosynthesis of spirocyclic compounds.

[3] Haibo, M.; Zizhen, Y.; Jiang, L.; Hailong, S.; Jianlin, H.; Recent Advances on the Electrochemical Difunctionalization of Alkenes/Alkynes. *Chinese Journal of Chemistry*. **2019**, *37*, 292.

lead to the opposite product. Future efforts would aim at demonstrating this relationship between our developing understanding of radical cation mechanisms and synthetic advances.

References

[1] Little, R.D.; Moeller, K. D.; Organic Electochemistry as a Tool for Synthesis: Umpolung Reactions, Reactive Intermediates, and the Design of New Synthetic Methods. *The Electrochemical Society – Interface* **2002**, *11*, 36

[2] Tang, F.; Chen, C.; Moeller, K.D.; Electrochemistry and Umpolung Reactions: New Tools for Solving Synthetic Challenges of Structure and Location. *Synthesis* **2007**, 3411.

[3] Miller, A. K.; Hughes, C. C.; Kennedy-Smith, J. J.; Gradl, S. N.; Trauner, D.; Total synthesis of (−)-heptemerone B and (−)-guanacastepene E. *J. Am. Chem. Soc.* **2006**, *128*, 17057.

[4] Ding, H.; DeRoy, P. L.; Perreault, C.; Larivee, A.; Siddiqui, A.; Caldwell, C. G.; Harran, S.; Harran, P. G.; Electrolytic macro- cyclizations: Scalable synthesis of a diazonamide-based drug development candidate. *Angew. Chem., Int. Ed.* **2015**, *54*, 4818.

[5] Badalyan, A.; Stahl, S. S.; Cooperative Electrocatalytic Alcohol Oxidation with Electron-Proton-Transfer Mediators. *Nature* **2016**, *535*, 406.

[6] Rafiee, M.; Miles, K. C.; Stahl, S. S.; Electrocatalytic alcohol oxidation with TEMPO and bicyclic nitroxyl derivatives: Driving force trumps steric effects. *J. Am. Chem. Soc.* **2015**, *137*, 14751.

[7] Wheeldon, I.; Minteer, S.D.; Banta, S.; Barton, C.; Atanassov, P.; Sigman, M.; Substrate channeling as an approach to cascade reactions. *Nature Chemistry* **2016**, *8*, 299.

[8] Hickey, D.P.; Schiedler, D.; Matanovic, I.; Doan, P.; Atanassov, P.; Minteer S.D.; Sigman, M.; Predicting Electrocatalytic Properties: Modeling Structure-Activity Relationships of Nitroxyl Radicals. *J. Am. Chem. Soc.* **2015**, *137*, 16179.

[9] Sevov, C. S.; Hickey, D. P.; Cook, M. E.; Robinson, S. G.; Barnett, S.; Minteer, S. D.; Sigman, M. S.; Sanford, M. S.; Physical Organic Approach to Persistent, Cyclable, Low-Potential Electrolytes for Flow Battery Applications. *J. Am. Chem. Soc*. **2017**, *139*, 2924.

[10] Kawamata, Y.; Yan, M.; Liu, Z.; Bao, D-H.; Chen, J.; Starr, J.T.; Baran, P.S.; Scalable, Electrochemical Oxidation of Unactivated C-H Bonds**.** *J. Am. Chem. Soc.* **2017**, *139*, 7448.

[11] Horn, E. J.; Rosen, B. R.; Chen, Y.; Tang, J.; Chen, K.; Eastgate, M. D.; Baran, P. S.; Scalable and sustainable electrochemical allylic C− H oxidation. *Nature* **2016**, *533*, 77.

[12] Rosen, B. R.; Werner, E. W.; O'Brien, A. G.; Baran, P. S.; Total synthesis of dixiamycin B by electrochemical oxidation. *J. Am. Chem. Soc.* **2014**, *136*, 5571.

[13] O'Brien, A. G.; Maruyama, A.; Inokuma, Y.; Fujita, M.; Baran, P. S.; Blackmond, D. G.; Radical C−H functionalization of heteroarenes under electrochemical control. *Angew. Chem., Int. Ed.* **2014**, *53*, 11868.

[14] Zhao, H.-B.; Liu, Z.-J.; Song, J.; Xu, H.-C.; Reagent-Free C–H/N–H Cross-Coupling: Regioselective Synthesis of *N*-Heteroaromatics from Biaryl Aldehydes and NH_3**.** *Angew. Chem. Int. Ed.* **2017**, *129*, 12732.

[15] Hou, Z.-W.; Mao, Z.-Y.; Song, J.; Xu, H.-C.; Electrochemical Synthesis of Polycyclic N-Heteroaromatics through Cascade Radical Cyclization of Diynes. *ACS Catal.* **2017**, *7*, 5810.

[16] Wu, Z.-J.; Xu, H.-C.; Synthesis of C3-Fluorinated Oxindoles Through Reagent-Free Cross Dehydrogenative-Coupling**.** *Angew. Chem. Int. Ed.* **2017**, *56*, 4734.

[17] Xiong, P., Xu, H.-H. and Xu, H.-C. Metal- and Reagent-Free Intramolecular Oxidative Amination of Tri- and Tetrasubstituted Alkenes. *J. Am. Chem. Soc.* **2017**, *139*, 2956.

[18] Zhao, H.-B.; Hou, Z.-W; Liu, Z.-J.; Zhou, Z.-F.; Song, J.; Xu, H.-C.; Amidinyl Radical Formation by Anodic N–H Bond Cleavage and Its Application in Aromatic C–H Bond Functionalization. *Angew. Chem. Int. Ed*. **2017**, *56*, 587.

[19] Fu, N.; Sauer, G. S.; Saha, A.; Loo, A; Lin, S.; Metal-catalyzed electrochemical diazidation of alkenes. *Science* **2017**, *357*, 575.

[20] Moeller, K.D.; Intramolecular Carbon-Carbon Bond Forming Reactions at the Anode. Moeller, K. D. *Topics in Current Chemistry* **1997**, *185*, 49.

[21] Moeller, K.D.; Synthetic Applications of Anodic Electrochemistry. *Tetrahedron* **2000**, *56*, 9527.

[22] Sperry, J. B.; Wright, D. L.; The Application of Cathodic Reductions and Anodic Oxidations in the Synthesis of Complex Molecules. *Chem. Soc. Rev.* **2006**, *35*, 605.

[23] Yoshida, J.; Kataoka, K.; Horcajada, R.; Nagaki, A.; Modern Strategies in Electroorganic Synthesis. *Chem. Rev.* **2008**, *108*, 2265.

[24] Wu, H.; Moeller, K.D.; Anodic coupling reactions: a sequential cyclization route to the arteannuin ring skeleton. *Org. Lett.* **2007**, *9*, 4599.

[25] Miller, L. L.; Stermitz, F. R.; Flack, J. R.; Electrooxidative cyclization of 1-benzyltetrahydroisoquinolines. Novel nonphenol coupling reaction. *J. Am. Chem. Soc.* **1973**, *95*, 2651.

[26] Liu, B.; Duan, S.; Sutterer, A.C.; Moeller, K.D. *J. Am. Chem. Soc.* **2002,** *124*, 10101,

[27] Hai-Chao Xu and Kevin D. Moeller *Angew. Chem. Int. Ed. Eng.* **2010**, *49*. 8004.

[28] IKA. (2019) ElectraSyn 2.0

[29] Tang, F.; Moeller, K.D.; Anodic oxidations and polarity: exploring the chemistry of olefinic radical cations. *Tetrahedron* **2009,** *65*, 10863.

[30] Lips, S.; Waldvogel, S.R.; Use of Boron-Doped Diamond Electrodes in Electro-Organic Synthesis. *Chem Electro Chem* **2019,** *6*, 1649.

[31] Schulz, L.; Waldvogel, S.R.; Solvent Control in Electro-Organic Synthesis. *Synlett* **2019**, *30*, 275.

[32] Huang, Y.; Moeller, K.D.; Anodic cyclization reactions: probing the chemistry of N,O-ketene acetal derived radical cations. *Tetrahedron* **2006**, *62*, 6536.

[33] Xu, G.; Moeller, K.D.; Anodic Coupling Reactions and the Synthesis of C-Glycosides. *Organic Letters* **2010,** *12*, 2590.

[34] Redden, A.; Moeller, K.D.; Anodic Coupling Reactions: Exploring the Generality of Curtin-Hammett Controlled Reactions. *Org. Lett.* **2011**, *13*, 1678.

[35] Campbell, J. 2013 'Anodic Olefin Coupling Reactions: Experimental and Computational Methods for Investigating the Intramolecular Cyclization Reactions of Electrooxidatively-Generated Radicals and Radical Cations' PhD Thesis, Washington University in St. Louis, St. Louis.

[37] Campbell. J.M.; Xu, H.;Moeller, K.D.; Investigating the Reactivity of Radical Cations: Experimental and Computational Insights into the Reactions of Radical Cations with Alcohol and p-Toluene Sulfonamide Nucleophiles. *J. Am. Chem. Soc.* **2012**, *134*, 18338.

[38] Campbell, J.M.; Smith, J.A.; Gonzalez, L.; Moeller, K.D. Competition studies and the relative reactivity of enol ether and allylsilane coupling partners toward ketene dithioacetal derived radical cations. *Tetrahedron Letters*, **2015,** *56*, 3595.

[39] Xu, H-C.; Moeller, K.D.; Intramolecular Anodic Olefin Coupling Reactions: Use of the Reaction Rate to Control Substrate/Product Selectivity. *Angew. Chem. Int. Ed.* **2010,** *49*, 8004.

[40] Graaf, M. 2015. "Manipulating Electron Transfer Reactions from Micro-to Preparative Scale." PhD Thesis. Washington University in St. Louis, St. Louis.

[41] Kauffman, G.; Fang, L; Purification of Copper (I) Iodide. *Inorganic Syntheses*, **1983**, *22*, 101

[42] Moeller, K.D.; Tinao, L.V; Intramolecular Anodic Olefin Coupling Reactions: The Use of Bis Enol Ether Substrates. *J. Am. Chem. Soc.*, **1992**, *114*, 1033.

[43] Feng, R.; Smith, J.A.; Moeller, K.D.; Anodic Cyclization Reactions and the Mechanistic Strategies that Enable Optimization. *Acc. Chem. Res.* **2017**, *50*, 2346.

[44] Smith, J.A.; Moeller, K.D.; Oxidative Cyclizations, the Synthesis of Aryl-Substituted C-Glycosides, and the Role of the Second Electron Transfer Step. *Organic Letters* **2013**, *15*, 5818.

[45] Wu, H.; Moeller, K.D.; Anodic Coupling Reactions: A Sequential Cyclization Route to the Arteannuin Ring Skeleton**.** *Organic Letters* **2007** *9*, 4599.

[46] Kotoku, N.;Fujioka, S.; Nakata, C.; Yamada, M.; Sumii, Y.; Kawachi, T.; Masayoshi, A.; Kobayashi, M.; Concise synthesis and structure-activity relationship of furospinosulin-1, a hypoxia-selective growth inhibitor from marine sponge. *Tetrahedron* **2011**, *67*, 6673.

[47] Schulz, L.; Waldvogel, S.R.; Solvent Control in Electro-Organic Synthesis. *Synlett* **2019,** *30*, 275.

[1] Yoshida, J.-i.; Watanabe, M.; Toshioka, H.; Imagawa, M.; Suga, S.; Selective electrochemical oxidation of heteroatom compounds having both silicon and tin on the same carbon as electroauxiliaries. J.*Electroanal. Chem*. **2001** ,*507*, 55.

[2] Sun, H.; Martin, C.; Kesselring, D.; Keller, R.; Moeller, K.; Building Functionalized Peptidomimetics: Use of Electroauxiliaries for Introducing N-Acyliminium Ions into Peptides. *J. Am. Chem. Soc.* **2006**, *128*, 13768.

[3] Haibo, M.; Zizhen, Y.; Jiang, L.; Hailong, S.; Jianlin, H.; Recent Advances on the Electrochemical Difunctionalization of Alkenes/Alkynes. *Chinese Journal of Chemistry.* **2019**, 37, 292.

Spectral Data

This section contains the ^{1}H NMR, ^{13}C NMR, and other NMR Data for the substrates I personally synthesized. They are arranged by chapter.

Chapter 2

This section contains NMR spectra for substrates I personally synthesized in chapter 2.

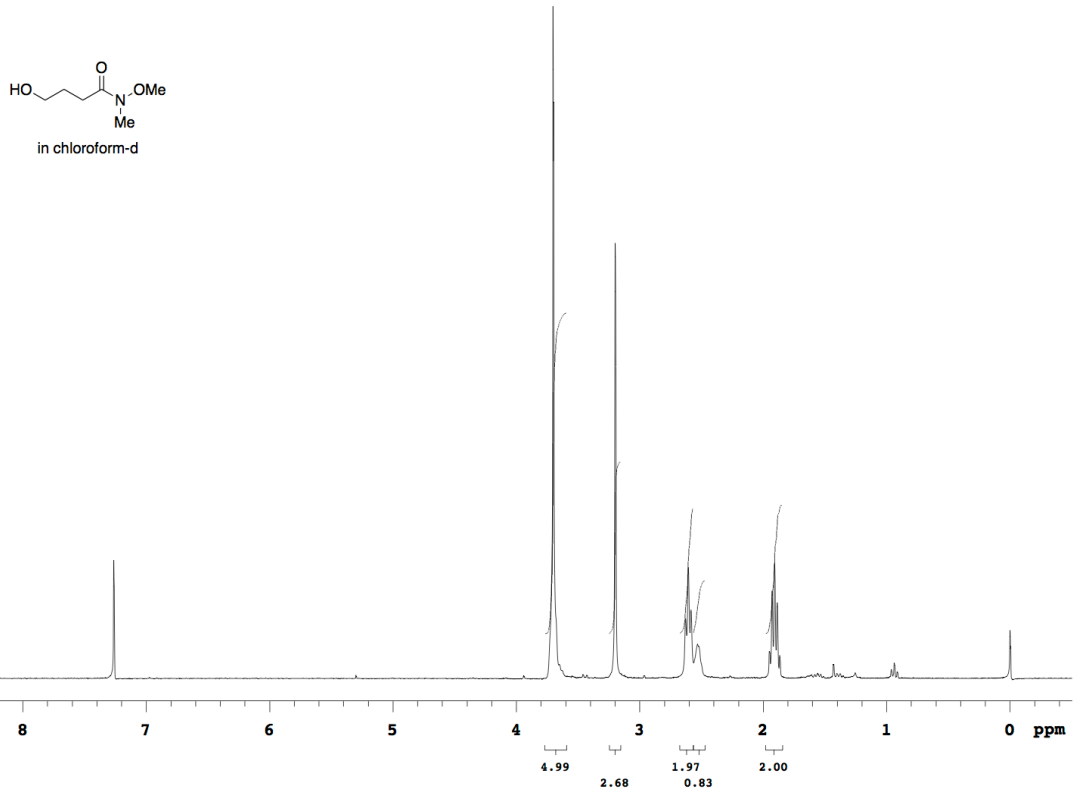
HO
O
N
OMe
Me
in chloroform-d
8
7
6
5
4
3
2
1
0
ppm
4.99
2.68
1.97
0.83
2.00

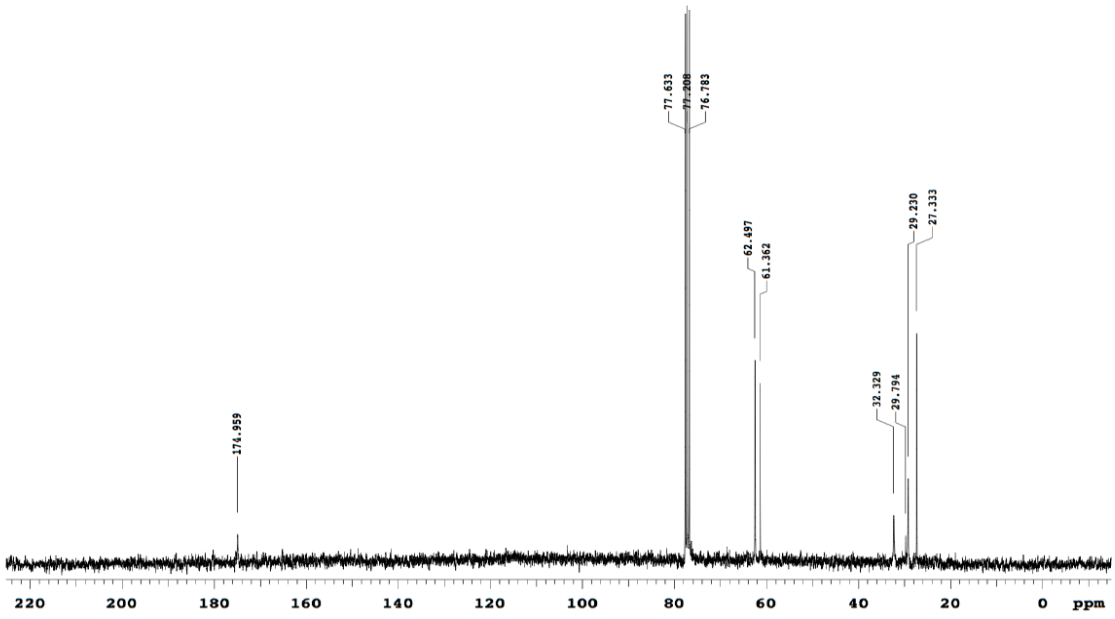
77.633
77.208
76.783
62.497
61.362
32.329
29.794
29.230
27.333
174.959
220
200
180
160
140
120
100
80
60
40
20
0
ppm

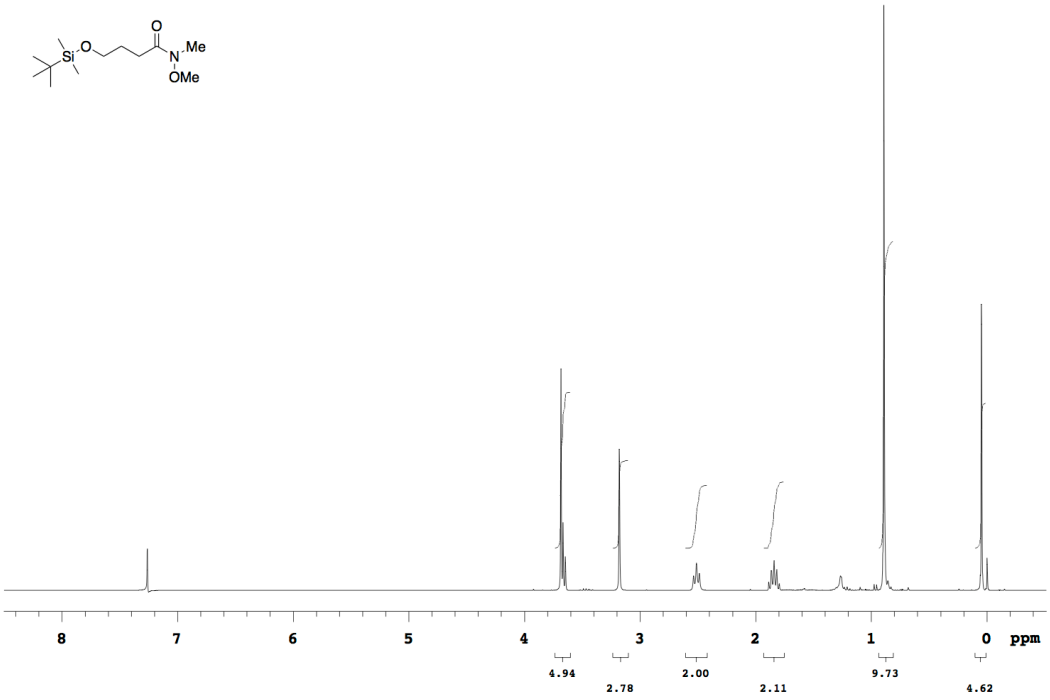
Si
O
N
Me
OMe
8
7
6
5
4
3
2
1
0
ppm
4.94
2.78
2.00
2.11
9.73
4.62

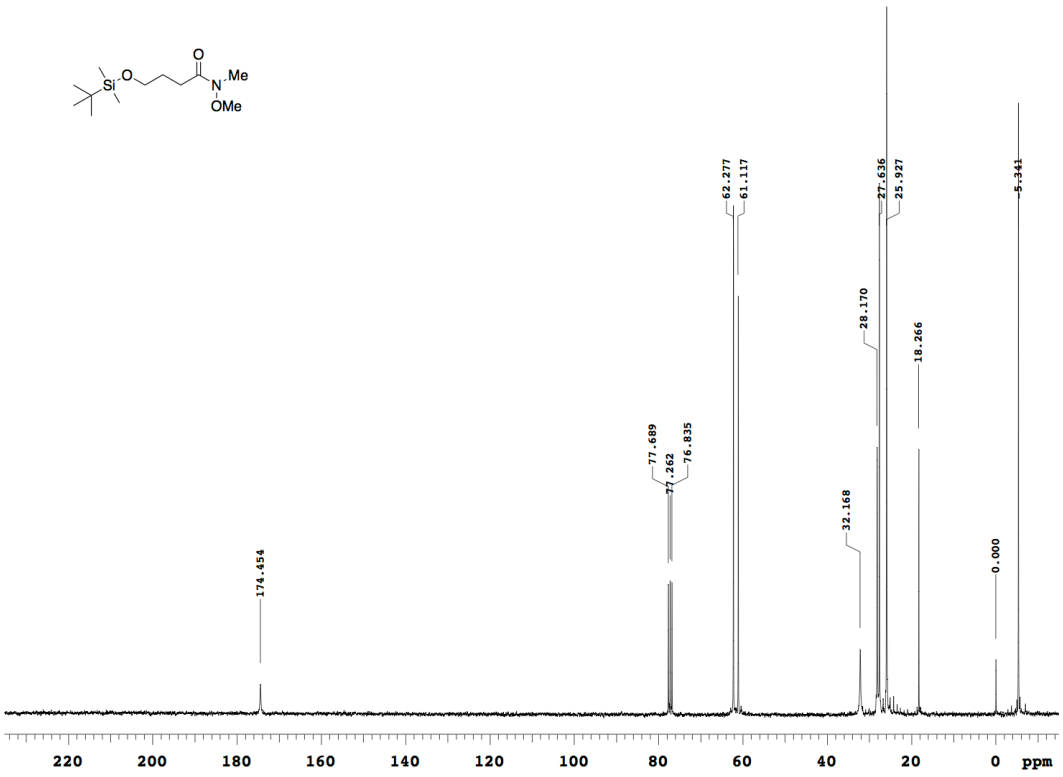
Si
O
N
Me
OMe
174.454
77.689
77.262
76.835
62.277
61.117
32.168
28.170
27.636
25.927
18.266
0.000
-5.341
220
200
180
160
140
120
100
80
60
40
20
0
ppm

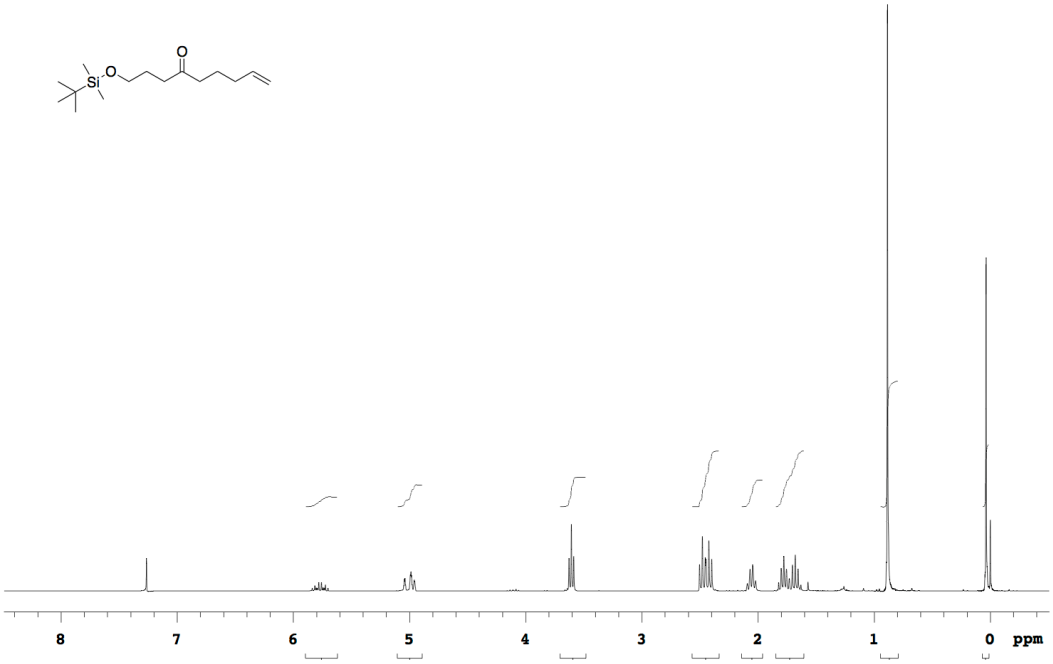
O
Si
O
8
7
6
5
4
3
2
1
0
ppm

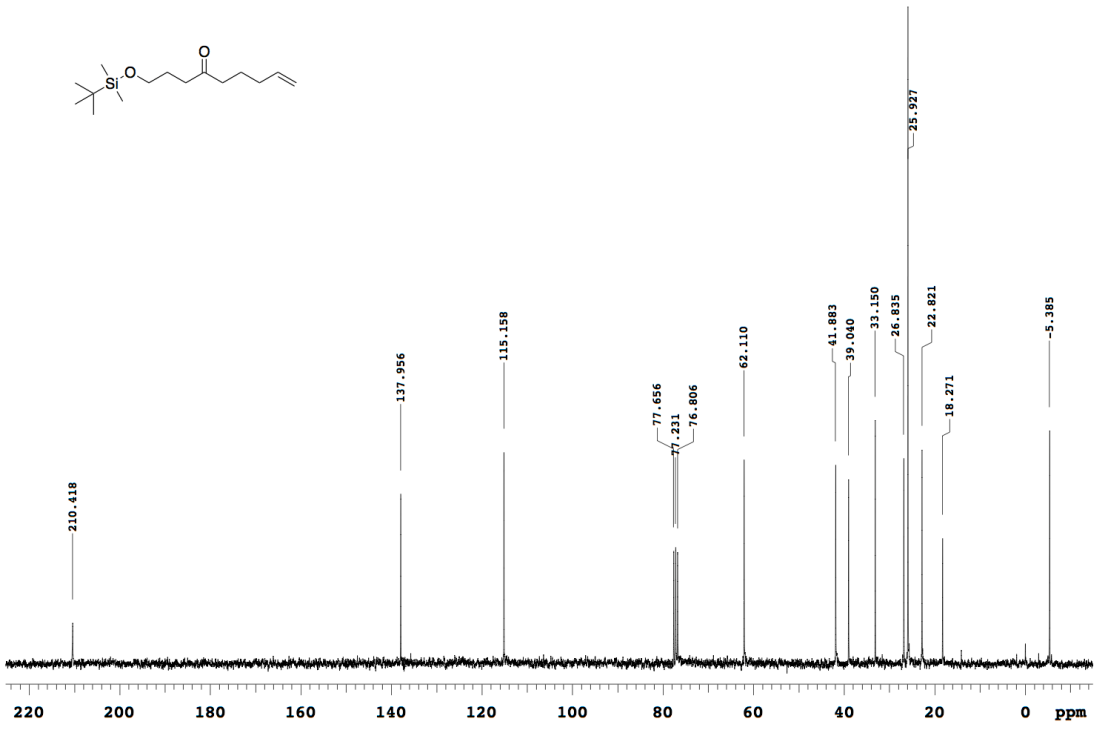
O
Si
O
210.418
137.956
115.158
77.656
77.231
76.806
62.110
41.883
39.040
33.150
26.835
25.927
22.821
18.271
-5.385
220
200
180
160
140
120
100
80
60
40
20
0
ppm

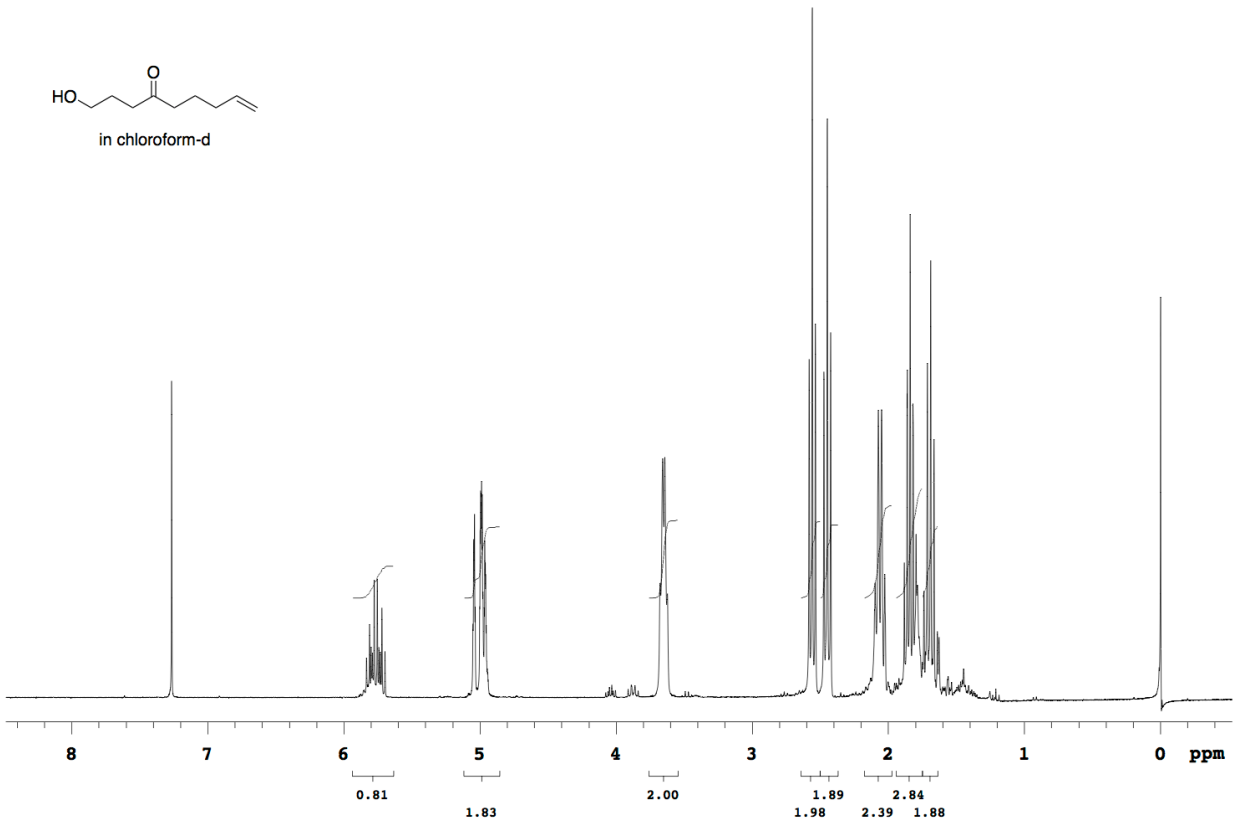
HO
O
in chloroform-d
8
7
6
5
4
3
2
1
0
ppm
0.81
1.83
2.00
1.89
1.98
2.84
2.39
1.88

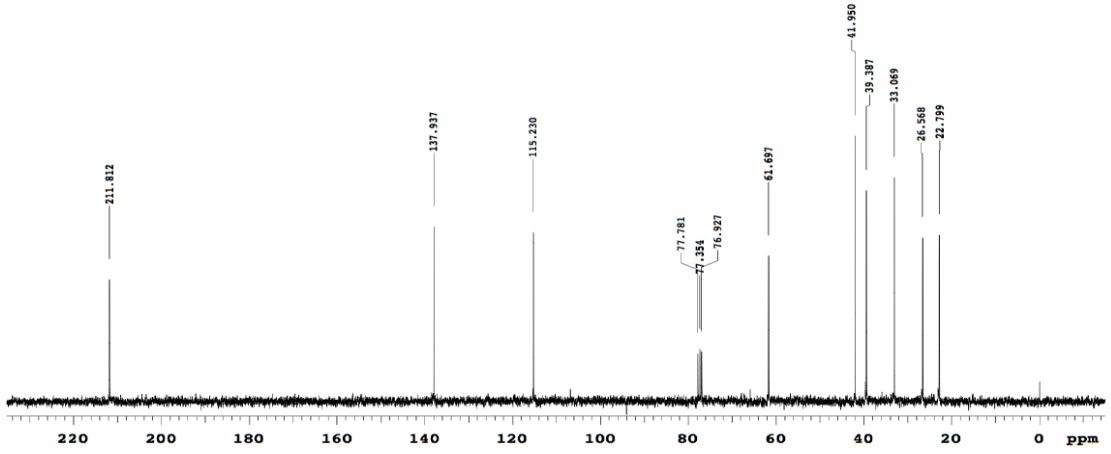
211.812
137.937
115.230
77.781
77.354
76.927
61.697
41.950
39.387
33.069
26.568
22.799
220
200
180
160
140
120
100
80
60
40
20
0
ppm

Chapter 3.

This section contains NMR spectra for substrates I personally synthesized in chapter 3.

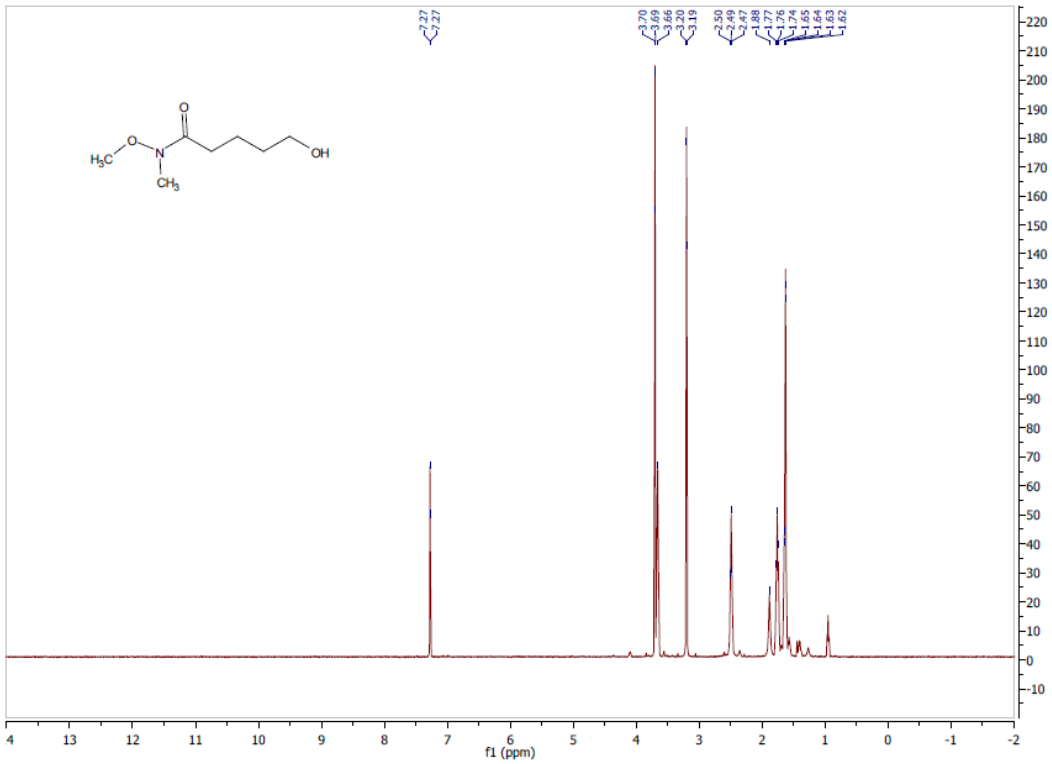
7.27
7.27
3.70
3.69
3.66
3.20
3.19
2.50
2.49
2.47
1.88
1.77
1.76
1.74
1.65
1.64
1.63
1.62
O
O
N
H3C
CH3
OH
f1 (ppm)

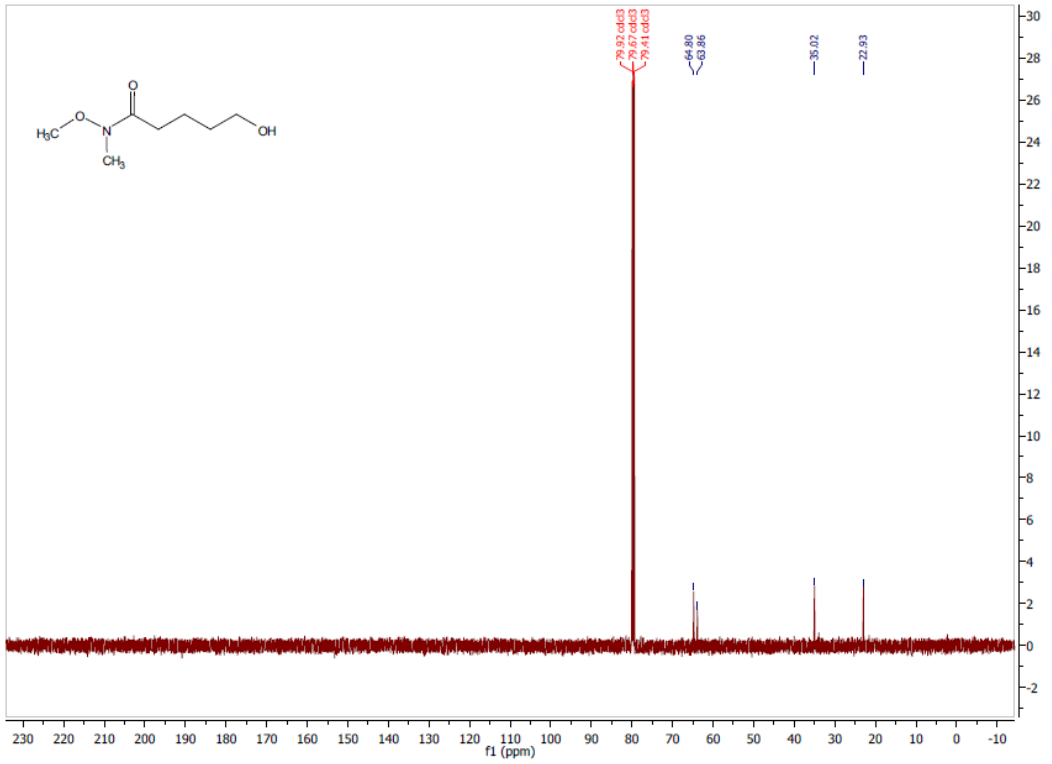
79.92 cdcl3
79.67 cdcl3
79.41 cdcl3
64.80
63.86
35.02
22.93
O
O
N
H3C
CH3
OH
f1 (ppm)

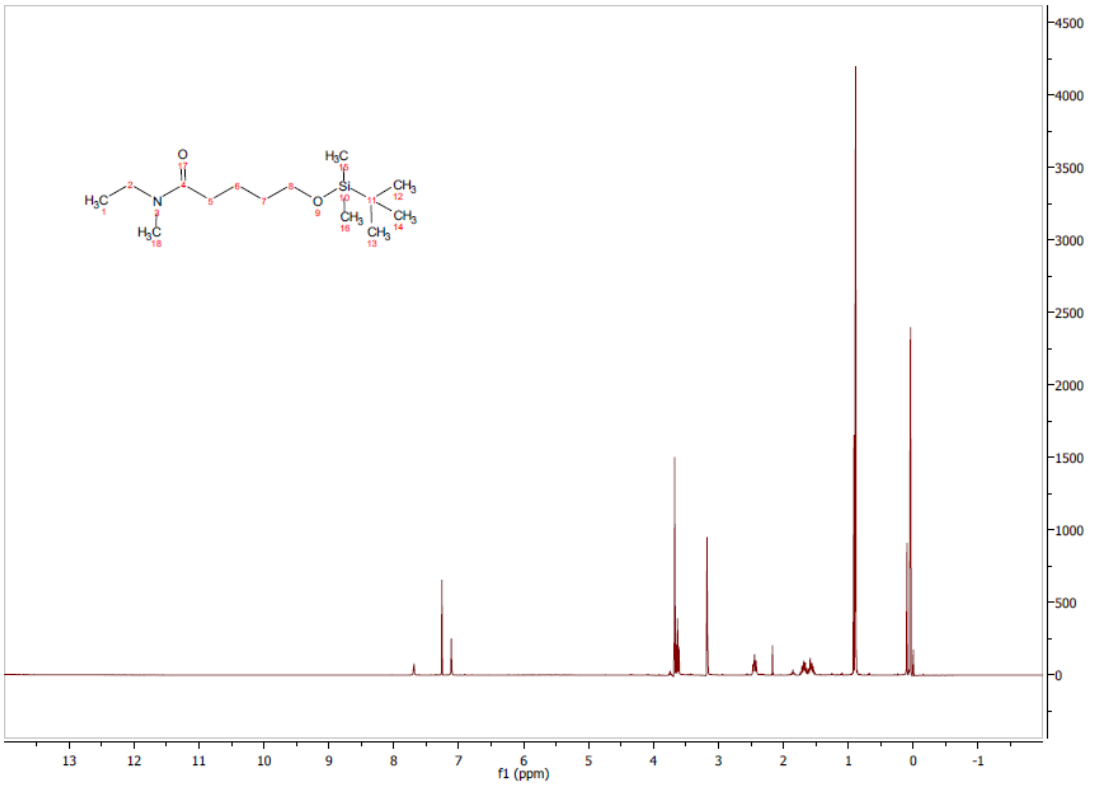
f1 (ppm)

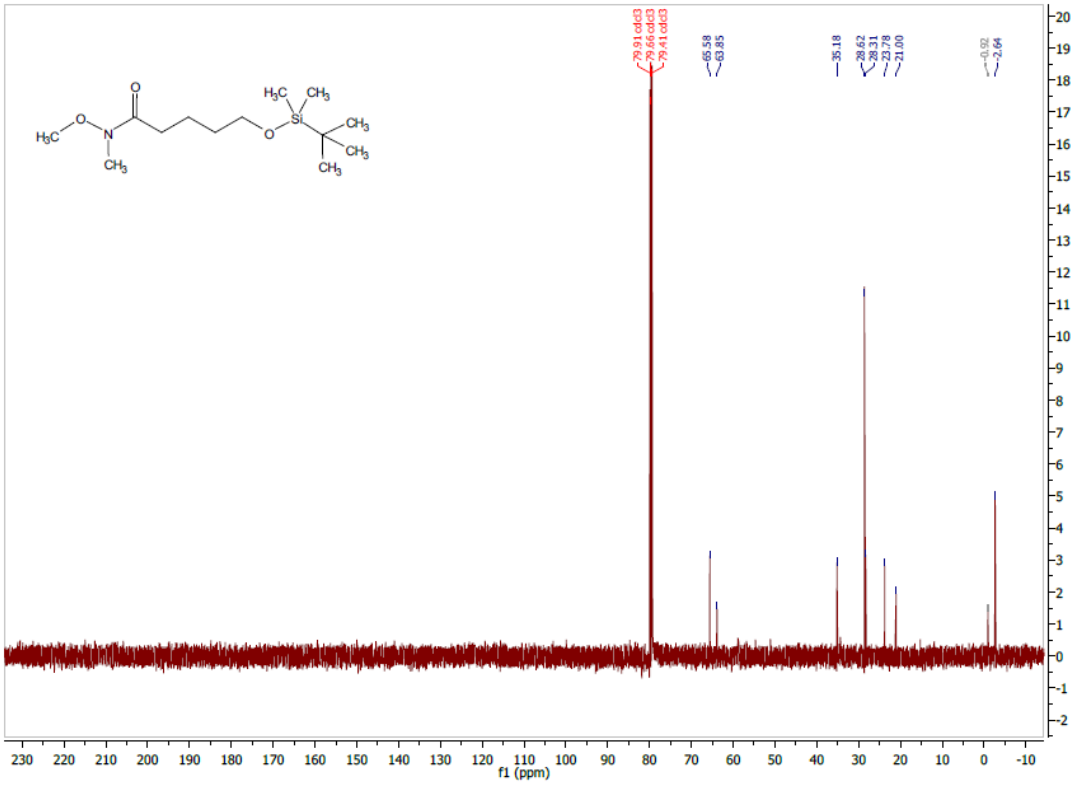
79.91 cdcl3
79.66 cdcl3
79.41 cdcl3
65.58
63.85
35.18
28.62
28.31
23.78
21.00
-0.02
-2.64
f1 (ppm)

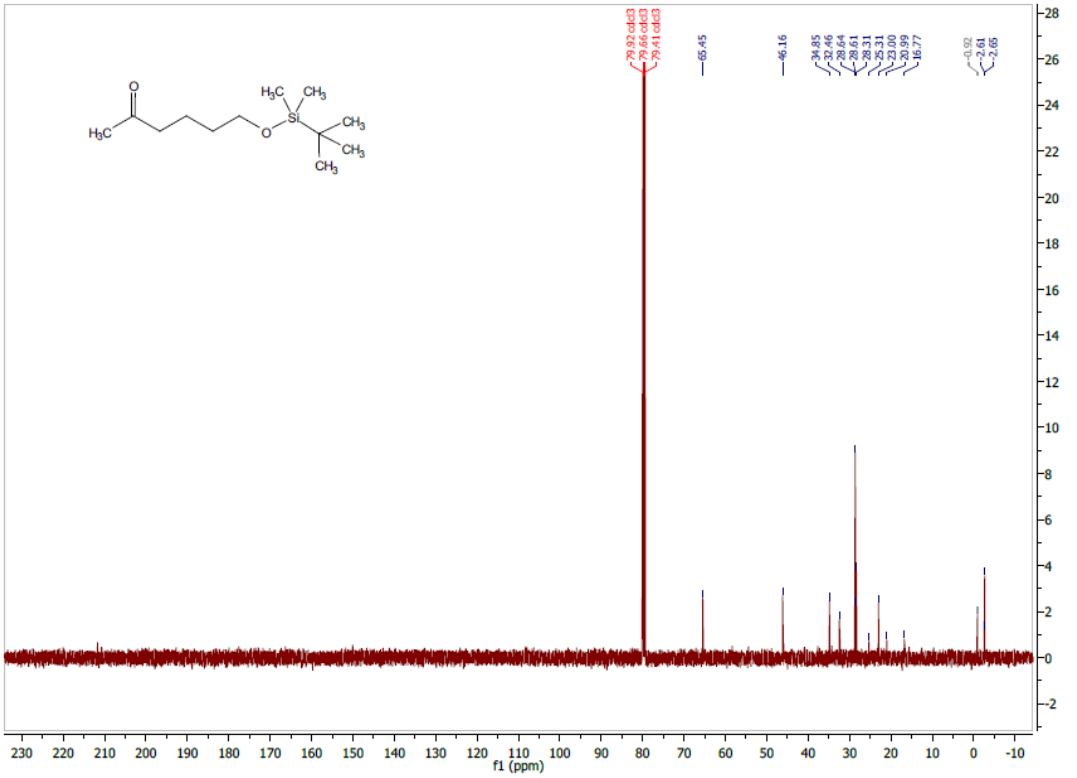
79.92 cdcl3
79.66 cdcl3
79.41 cdcl3
65.45
46.16
34.85
32.46
28.64
28.61
28.31
25.31
23.00
20.99
16.77
-0.02
-2.61
-2.65
f1 (ppm)

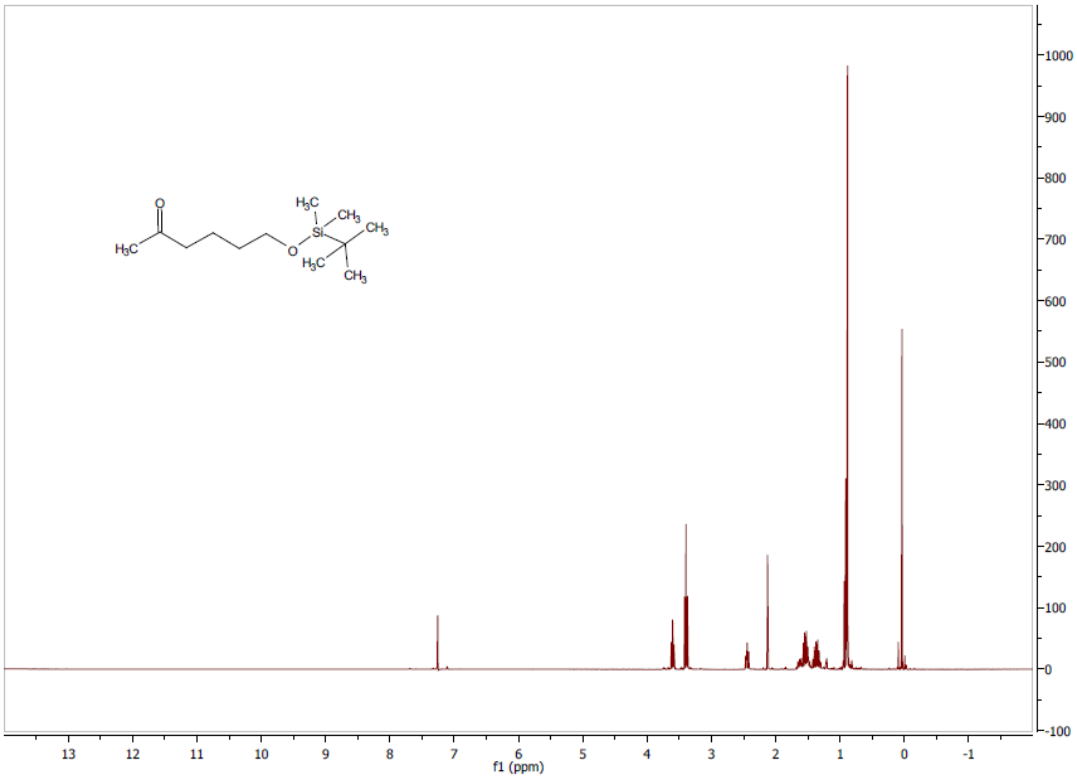
f1 (ppm)

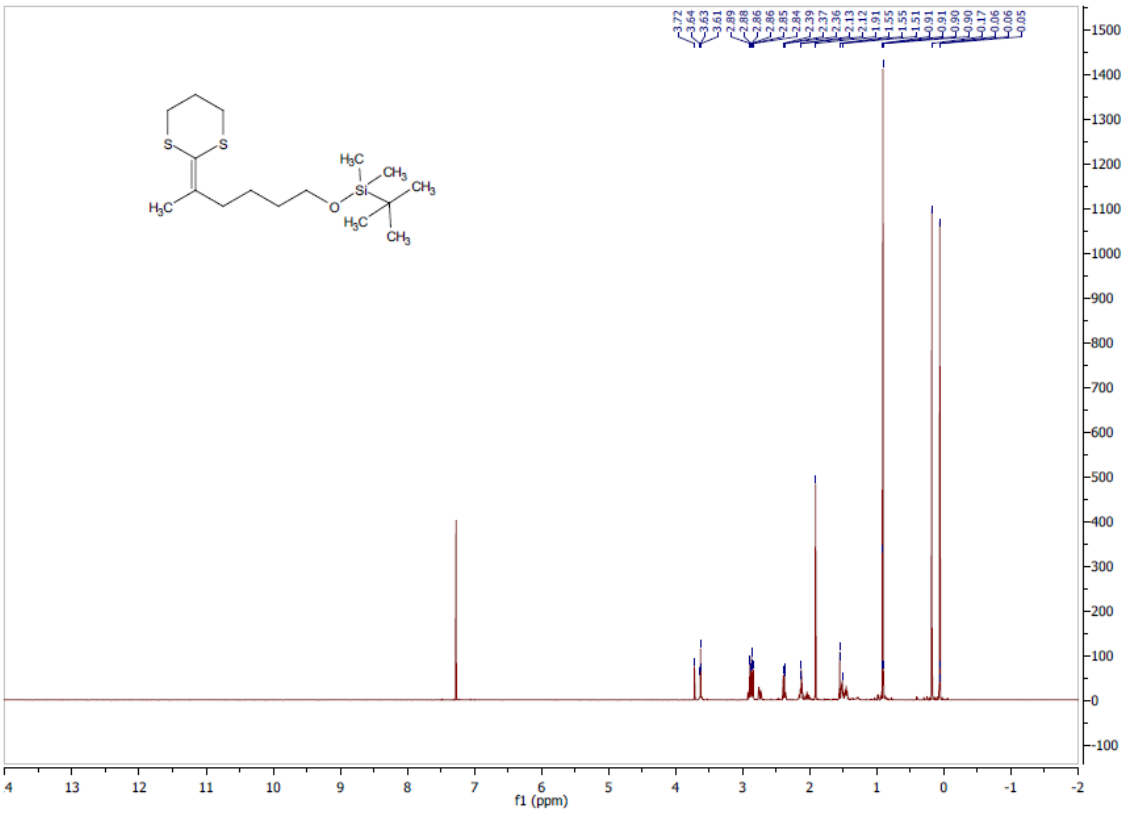
3.72
3.64
3.63
3.61
2.89
2.88
2.86
2.85
2.84
2.39
2.37
2.36
2.13
2.12
1.91
1.55
1.55
1.51
0.91
0.90
0.90
0.17
0.06
0.06
0.05
f1 (ppm)

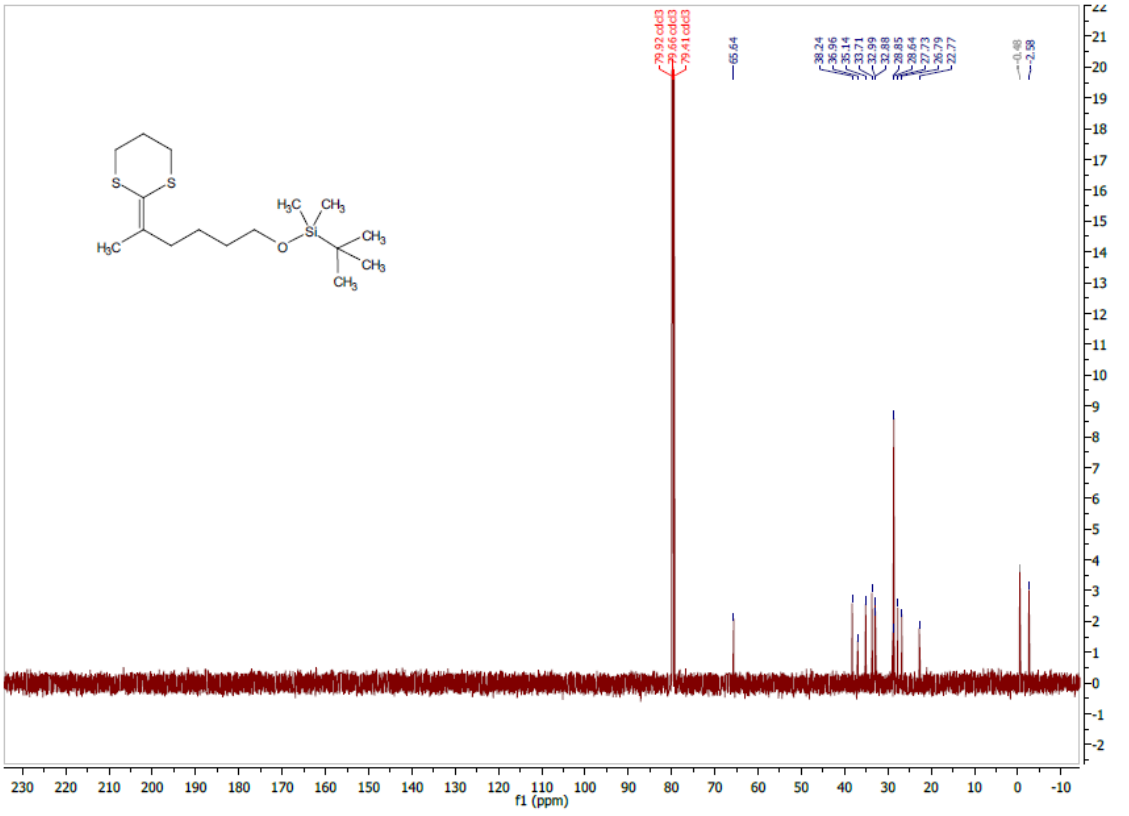
79.92 cdcl3
79.66 cdcl3
79.41 cdcl3
65.64
38.24
36.96
35.14
33.71
32.99
32.88
28.85
28.64
28.23
26.79
22.77
-0.48
-2.98
f1 (ppm)

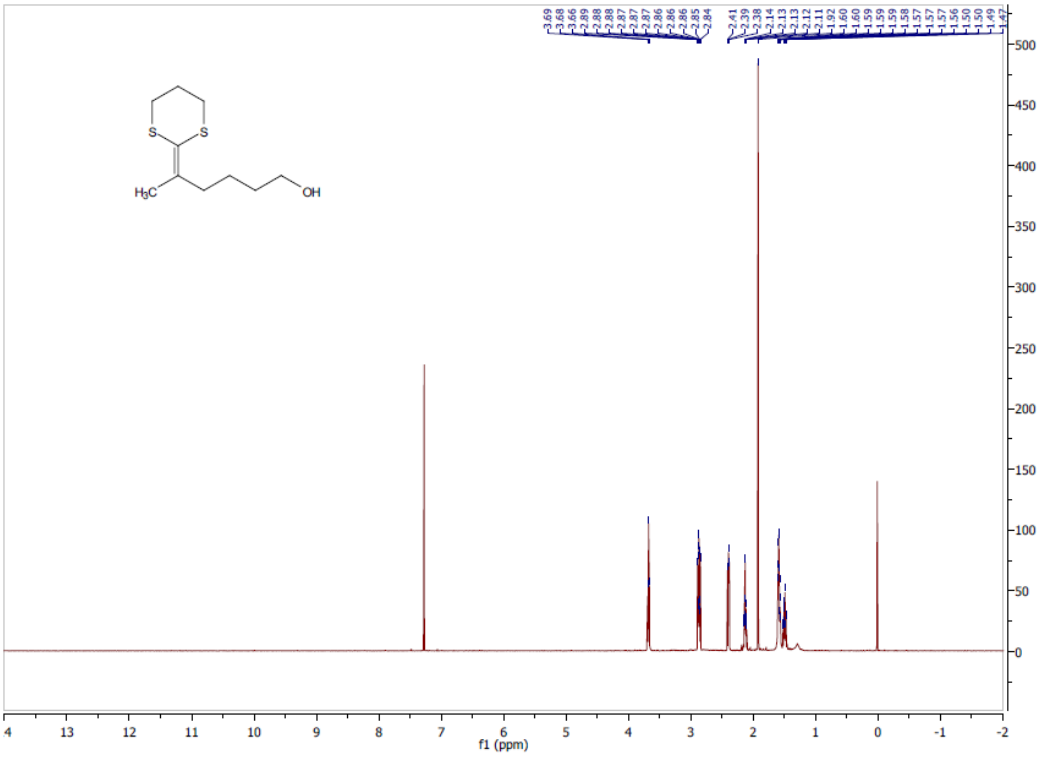
S
S
H3C
OH
f1 (ppm)

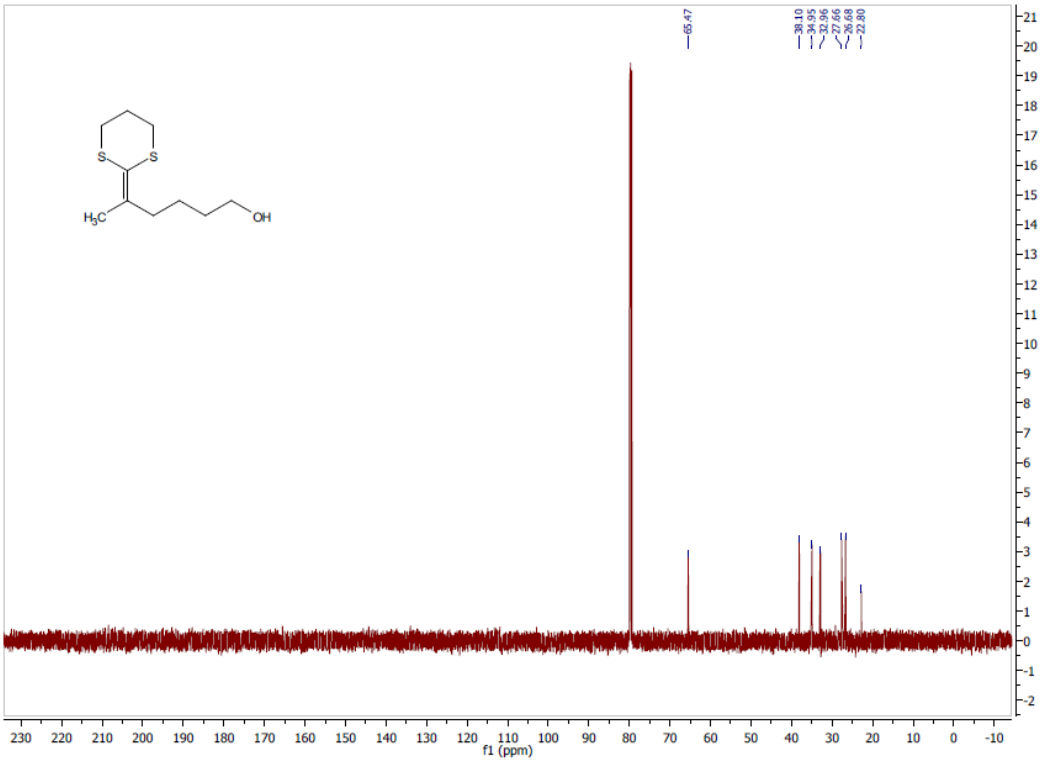
65.47
38.10
34.95
32.96
27.66
26.68
22.80
S
S
H3C
OH
f1 (ppm)

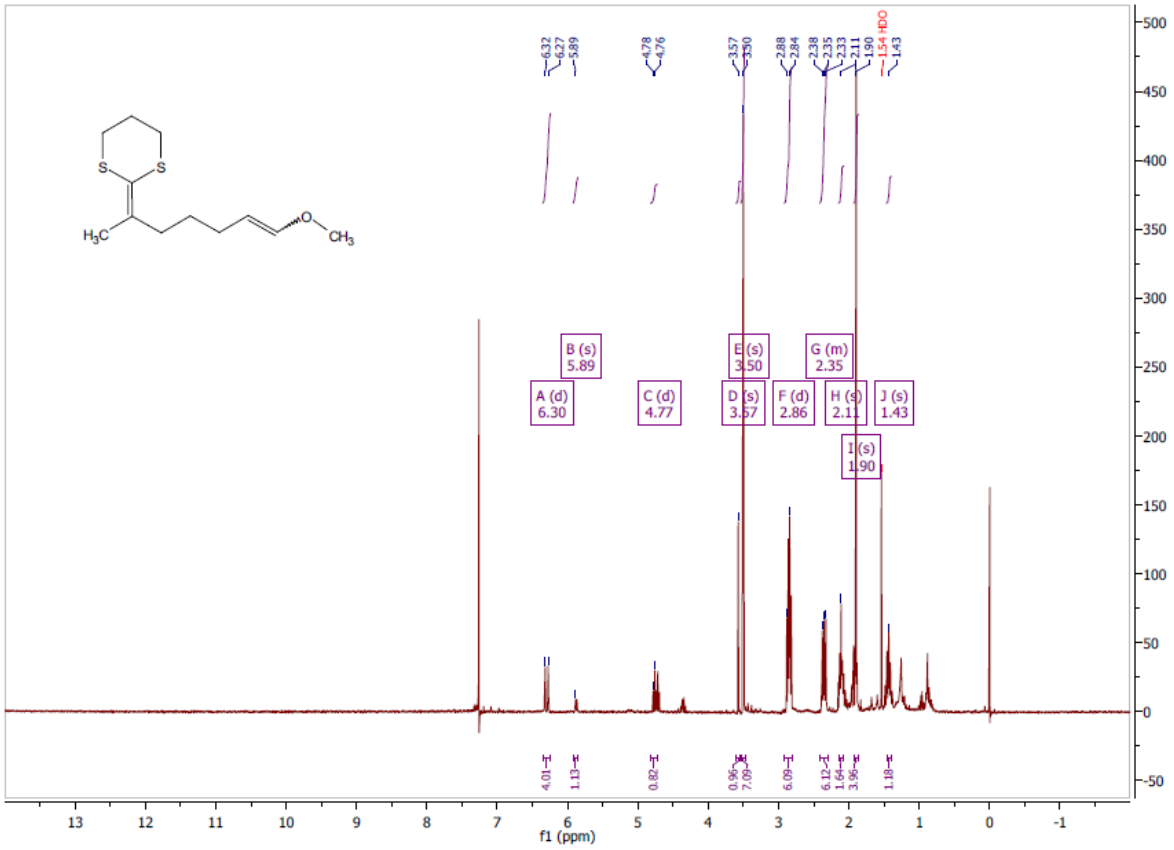
6.32
6.27
5.89
4.78
4.76
3.57
3.50
2.88
2.84
2.38
2.35
2.33
2.11
1.90
1.54
HDO
1.43
B (s)
5.89
E (s)
3.50
G (m)
2.35
A (d)
6.30
C (d)
4.77
D (s)
3.57
F (d)
2.86
H (s)
2.11
J (s)
1.43
I (s)
1.90
4.01
1.13
0.82
0.96
7.09
6.09
6.12
1.64
3.96
1.18
f1 (ppm)

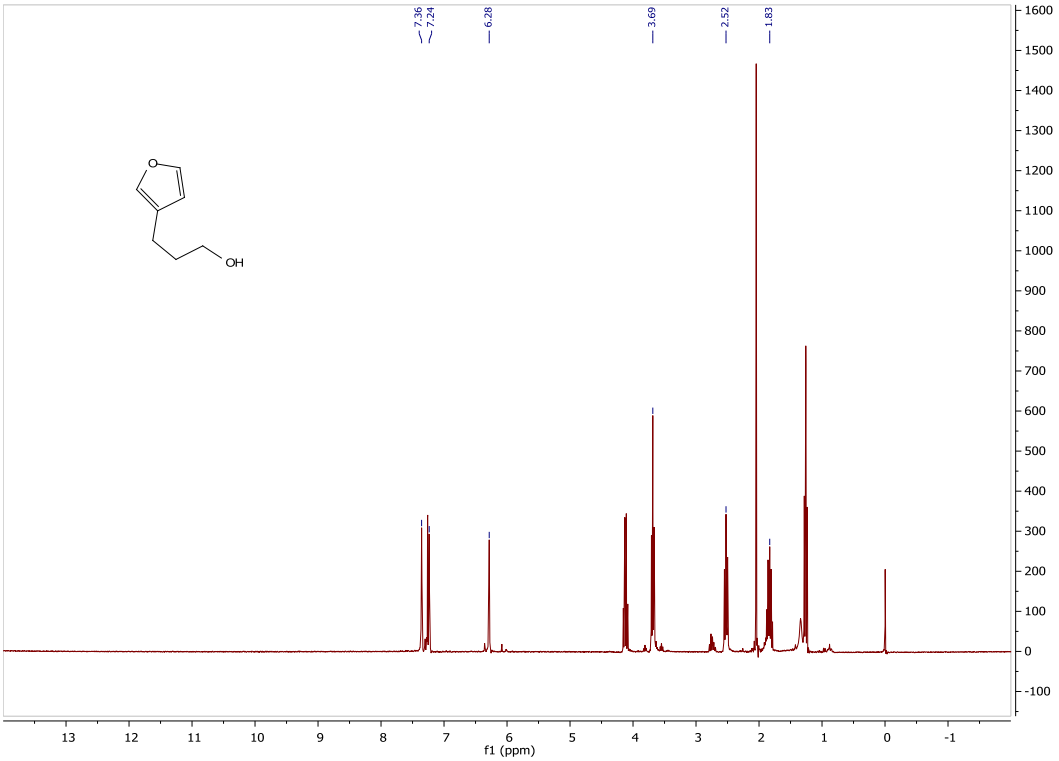
7.36
7.24
6.28
3.69
2.52
1.83
O
OH
f1 (ppm)

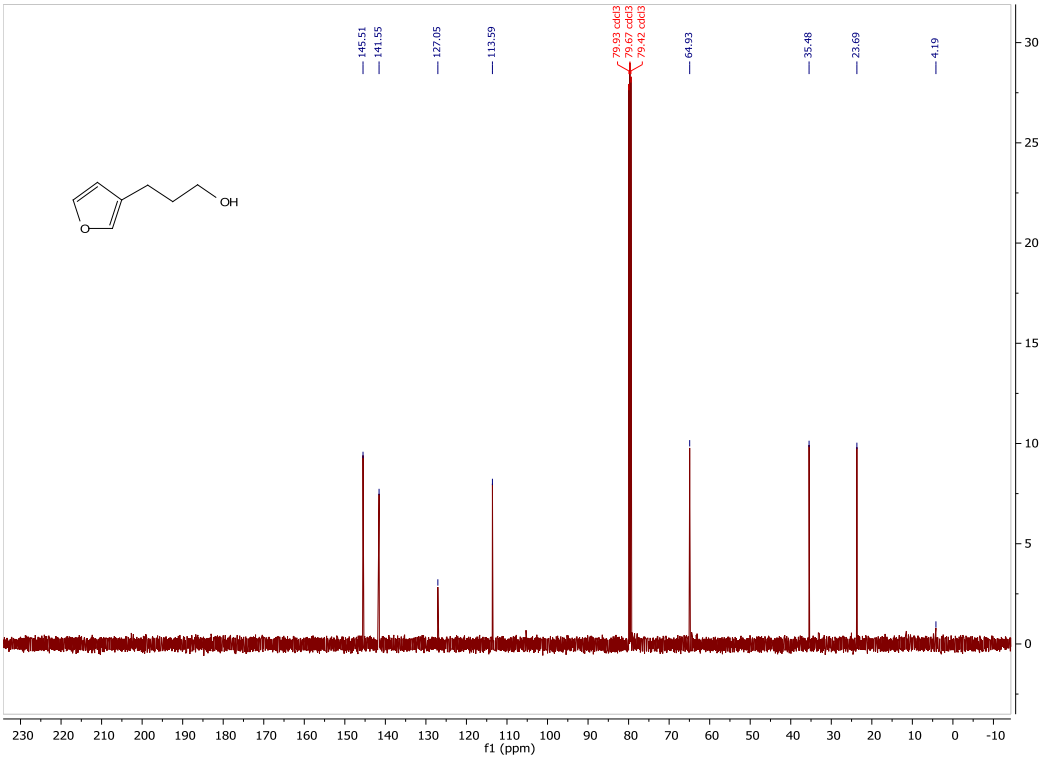
145.51
141.55
127.05
113.59
79.93 cdcl3
79.67 cdcl3
79.42 cdcl3
64.93
35.48
23.69
4.19
OH
O
f1 (ppm)

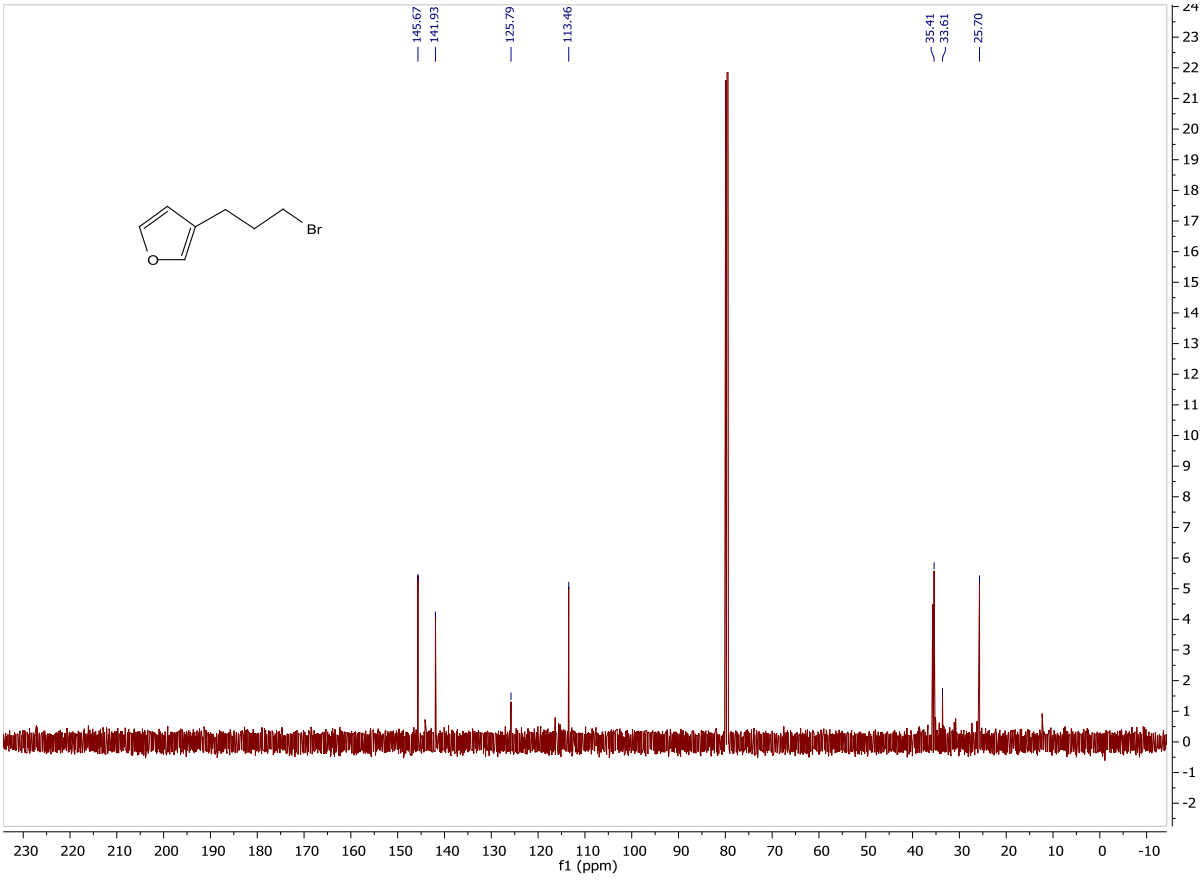
145.67
141.93
125.79
113.46
35.41
33.61
25.70
Br
O
f1 (ppm)

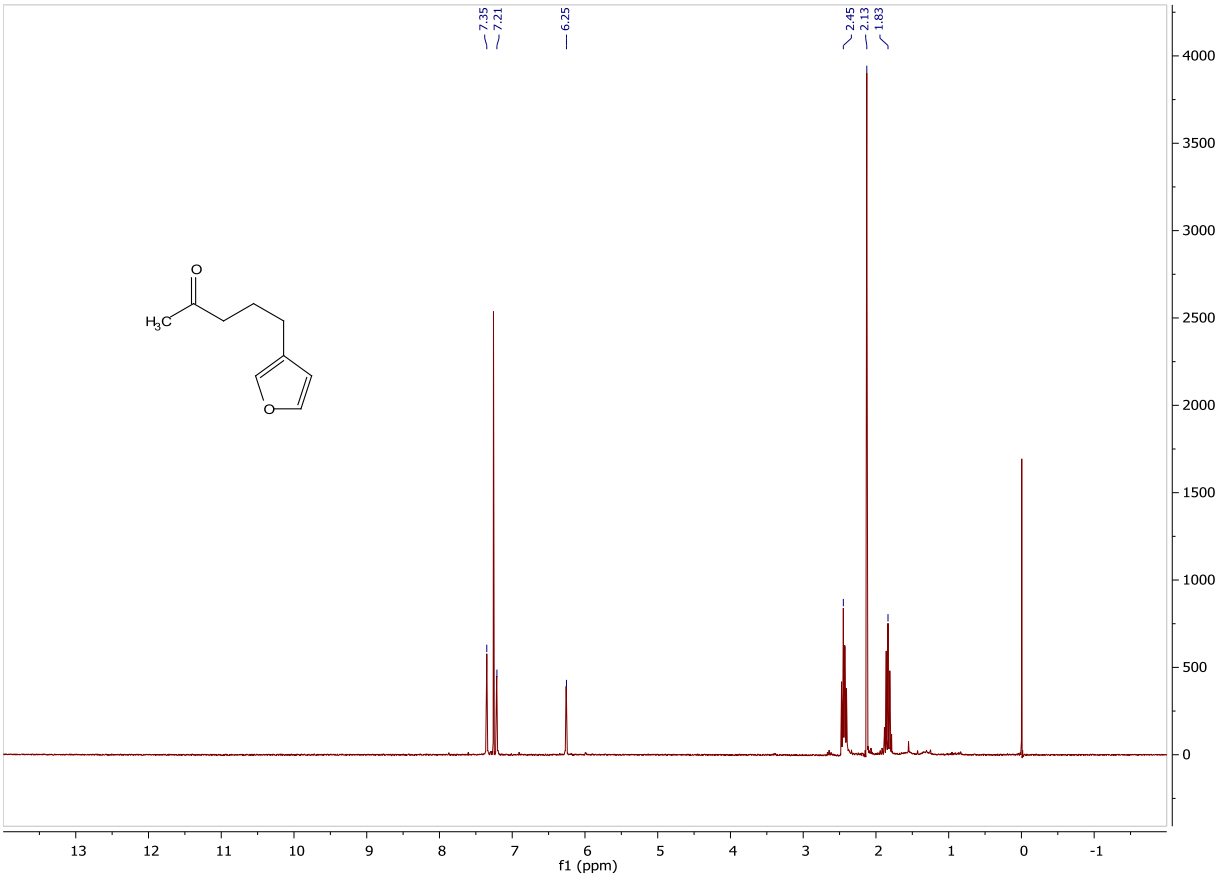
7.35
7.21
6.25
2.45
2.13
1.83
O
H3C
O
4000
3500
3000
2500
2000
1500
1000
500
0
13
12
11
10
9
8
7
6
5
4
3
2
1
0
-1
f1 (ppm)

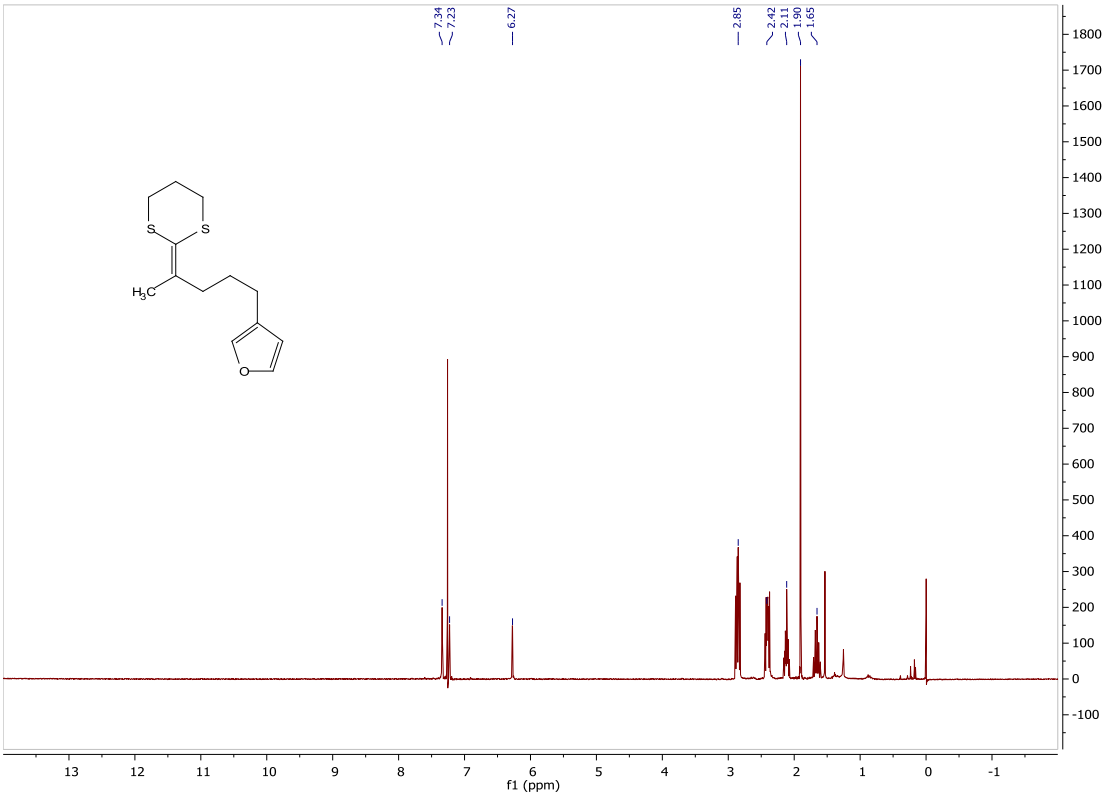
7.34
7.23
6.27
2.85
2.42
2.11
1.90
1.65
S
S
H3C
O
f1 (ppm)

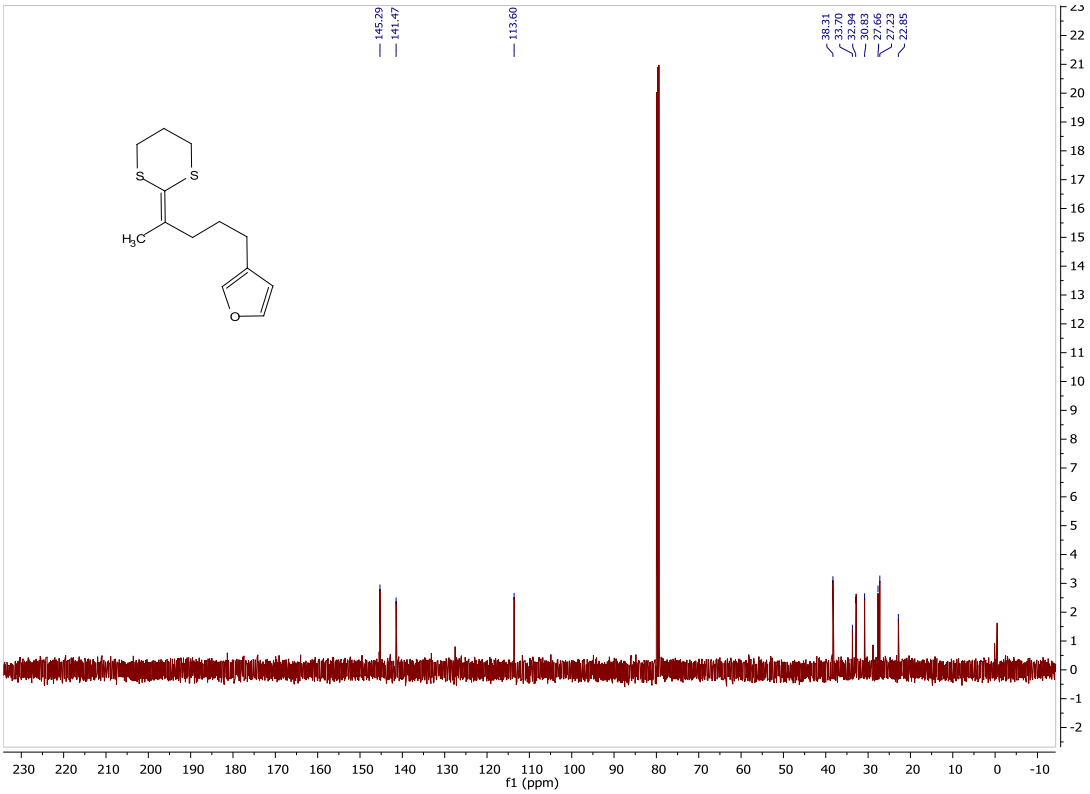
145.29
141.47
113.60
38.31
33.70
32.94
30.83
27.66
27.23
22.85
S
S
H3C
O
f1 (ppm)

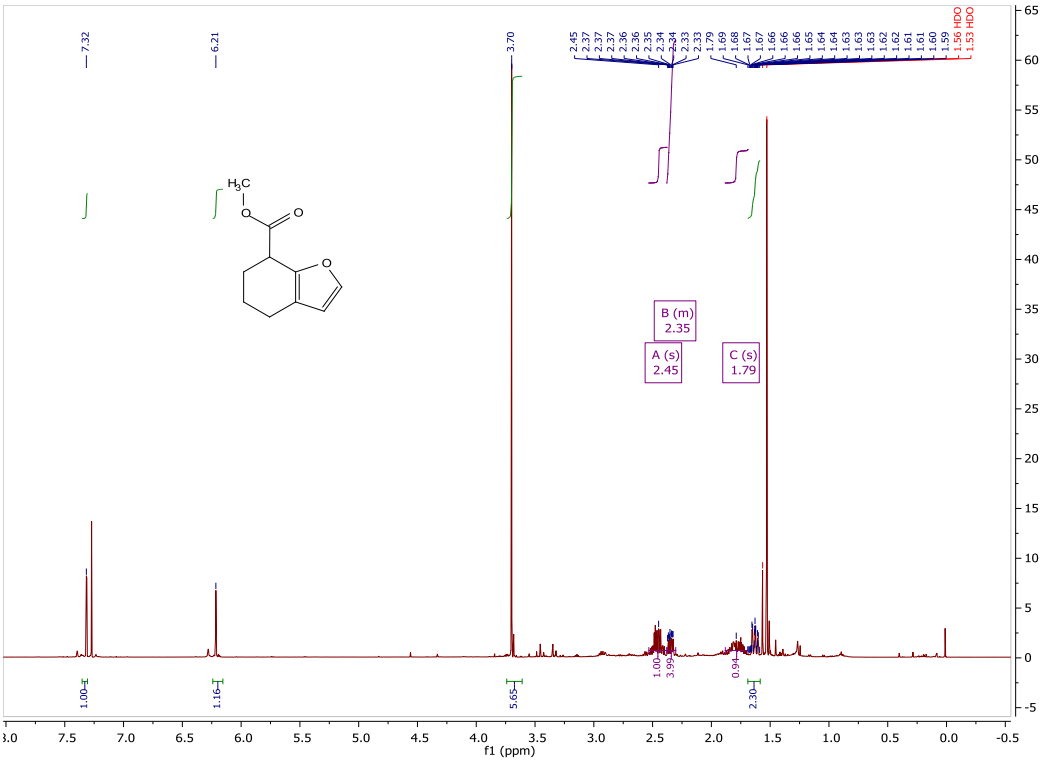
7.32
6.21
3.70
2.45
2.37
2.37
2.37
2.36
2.36
2.35
2.34
2.34
2.33
1.79
1.69
1.68
1.67
1.67
1.66
1.66
1.65
1.64
1.64
1.63
1.63
1.62
1.62
1.61
1.61
1.60
1.56 HDO
1.53 HDO
B (m)
2.35
A (s)
2.45
C (s)
1.79
1.00
1.16
5.65
1.00
3.99
0.94
2.30
f1 (ppm)

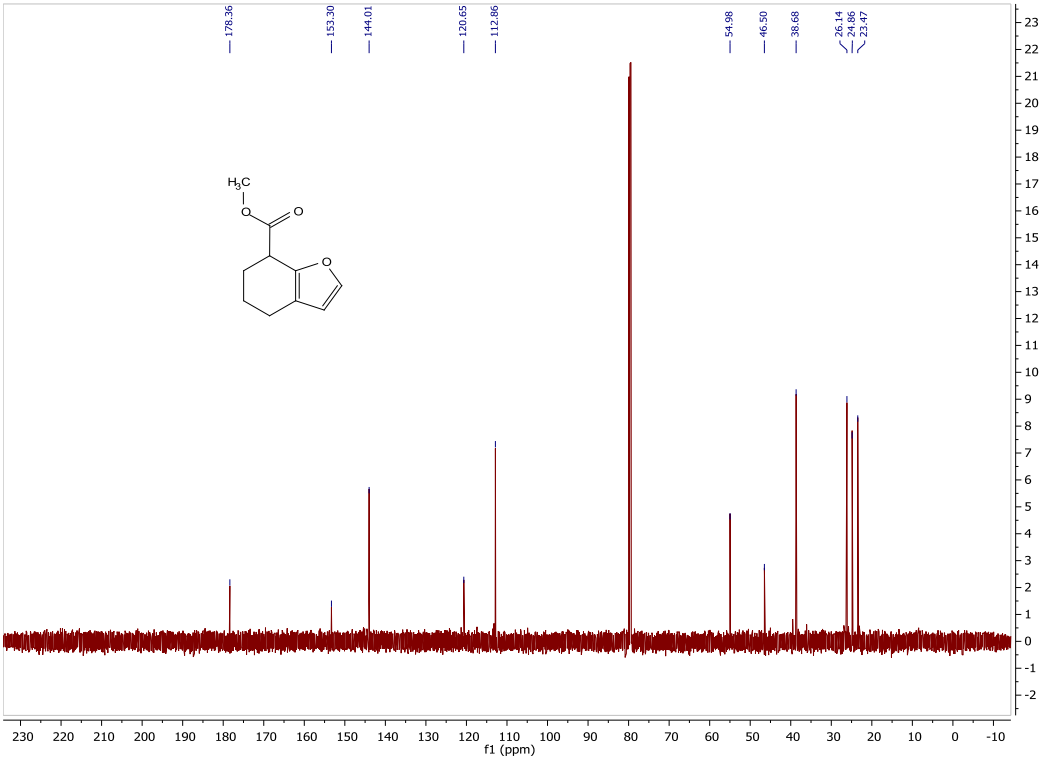
178.36
153.30
144.01
120.65
112.86
54.98
46.50
38.68
26.14
24.86
23.47
f1 (ppm)